Using an engineered human hexosaminidase as an enzyme replacement therapy to treat a mouse model of Tay-Sachs Disease

By

Mehrafarin Ashiri

A Thesis submitted to the Faculty of Graduate Studies of

The University of Manitoba

in partial fulfillment of the requirements for the degree of

Master of Science

Department of Biochemistry and Medical Genetics

University of Manitoba

Winnipeg, Manitoba, Canada

Abstract:

Tay-Sachs disease (TSD) is a rare genetic disorder arising from mutations in the gene encoding the α-subunit of β-hexosaminidase A (HexA). Hexosaminidase A is a member of a family of enzymes that are involved in the degradation of glycoconjugates including glycolipids and glycosphingolipids. These molecules are components of cell membranes and have important roles in cellular signaling processes, cell-surface recognition, cell proliferation, and neurotransmission, among other functions.

HexA enzyme deficiency leads to progressive buildup of GM2 ganglioside in the central nervous system (CNS) and other tissues throughout the body. Excessive GM2 ganglioside storage in the CNS leads to neuronal death with devastating neurological and psychiatric consequences such as cognitive impairment and intellectual disability, locomotion dysfunction, seizures, and respiratory failure.

Although various treatment strategies have been investigated, there are no known effective treatments for TSD other than mitigating the associated symptoms. Lack of an effective treatment results in death at the age 4-5 in the most severe form of TSD known as infantile TSD.

One of the therapeutic strategies which is based on the ability of cells to take up exogenous enzyme is enzyme replacement therapy (ERT). Therefore, ERT can increase the enzyme activity in enzyme deficient cells to therapeutic levels, which is known as an effective treatment strategy for other lysosomal storage disorders (LSDs).

In the present study we used HexM, a human based engineered enzyme harbouring the critical aspects of HexA enzyme, which made it a suitable candidate to improve the efficacy of ERT.

To evaluate the therapeutic efficiency of a M6P-HexM and its hyperphosphorylated form; M6P-PhosHexM, we used intracerebroventricular (ICV) ERT in a TSD comparable mouse model.

Assessing the biodistribution of enzymes suggested that M6P-HexM had a longer circulation time in the blood compared to M6P-PhosHexM. We also observed that after administrating the enzymes through the vein, liver enzyme activity was significantly enhanced in comparison to activity in HexA deficient animals. Brain's enzyme activity suggested an elevation post M6P-HexM IV-infusion compared to controls. Histological analysis of brain tissue post ICV-ERT showed a reduction in the accumulated GM2 ganglioside.

Delivering the enzymes directly into the cerebrospinal fluid through ICV-cannulation resulted in an increase in the ratio of GM3/GM2 ganglioside in the hippocampal region and near the implanted cannula.

Acknowledgements:

Words cannot express my gratitude to my supervisors Dr. Barbara Triggs-Raine and Dr. Brian Mark who provided me with the invaluable opportunity to achieve my master's degree. I cannot thank you enough for never stop believing in me and for patiently guiding me throughout my project and finalizing it. You are second to none!

I have had the pleasure to work with Brian, an experienced mentor and an incredible scientist who has been always, inspiring to me. He always has been accessible, encouraging, and supportive whenever I asked for help.

I would like to express my deepest appreciation to Barb an exceptional teacher, a knowledgeable and experienced mentor and a passionate scientist who has been always humble, accessible, understanding, supportive, encouraging, and taught me to never give up. Working with you gave me great confidence throughout this process.

Also, I could not have undertaken this journey without the chair of department Dr. Etienne League and my committee members, Dr. Donald Miller and Dr. Geoff Hicks who generously provided knowledge and expertise. Additionally, this endeavor would not have been possible without the generous supports and suggestions from my current and past lab members in Mark and Barb's lab, especially Dr. Rick Hemming, Emily Barker, Elaine Anjos, Deanne Miao, Veronica Larmor, Grace Saliga, and Anuradha De Silva.

I would like to extend my sincere thanks to our collaborators in M6P therapeutics (M6PT), Dr. Shawn Whitehead and Wenxuan Wang in Western university, and all the funding agencies.

I wish to acknowledge the help provided by BMG mentorship group, the technical and support staff in the in the Biochemistry and medical genetics department.

I would also like to acknowledge the central animal care services staff especially Agnes Fresnoza and Rhonda Kelley for their kind support.

I would also like to thank my wonderful friends for all the kindness, help, discussions, and encouragements.

I would like to thank all the people who believed in me and supported me to grow, and I would like to thank people who never believed in me, and made me a stronger fighter!

Finally, and most importantly, I would like to thank my amazing family and my Azarory for their unwavering love and support through the good times and hard times.

Dedication

I would like to dedicate this thesis to the brave women and men in Iran who are fighting for their freedom.

To women, to life, to freedom.

Table of Contents

List of Tables

List of Figures

Abbreviations:

A	Alpha
A260	Absorbance at 260 nm
Ab	Antibody
aCSF	artificial Cerebrospinal fluid
AP	Anterior-Posterior
AAV	Adeno-associated virus
AAVrh8	Adeno-associated virus rhesus isolate 8
AMR	Ashwell–Morell receptor
B	Beta
BBB	Blood-brain barrier
Bis-Tris	Bis(2-hydroxyethyl) amino-tris(hydroxymethyl)methane
BMT	Bone marrow transplantation
BSA	Bovine Serum Albumin
CD-MPR receptors	Cation-dependent mannose-6-phosphate receptor
CDM-HD	Chemically defined medium for high density
cDNA	Complimentary DNA
CI-MPR	Cation-independent mannose-6-phosphate receptor
CMV	Cytomegalovirus
CLN2	Neuronal ceroid lipofuscinoses type II
CNS	Central nervous system
CP buffer	Citrate-phosphate buffer
CRISPR	Clustered regularly interspaced short palindromic repeats
CSF	Cerebrospinal fluid
°C	Degrees Celsius
Da	Dalton
DAN	1,5-Diaminonapthalene
ddH2O	Double deionized water
dKO	Double knock out

DMEM	Dulbecco's modified Eagle medium
DMSO	Dimethyl sulfoxide
DNA	Deoxyribonucleic acid
dNTP	Deoxynucleotide triphosphate
DV	Dorsal-Ventral
ER	Endoplasmic reticulum
ERAD	Endoplasmic reticulum-association degradation
ERT	Enzyme replacement therapy
FBS	Fetal bovine serum
FDA	United States Food and Drug Administration
g	Gram
GalNAc	N-acetyl-β-galactosamine
GC buffer	Glycine-Carbonate buffer
GD1	type 1 Gaucher disease
GM1	GM1 ganglioside
GM2	GM2 ganglioside
GM3	GM3 ganglioside
GM4	GM4 ganglioside
GM2A	GM2 activator gene
GM2AP	GM2 activator protein
GT	Gene therapy
GVHD	graft-versus-host disease
HEK 293T	Human embryonic kidney 293T
HexA	β-hexosaminidase A
HEXA	*HEXA* gene
Hexa$^{-/-}$	HexA knock out
HexB	β-hexosaminidase B
HEXB	*HEXB* gene
HexM	β-hexosaminidase M
HexS	β-hexosaminidase S

HRP	Horseradish peroxidase
ICV	Intracerebroventricular
IGF2R	Insulin-like growth factor 2 receptors
IHC	Immunohistochemistry
IMAC	Immobilized metal affinity chromatography
ITO	Indium-Tin-Oxide
iPSCs	Induced pluripotent stem cells
kb	Kilobase
kDa	Kilodalton
LSD	Lysosomal storage disorders
µg	Microgram
µl	Microlitre
µM	Micromolar
MALDI-MSI	Matrix assisted laser desorption/ionization mass spectrometry imaging
M6P-HexM	HexM provided by M6P-Theraputics
M6P-PhosHexM	PhosHexM provided by M6P-Theraputics
MPR	Mannose-6-phosphate Receptor
MCB	Membranous cytoplasmic bodies
mg	Milligram
ml	Millilitre
ML	Medial-Lateral
mM	Millimolar
MPS I	Mucopolysaccharidosis type I
MPS II	Mucopolysaccharidosis type II
MR	Mannose receptor
MPS VI	Mucopolysaccharidosis type VI
MUG	4-Methylumbelliferyl 2-acetamido-2-deoxy-β-D-glucopyranoside
MUGS	4-Methylumbelliferyl 6-sulfo-2-acetamido-2-deoxy-β-D-glucopyranoside
M6P	Mannose 6-phosphate
M6PR	Mannose 6-phosphate receptor

MW	Molecular weight
NAGPA	N-acetylglucosamine-1-phosphodiester-N-acetylglucosaminidase
ng	Nanogram
Ni-NTA	Nickel-nitrilotriacetic acid
Neu3	Neuraminidase3 gene
Nue3$^{-/-}$	Neu3 knock out
nm	Nanometer
LSD	Lysosomal storage disorder
PBS	Phosphate-buffered saline
PCR	Polymerase chain reaction
pM	Picomolar
PTMs	Post translational glycosylation
PYR	Pyrimethamine
RER	Rough endoplasmic reticulum
RFU	Relative fluorescence units
rGM2AP	Recombinant human GM2AP
ROI	Region of interest
RSV	Respiratory syncytial virus
s	Second
S1S3 PTase	Modified GlcNAc-1-phosphotransferase
SEC	Size exclusion chromatography
Sc-AAV	Self-complementary adeno-associated virus
SD	Sandhoff disease
SDS-PAGE	Sodium dodecyl sulfate polyacrylamide gel electrophoresis
SRT	Substrate reduction therapy
TGN	Thioguanine
T_m	Melting temperature
TSD	Tay-Sachs disease
UV	Ultraviolet
Vmax1	Maximum enzyme velocity

WB	Western Blot
4-MU	4-methylumbelliferone

1 Introduction

1.1 The lysosomes

Christian de Duve, in 1955, first discovered lysosomes which are recognized as membrane bound organelles containing acidic hydrolases and lysosomal enzymes [1].

Not only are lysosomes involved in degradation and recycling of intracellular material though autophagy, but they are also involved in the degradation of extracellular material through endocytosis and phagocytosis [2]. Further, lysosomes are known to participate in vital biological processes including the regulation of energy metabolism and cell growth, plasma membrane repair, maintenance of cell and cholesterol homeostasis, immune reactions and apoptosis [2–4].

Due to the involvement of lysosomes in multiple cellular processes, their normal function is critical. Defects in many lysosomal components lead to lysosomal storage disorders (LSD), however, lysosomal dysfunction has also been observed in other diseases such as cancer and Alzheimer's disease [4,5].

1.2 Lysosomal storage diseases

LSD refers to over 50 hereditary metabolic disorders characterized by progressive storage of a specific substrate(s) due to the lack of a specific enzyme or nonenzymatic protein. Combined, LSDs are estimated to have an incidence of 1 in 5000-8000 births [2–4,6].

LSD clinical manifestations vary depending on the affected enzyme/protein and the degree of substrate storage. The cellular and organ damage due to pathological accumulation of substrate in the lysosomes can affect almost any tissue/organ depending on the abundance of the accumulating substrate in that tissue. Cognitive and neurologic impairment, skeletal and muscular abnormalities, and organomegaly of the heart, liver, and/or spleen are some of the common problems that result in morbidity and early death [6–9].

1.3 GM2-gangliosidoses

The GM2-gangliosidoses are a group of hereditary neurodegenerative LSDs that arise from loss-of-function mutations in *HEXA, HEXB or GM2A* genes. Homozygosity for mutations in any one of these genes results in β-hexosaminidase (Hex) deficiency and gradual storage primarily of GM2 ganglioside within lysosomes [10,11].

HEXA and *HEXB* genes encode the α and β subunits respectively, which dimerize to form three different Hex isozymes including a heterodimer of αβ subunits called β-hexosaminidase A (HexA), a homodimer of ββ subunits called β-hexosaminidase B (HexB), and a less stable homodimer of αα subunits called β-hexosaminidase S (HexS) [12–15].

Mutations in *HEXA* cause Tay-Sachs disease (TSD, OMIM 272800); while mutations in *HEXB* cause Sandhoff disease (SD, OMIM 268800). Also, mutations in *GM2A* cause deficiency in the GM2 activator protein (GM2AP) leading to a rare form of GM2-gangliosidosis called the AB-variant (OMIM 272750) [16].

1.4 GM2-ganglioside structure, distribution, and biological function

Gangliosides were first discovered by Ernst Klenk in the 1930s [17,18] in a post-mortem assessment of brain lipids from a TSD patient [19]. Gangliosides are found in all tissue types, and predominantly located in the neuronal membrane [20], where they contribute to critical cellular processes such as cell recognition, axon-myelin connections, membrane protein regulation, cell signaling and Ca^{2+} maintenance as well as overall brain function and development [5,10,21].

Gangliosides are comprised of a glycosphingolipid backbone that is linked to sialic acid moieties through an oligosaccharide structure [22]. In humans, the majority of distributed

ganglioside in the visceral organs such as liver, heart and connective tissues such as platelets and fat are GM3 ganglioside [22]. Of the ganglioside content in the brain, about 95% of it is comprised of GM1, GD1a, GD1b and GT1b gangliosides and the remaining 5% is GM2 and other gangliosides [20,23,24]. Ganglioside degradation involves a variety of target-specific lysosomal enzymes, and it happens through the consecutive removal of neutral sugar residues and sialic acid [19,25]. GM2 ganglioside[1] (GM2) is an intermediary glycosphingolipid produced by recycling complex gangliosides of the brain (**Fig. 1-1**) [10,26].

[1] β-GalNAc-(1-4)-[α-Neu5Ac-(2-3)]- β-Gal-(1-4)- β-Glc-(1-1)-Cer

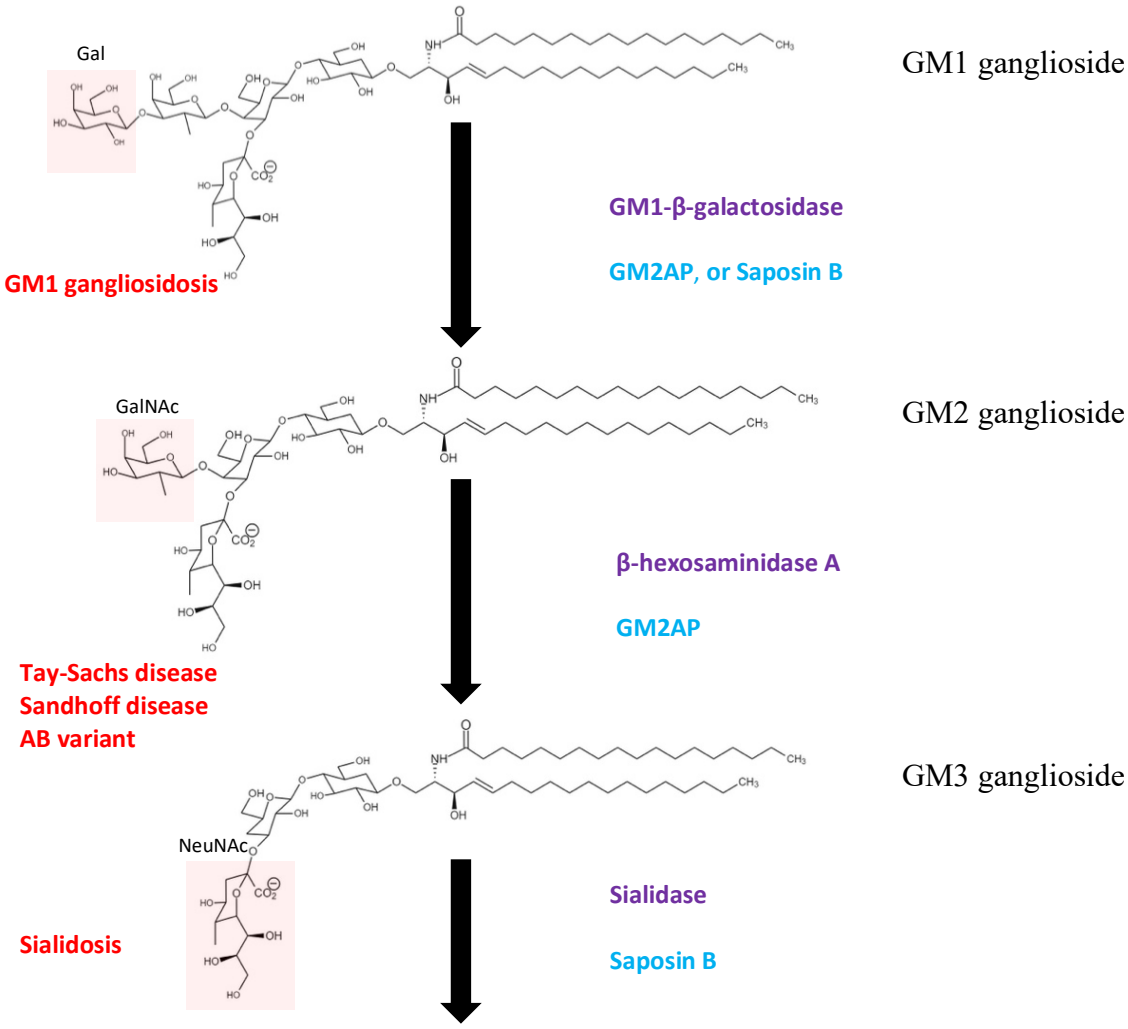

Figure 1-1. The catabolism pathway of GM1 ganglioside to GM3 ganglioside in humans.

Stepwise degradation of gangliosides to sphingosine involves different enzymes and coenzymes. GM1-β-galactosidase enzyme mediates the removal of terminal galactose from GM1 ganglioside and converts it to a GM2 ganglioside. In the next step, β-hexosaminidase A facilitates the conversion of GM2 ganglioside to GM3 ganglioside by removal of the terminal N-acetyl-β-galactosamine (GalNAc) residue 19. Then N-acetylneuraminic acid residue of GM3 ganglioside is removed by sialidase to form lactosylceramide (not shown)[27]. Enzymes and coenzymes are shown in purple and cyan respectively. Disruption of this catabolic pathway can result in different lysosomal storage diseases, indicated in red. Figure is modified from Sandhoff et al. 2013 and Konrad Sandhoff et al 1995 under the license number of 5450971458959 [19,28].

1.5 Tay-Sachs disease (TSD) and classification

In 1881, an ophthalmologist named Warren Tay first characterized TSD in an infant patient with a macular cherry-red spot [29]. At the same time, a neurologist Bernard Sachs, described the pattern of inheritance, underlying cellular modifications such as swollen ganglion cells and cellular vacuolization while studying TSD in affected Ashkenazi Jewish infants [30,31]. Based on the severity of mutations' impact on the HexA activity, there are three different classifications of GM2 gangliosidosis resulting from HexA deficiency that differ in clinical symptoms and onset age infantile, juvenile, and late-onset [32].

The most severe form is the infantile form, also known as TSD, which is described with the lowest enzyme activity (below 0.1% normal) [10,32,33]. Individuals affected by this form of TSD appear normal at birth; however, due to the absence of enzyme activity rapid disease progression occurs [34]. Clinical symptoms are exhibited by 3-6 months of age, including a retinal cherry red spot and abnormal startle response. This is followed by regression of developmental milestones, developmental delay in motor and mental skills, swallowing problems, and seizures ultimately leading to death typically before 4 years of age [10,12,32,35–37].

Other forms of GM2 gangliosidosis resulting from mutations in HexA show a higher residual enzyme activity. Although the onset is highly variable, clinical symptoms typically become evident between 2 and 5 years of age for juvenile GM2 gangliosidosis and in early/mid-teens or later for the adult-onset form of GM2 gangliosidosis [36,38]. Clinical symptoms in juvenile patients consist of an inability to control muscles, difficulty in swallowing and speaking, hypotension, recurring spasms, and death by age 15 years old. A less severe and broader range of symptoms are observed in late onset GM2 gangliosidosis with progressive motor, cerebral and spinocerebellar dysfunction [12].

1.5.1 TSD incidence and prenatal screening

While rare in the general population with an incidence of 1 in 360,000 and an estimated carrier frequency of 1 in 300 [39,40], TSD was initially found to have a higher carrier frequency in certain populations such as Ashkenazi Jews with 1 in 30 and eastern Quebec French Canadians with a carrier frequency of 1 in 14 [39–41].

To address the high carrier frequency in aforementioned populations, prenatal screening and genetic counseling have been offered which in turn resulted in a notable reduction in the incidence of TSD among the Ashkenazi Jewish population in Northern America [40,42,43].

Previously, screening tests relied on biochemical tests on leukocytes and/or serum, cultured skin derived fibroblasts, or amniotic fluid using synthetic substrates known as MUGS[2] or using MUG[3] followed by thermal differentiation to distinguish the activity associated with the HexA and HexB isozymes [42,44–48]. However DNA analysis is a more reliable method to detect the underlying mutations in the *HEXA* gene and differentiate the disease causing from benign mutations [12,32,36,39,40,43,44,46,47].

[2] 4-methylumbelliferyl- GlcNAc-6-sulfate
[3] 4-methylumbelliferyl-β-N-acetylglucosamine

1.5.2 TSD common mutations

About 170 different mutations including single base substitutions, deletions, insertions and indels have been recognized to be associated with HexA enzyme deficiency and TSD, while a 7.6 kb deletion has been defined as one of the prevalent TSD causing mutations in French Canadians [44,49–51]. Mutations which are commonly assessed in TSD screening are the G269S substitution associated with late onset TSD [52,53], and two other mutations associated with infantile TSD in Ashkenazi Jewish patients including a 4 base-pair insertion (c.1278insTATC) which causes a frameshift in exon 11 of *HEXA* gene and introduces a premature stop codon and a G→C transversion (c.1421+ 1G3 > C) affecting the splicing of *HEXA* [43,54–57].

1.5.3 HexA enzyme synthesis, transport and GM2 ganglioside degradation

The synthesis and post translational glycosylation (PTMs) of both HexA subunits occurs in the endoplasmic reticulum (ER) [58]. The PTM events are vital since they are necessary for the further targeting of lysosomal enzymes to their assigned destinations, and determine their pharmacokinetic characteristics [59,60]. Proper folding and intramolecular disulfide bond formation between the α and β subunits of the heterodimer also occur in the ER and are necessary to form a catalytically functional HexA enzyme [61].

The HexA enzyme is then transferred to the Golgi apparatus where it acquires mannose-6-phosphate (M6P) as recognition tags on specific N-linked glycans by consecutive action of two enzymes. In the first step, GlcNac-1-phosphotransferase mediates transmission of GlcNac-1-phosphate moiety from UDP-GlcNac[4] to terminal mannose residues on the attached glycans [62].

[4] Uridine diphosphate N-acetylglucosamine

In the second step, N-acetylglucosamine-1-phosphodiester-N-acetylglucosaminidase (NAGPA) exposes the Man6P recognition tags by removing GlcNAc [63]. Exposed M6P-tags on the enzyme are recognized by M6P receptors existing in the Golgi which ensures the accurate trafficking of HexA enzyme to its destination, mainly to lysosomes [60,61]. The low pH condition in the lysosomes promotes proteolytic cleavage of α and β subunits and trimming of oligosaccharides resulting in the formation of the mature form of catalytically active enzyme [61].

A protein known as the GM2 activator protein (GM2AP) extracts GM2 ganglioside from lysosomal membranes and presents it to HexA for further degradation by removal of the terminal N-acetyl-D-galactosamine (GalNAc) moiety from GM2 ganglioside (**Fig. 1-2**) [20,64]. However, mutations in the α subunit of HexA can adversely affect proper folding of this subunit and subsequently impact its ability to make a heterodimer with β subunit required for formation of HexA active enzyme. The misfolded or truncated α subunits made in ER will be eliminated through ERAD[5] process [55]. Disruption of this degradative pathway eventually causes pathological accumulation of GM2 mainly in the CNS, and peripheral nervous system, which results in GM2 gangliosidosis [65].

[5] ER-associated degradation

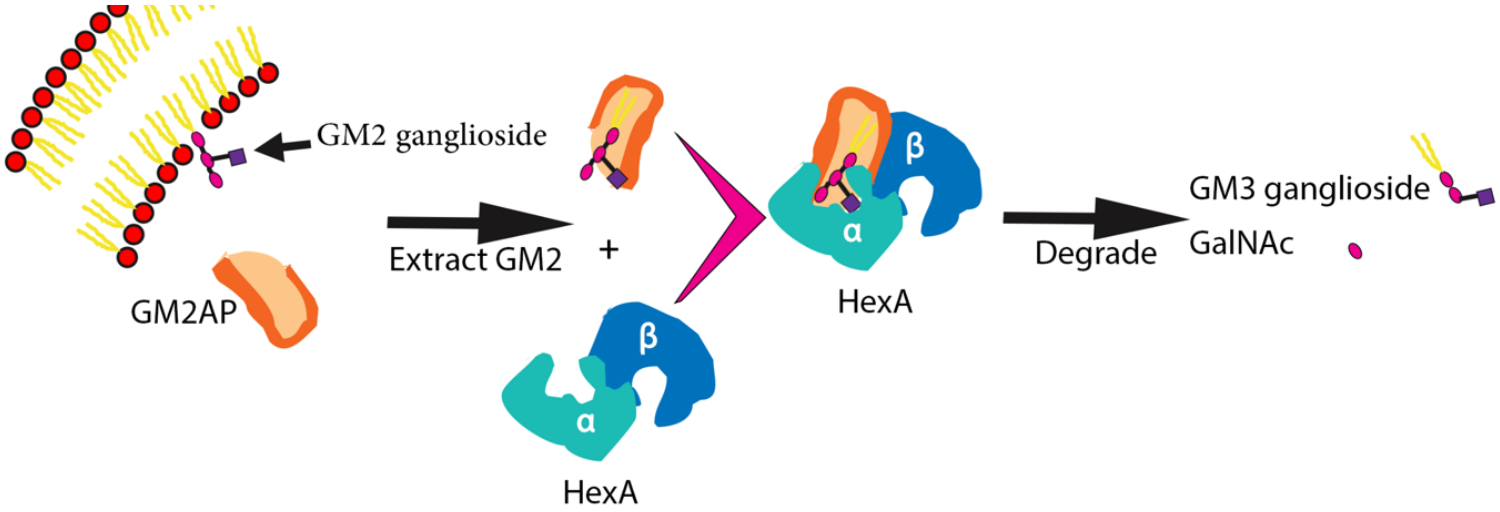

Figure 1-2. Schematic of GM2AP's role in GM2 ganglioside degradation.

GM2AP binds GM2-ganglioside in the lysosome membrane and makes it accessible to the α-subunit active site and forming a stable quaternary complex with the β subunit to degrade GM2-ganglioside. Reproduced from Sandhoff et al. 2013 [19] (Creative Commons Attribution-Non-commercial-Share Alike 3.0 Unported License (CC-BY-NC-SA)).

1.6 Potential therapies

HexA deficiency results in the progressive storage of GM2 ganglioside primarily in lysosomes of neurons. Accumulated GM2 ganglioside results in the formation of membranous cytoplasmic bodies (MCB) which consequently manifest with a destructive impact on motor and cognitive development [12,37]. As the disease progresses, increased levels of MCBs cause neuronal death and provoke a widespread neuroinflammatory response characterized by microglial and astrocyte activation [12,66]. The toxic GM2 accumulation and subsequent events can cause death as early as age 3 - 4 in the infantile TSD, highlighting the significance of developing an effective treatment to address this disease [36].

Although a variety of approaches to manage and treat GM2 gangliosidosis have been attempted, there is still no successful treatment for these disorders [32].

Conzelmann and Sandhoff in 1992 conducted an experiment on skin fibroblasts from patients with differing severities of GM2 gangliosidosis. They used radiolabelled GM2 ganglioside as a substrate to demonstrate a correlation between substrate clearance and the residual HexA enzyme activity [67]. This led to the definition of a threshold of 10-15% of normal HexA activity as the minimum level of residual enzyme activity that is required for a normal phenotype [67]. Conzelmann and Standoff's study provided a foundation to develop therapeutic strategies for GM2 gangliosidosis because it demonstrated the critical threshold that would need to be reached to allow normal substrate turnover. Therapeutic strategies include but are not limited to enzyme enhancing therapy, substrate reduction therapy, stem cell transplantation, gene therapy (GT) and enzyme replacement therapy (ERT) [12].

1.6.1 Enzyme enhancing therapy

Enzyme enhancing therapy takes advantage of small molecules that act as specific inhibitors at low concentrations or molecules that bind to proteins in a non-selective manner [55,68,69]. This interaction stabilizes and rescues the misfolded α subunit enzyme which otherwise will be degraded through the ERAD pathway [55,68,69].

The small molecules used in this strategy act as chaperones to stabilize the properly folded conformation which helps the enzyme to translocate from the ER to the Golgi apparatus for subsequent delivery to the lysosomes. There, the lower pH and high content of its substrate will favor the dissociation of the chaperone from the enzyme, allowing it to degrade its substrate [16,70]. Maegawa et al. in 2007 conducted a detailed examination of over a thousand FDA-approved

small molecules [16]. It was revealed that thioguanine (TGN) and pyrimethamine[6] (PYR) were demonstrated with inhibitory properties toward HexB [16]. However TGN was excluded from further studies due to its toxicity when applied to fibroblast cell lines in the required concentration [16]. PYR acts as a competitive inhibitor with maximum inhibition at neutral pH, which makes it an ideal pharmacological chaperone [16]. Further investigation of the effect of PYR on the late onset TSD fibroblast cell lines showed that it resulted in residual HexA activity approximately higher than 10 % of normal enzyme activity [16]. Although this therapeutic strategy results in the higher residual enzyme activity, it is limited to specific mutations that cause a misfolded enzyme subunit [68]. An additional complication of chaperone therapy is that determining the appropriate dosage of the inhibitor to rescue the residual enzyme activity is challenging [16,69]. One of the only chaperones used clinically for LSDs is Migalastat which is an FDA approved orally administered treatment for Fabry's Disease [71].

1.6.2 Substrate reduction therapy (SRT)

Substrate reduction therapy is another approach to prevent TSD progression that works by inhibiting the first step in the biosynthesis of glycolipids, resulting in a reduction in the accumulation rate of the GM2 ganglioside [72]. Miglustat[7], commercially available as Zavesca® is an iminosugar that acts as an inhibitor for glucosylceramide synthase, and it has been established that it has a broad biodistribution even to the hard-to-reach organs like brain and bone marrow [73,74]. Miglustat is a FDA approved treatment for treating some of the LSDs including, type 1 Gaucher disease (GD1) [72]. The efficacy of Miglustat as a SRT has been demonstrated in TSD

[6] PYR (2,4-diamino 5-(4-chlorophenyl)-6-ethylpyrimidine
[7] N-butyldeoxynojirimycin, NB-DNJN

and Sandhoff disease animal models. Although clinical administration of Miglustat did not improve the lifespan for the infantile form of TSD, it delayed some of neuropathological manifestation such as macrocephaly which otherwise would have developed due to substrate accumulation[75]. It also resulted in a considerable increase in levels of Miglustat in the CSF.

1.6.3 Stem cell transplantation

Stem cell transplantation is another approach to treat TSD by providing HexA deficient patients with healthy donor cells [14,67]. The stem cells are derived from different sources including bone marrow, peripheral blood or umbilical cord blood [76]. This approach has been promising in treating mucopolysaccharidosis (MPS) type I and II, and Gaucher disease type 1 and 2 [20]. Using hematopoietic stem cell transplant in the infantile form of TSD did not improve the life span nor alleviate the neurological symptoms [77]. Another study reported an increase in the lifespan of 2 patients with infantile TSD after an umbilical cord blood transplant from an unrelated healthy donor [78]. A different study on the juvenile form of TSD resulted in an increase in the HexA activity in leukocytes and plasma a month after transplantation. The enzyme activity in these patients gradually decreased and reached levels lower than normal in the following 3 months [79]. Also, the progressive neurodegeneration due to the accumulated substrate was not improved [79].

Although this approach has had some success in increasing the enzyme activity levels in the visceral organs, the presence of the blood brain barrier (BBB) hinders the enzyme delivery to the CNS [14]. Further, finding a donor with the best match for bone marrow transplant is difficult, and the recipient of the stem cell transplants are at the risk of developing graft-versus-host disease (GVHD) or graft failure [78]. Moreover, early intervention is critical, as the disease progress is rapid, especially in the infantile form of TSD [80].

1.6.4 Gene therapy (GT)

Gene therapy is a therapeutic strategy which takes advantage of viral vectors to deliver wild-type gene(s) to affected cells to compensate for loss of function mutations in the genome of the recipient [12,81]. Secretion of enzyme from the transduced cells can lead to cross correction in the enzyme deficient cells [82–84].

Different viral vectors have been developed to overcome some of the common challenges associated with the GT approach including, higher capacity to carry longer DNA sequences, vectors with improved ability to pass through the BBB, reduced immunogenicity, and improved target specificity [81]. Adenoviruses, retroviral and non-replicable herpes simplex virus are among the most common viral vectors used for this strategy [36,85]. Early attempts to use this approach were introduced by Akli and his colleagues in 1996 in which they used a nonreplicable adenoviral vector[8] (pAdRSV-Hexα) to transduce fibroblasts cells derived from a TSD patient with wildtype α-subunit cDNA. Post transduction results revealed an increase in the HexA activity and a 25-fold increase in the α-subunit secretion compared with the non-transfected TSD fibroblasts [86]. Later, Guidotti et al. demonstrated that intravenous co-injection of adenoviral vectors with α and β subunit cDNAs (pAdRSV-Hexα and pAdCMV-Hexβ[9]) in the HexA deficient mice resulted in HexA levels of activity greater than the defined threshold for the normal enzyme activity in the serum, liver, and other peripheral organs such as spleen, heart, kidney, and skeletal muscle. However, the co-administration of adenoviral vectors did not significantly improve the brain's enzyme activity indicating the inability of adenoviral vectors to

[8]Replication-deficient pAdRSV-Hexα

[9] Replication-deficeint pAdCMV-Hexβ

transduce the CNS effectively [87]. In another study conducted on HexA deficient mice by Martino et al. in 2005, a single dosage of a replication deficient herpes simplex vector encoding the α-subunit was used to unilaterally inoculate the brain internal capsule which resulted in the widespread diffusion of the vector from the injection site, most notably in the spinal cord and cerebellum [85]. A month after injection, the vector transduced neurons and astrocytes were mainly close to the injection site, with just a few transduced neurons away from the injection site. Widespread reduction in the GM2 levels was reported along with an increase in the HexA activity to about 60–70% of the activity in the healthy animals [85]. Several studies in the following years using different serotypes of adeno-associated viral vectors in the SD mice model co-administered the α- and β-subunit encoding genes through intracranial infusion. These resulted in an improvement in survival, extensive enzyme diffusion, retarded neuropathological progression and reduced GM2 storage throughout the CNS [88,89]. In another study conducted by Walia et al. a single viral inoculation with AAV9-HexB vector in neonatal SD mice model improved the survival. Despite the positive outcome, the study reported a formation of tumors in the lung and liver [90].

Tropak et al. in 2016, introduced a self-complementary adeno-associated viral vector serotype 9 (scAAV9) with a novel insert encoding an engineered HexA α-subunit known as the μ-subunit that had the capability to dimerize into a catalytically active homodimer known as HexM, which could productively turnover GM2 ganglioside in a GM2AP dependent manner. Using a single subunit allowed an effective transduction of cells instead of using co-transduction of two viral vectors. Also, intracranial injection of the designed vector resulted in the attenuation of the GM2 levels in the brain [91]. Intravenous injection of the same construct into HexA deficient mice resulted in the widespread distribution of the vector in the CNS and visceral organs such as

liver, lung and heart and a reduction in the accumulated GM2 substrate compared with the HexA knock out control animals [92]. Previous research evaluating the intracranial co-administration of α and β subunits using adeno associated viral vectors in the TSD sheep model showed widespread distribution of the viral vector throughout the brain and CNS and to a lesser extent in the spinal cord, resulting in an attenuated neuroinflammatory response, increased HexA activity, and reduced GM2 ganglioside storage. Despite the positive clinical outcome, this study did not result in increased survival of the animal model. This might be due to the excessive GM2 ganglioside storage in the cerebellum and spinal cord of treated animals [93]. In a recent clinical trial, investigators examined the effects of intrathecal co-administration of AAV gene therapy using α-subunit and β-subunit cDNAs (AAVrh8-α and AAVrh8-β [10]) on two infantile TSD patients. The results were promising because they maintained the HexA activity levels in the CSF and serum, improved myelination, and slowed the disease progression [32]. However, the risks associated with the thalamic injection, estimation of the viral vector dose required for each individual, immune reactions and long-term effects of the intervention are to be addressed [32].

1.6.5 Enzyme replacement therapy (ERT)

It has been established that a small portion of synthesized enzyme with M6P-recognition tags on their N-linked oligosaccharides is secreted into the extracellular space from the trans-Golgi network (TGN). These lysosomal enzymes subsequently can be detected and internalized in an M6PR-mediated manner and targeted to the lysosomes where it is needed. This procedure is known as the cross-correction mechanism (**Fig. 1-3**) [31,55,82–84].

[10] Adeno-associated virus rhesus isolate 8

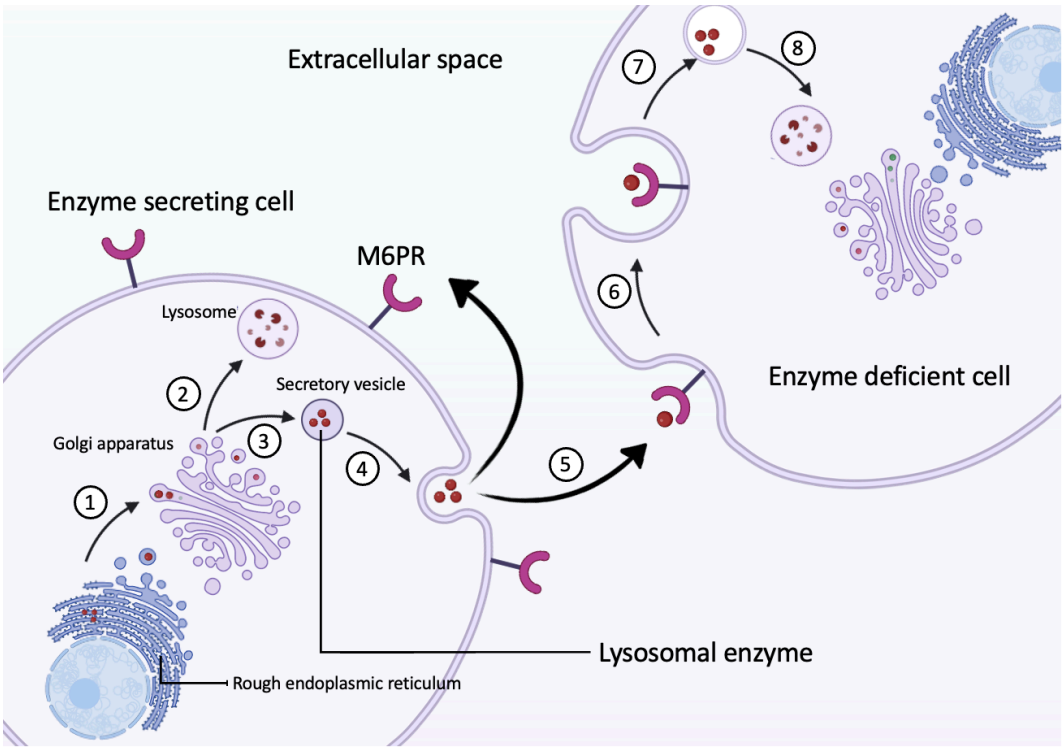

Figure 1-3. Mechanism of lysosomal cross-correction.

After the production of lysosomal proteins in the rough endoplasmic reticulum (indicated as red circles), they will be transferred to the trans-Golgi network (step 1) wherein they acquire the terminal mannose 6-phosphate tags (M6P). The majority of the M6P-tagged enzyme goes to lysosomes (step 2). After secretion into the extracellular space (steps 3, 4 and 5), these tags will target the enzyme to lysosomes in an M6PR-mediated way (steps 6, 7 and 8). Regenerated from Sands et al. 2006 (Adopted under the Creative Commons Attribution-Non Commercial-No Derivatives License (CC BY NC ND), http://creativecommons.org/licenses/by-nc-nd/4.0/) [6]. Created with BioRender.com.

ERT refers to providing catalytically active enzyme to enzyme deficient cells relying on the cross-correction mechanism to recapture the exogenous enzyme [6,20,82]. Continuous absorption of active HexA through the cross-correction mechanism could potentially increase the residual enzyme activity to nearly 10% of normal enzyme activity in order to prevent the pathological build-up of GM2 ganglioside and treat TSD [33].

A considerable body of literature has been published on ERT as an efficient treatment strategy for some LSDs. Currently, IV-ERT is an FDA approved treatment for Gaucher, Fabry, Pompe, MPS I, II, and VI [20,94,95].

In 1973, for the first time, Johnson et al. conducted ERT in a SD patient by intravenous administration of purified HexA which resulted in the detection of enzyme in the liver [96]. However, lack of enzyme activity in the CSF or brain post IV-ERT revealed a serious limitation of the IV-ERT approach for CNS-based LSDs due to the inability of enzyme to cross the BBB [20,97]. The results presented in this study highlighted the importance of an administration method to overcome the BBB and improve the efficacy of ERT to alleviate the neuropathological symptoms caused by substrate storage in the CNS [12,98].

Over the past decades, researchers attempted to advance the ERT approach for TSD by generating the HexA enzyme in large quantities in a cost-effective way, as it is necessary to have a sustainable and reliable source of active enzyme for a long-term infusion [99]. To address this issue, Akeboshi and co-workers in 2007 used a mutant yeast to produce a recombinant HexA with the highest yield of 13 mg per each liter of medium [99]. However, further assessment revealed that the recombinant protein was truncated in the C-terminus of the β-subunit which is required for proper dimerization [99]. This truncation of the C-terminus was due to a yeast-specific proteolytic activity which subsequently resulted in the shift in the ratios of isozyme dimers, with

the least amount for HexA and HexB isozymes [99]. Since the BBB adversely affected the efficacy of ERT because the enzyme could not pass through it, intracerebroventricular (ICV) administration of therapeutics to the CNS resulted in a promising outcome to the extent that it is now an accepted clinical practice to bypass the BBB in some LSDs such as neuronal ceroid lipofuscinoses type II (CLN2) [96,100].

For further investigation of ICV-ERT to overcome the BBB, Tsuji et al. in 2011 carried out an experiment using a hyper-phosphorylated form of a recombinant HexA enzyme in a SD mouse model [97]. The results of this study revealed that intraventricular enzyme delivery enhanced the enzyme distribution and improved the enzyme activity in different regions of the brain compared with the control animals, reduced the neuronal GM2 content and increased the survival rate in SD mice model [97]. The study did not report any significant immunoreactivity post injection.

In another study conducted by Matsuoka (2011), ICV administration of an engineered HexB enzyme produced in a mammalian cell line was investigated in the SD mice model and TSD derived fibroblast cells [101]. The designed HexB containing critical α-subunit amino acids was found to be taken up through the M6P receptors, interacted with the GM2AP and reduced the GM2 content in the TSD fibroblast cells [101]. Also, ICV-ERT of the modified HexB in the SD mouse model showed an increase in the enzyme activity and a reduction in the parenchymal GM2 content [101]. Recently, Vu et al. evaluated ERT of a codon optimized recombinant HexA produced in yeast on neuronal stem cells derived from a TSD patient's induced pluripotent stem cells (iPSCs) ; a reduction in the lysosomal GM2 storage was observed [102].

Although ERT is a potential therapeutic strategy to compensate for HexA deficiency, several considerations need to be made for the HexA-based ERT approach to work [12,91]. Firstly,

to provide purified and active HexA (αβ) enzyme for ERT, both α and β subunits have to be produced and production of HexA(αβ) needs to be optimized [91,99]. On the other hand, presence of endogenous isozymes in the cell line can impact the isolation steps of recombinant enzyme [91,97,101]. Secondly, HexA has to be produced in large quantities at a low-cost for subsequent long-term ERT treatment, while preserving the native post translational modifications due to the selected expression system [12,99].

1.7 HexM and PhosHexM enzyme

The Mark lab in collaboration with the Mahuran Lab (Toronto SickKids Hospital), developed called HexM that is an engineered version of human hexosaminidase A enzyme according to the X-ray analysis of HexA (αβ) and HexB (ββ) crystal structures [91,103]. The novel design helped to address the previous challenges regarding the necessity of co-expressing both α and β subunits [97,101]. Also, the endogenous hexosaminidase enzymes from the host cell line was eliminated, so there is no interference from the HexM cell line [97,101].

HexA subunits share a high amino acid identity (~ 60%) which helped for designing HexM as a homodimer of two identical μ-subunits [104]. Each subunit contains an α-subunit active site as well as the essential aspects of the α and β-subunits involved in the GM2 turnover in a GM2AP dependent manner, and β-subunit residues which are involved in stabilizing the dimer (**Fig. 1-4**) [63,91,103,104].

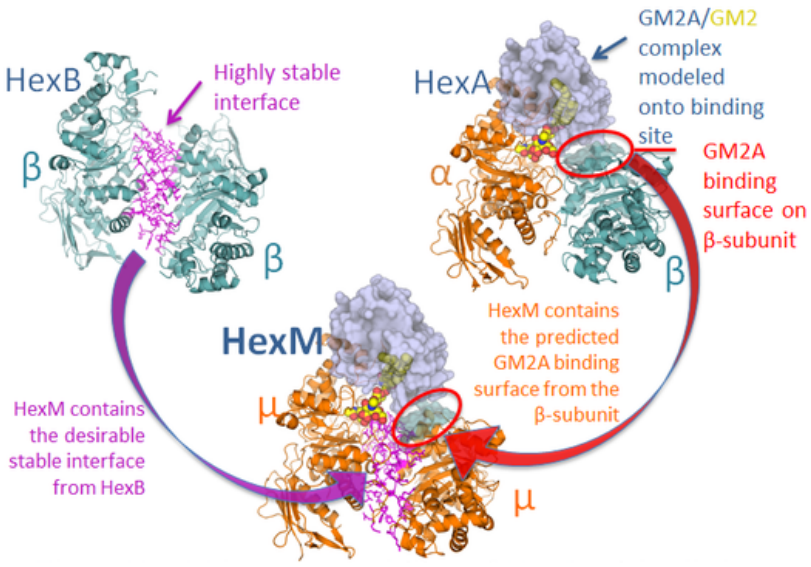

Figure 1-4. Design of HexM.

A single μ-subunit contains critical residues of the α-subunit active site, the β-subunit stabilizing interface, and unique, essential areas of each subunit for GM2AP interaction. Thus, HexM is a homodimer with higher efficiency for degrading GM2 ganglioside due to two α-subunit derived active sites. Molecular structure is obtained from Tropak et al. 2016 (Reproduced with permission of ASGCT under Creative Commons Attribution–Non Commercial–NoDerivs (CC BY-NC-ND 4.0)) [91].

Remarkably, the unique design of *HEXM* makes it more feasible to transfect cells with only one vector to overexpress the homodimeric functional enzyme required for the future gene therapy approach for treating TSD [63,91]. On the one hand, HexM is a homodimeric enzyme which resolves the need for separating it from its isozymes otherwise [91]. Further, the mammalian cell line used for HexM overexpression under a tetracycline inducible promotor is deficient for both endogenous *HEXA* and *HEXB* genes (HEK-ABKO-HexM) and the enzyme is tagged with His-6 or HPTC peptide resulting in easier downstream purification of enzyme [91]. Experiments conducted on purified HexM conclusively showed that it has higher heat stability than HexA,

and its V_{max} for MUGS is almost twice that of HexA, confirming the presence of two active sites in HexM. It was also shown that HexM can degrade NBD-GM2[11] in a GM2AP dependent manner in cultured cells and in-vitro in the presence of recombinant human GM2AP (rGM2AP) [91]. Also, when provided to TSD fibroblast cells, HexM was able to enter through an M6PR-dependent manner paving the way for ERT [91].

Investigation of glycosylation patterns of HexA and HexB revealed a total of seven glycosylation sites on both α and β subunits (αAsn115, αAsn157, αAsn295, βAsn84, βAsn142, βAsn190, and βAsn327) [61,105–107]. However, only two of the glycans on the α-subunit (αAsn115, αAsn295) and one on the β-subunit (βAsn84) undergo further phosphorylation to obtain M6P-tags on the terminal mannose of these glycan chains [103]. Mass spectroscopy analysis of HexA and HexM showed similarly low levels of phosphorylation on one glycan chain[63]. It is now understood that these M6P-tags on the enzyme play an important role in the cellular uptake through M6PR receptors [99,108], so increasing the phosphorylation levels on the N-linked glycans can potentially improve the cellular uptake and ERT efficacy [63,99]. However previous attempts in producing hyperphosphorylated recombinant HexA enzyme in the yeast *Ogataea minuta*, resulted in changes in the length and mannose content of N-glycans, and low phosphorylation levels on N-glycans [99]. In a study conducted by Benzie et al. 2022, simultaneous expression of HexM with S1S3 PTase[12], a truncated active form of GlcNac-1-PT [63,109] improved the phosphorylation levels of HexM to nearly 20% higher than HexA [63]. The hyperphosphorylated

[11] NBD-GM2 is a fluorescent artificial analog for GM2 ganglioside in which nitro-2,1,3-benzoxadiazol (NBD)-4-yl bonds to sn2 acyl chain of lyso-GM2 ganglioside.

[12] Modified GlcNAc-1-phosphotransferase

form of HexM (PhosHexM) showed a significant enhancement in enzyme uptake through a M6P-receptor mediated manner in TSD cells [63].

Taken together, the findings from previous studies on HexM provide support for the hypothesis that distinctive features of HexM including its high expression in a mammalian cell expression system, simple purification in large quantities (in gram scale) through the C-terminal His-tag or HPC4-tag, presence of two catalytic sites for degrading substrate and higher heat stability, made HexM as an ideal candidate for the ERT approach [63]. Further, by expressing HexM in combination with a promiscuous phosphotransferase into the media, its uptake should be increased.

1.8 TSD animal model

It is essential to work with a valid animal model of TSD disease that has a comparable clinical phenotype to evaluate ERT as a potential therapeutic strategy [21,68,110]. GM2 gangliosidosis has been described in different animals such as cats and dogs. However, Jacob sheep and most recently a pig model are the only recognized TSD models in research with clinical signs comparable to TSD in humans [21,37,111,112]. Although Jacob sheep can be used as a juvenile or late onset form of TSD and the described pig model can be used as an infantile form of TSD [112,113], these animal models are not readily used in practice. The large size of these animals, high cost of maintaining them for long-term interventions, long gestation time, smaller litter size, and fewer available reagents for the species are some of the factors that make these models challenging to use [21,112]. To overcome the challenges in using bigger animal models of TSD, researchers tried to develop a translatable mouse model of TSD.

The first attempts to generate a TSD mouse model in 1995 by Taniike et al. and later by Phaneuf et al. in 1996 were unsuccessful [114,115]. Taniike established that disruption of the α-subunit of the HexA enzyme (*Hexa* knockout) did not result in the expected severe neurological deterioration, although it did result in the progressive formation of membranous cytoplasmic bodies (MCBs) observed in the neurons of human TSD patients. However pathological accumulation of GM2 ganglioside was only localized in certain areas of the CNS which were detected in the mouse model as early as two months old [37,115]. Similarly, Phaneuf et al. in 1996 found that despite a drastic reduction in the MUGS activity in the brain and liver of the $Hexa^{-/-}$ knockout mouse, the model didn't exhibit the expected widespread GM2 ganglioside accumulation in CNS, nor the neurological and behavioral changes that characterize TSD patients [114]. These studies suggested the presence of a murine-specific alternative pathway to degrade GM2 to GA2 ganglioside [114,115]. Subsequent degradation of GA2 through action of HexB enzyme results in the formation of lactosylceramide and prevented the pathological storage of GM2 ganglioside that would result in early neurological symptoms [116,117]. Twenty-three years later, Seyrantepe et al. in 2018, indicated that a membrane bound sialidase, called neuraminidases 3 (Neu3) facilitated the removal of terminal sialic acid residues from the glycans of glycolipids and was responsible for the bypass present in the previous $Hexa^{-/-}$ knock-out TSD mouse models (**Fig. 1-5**) [10].

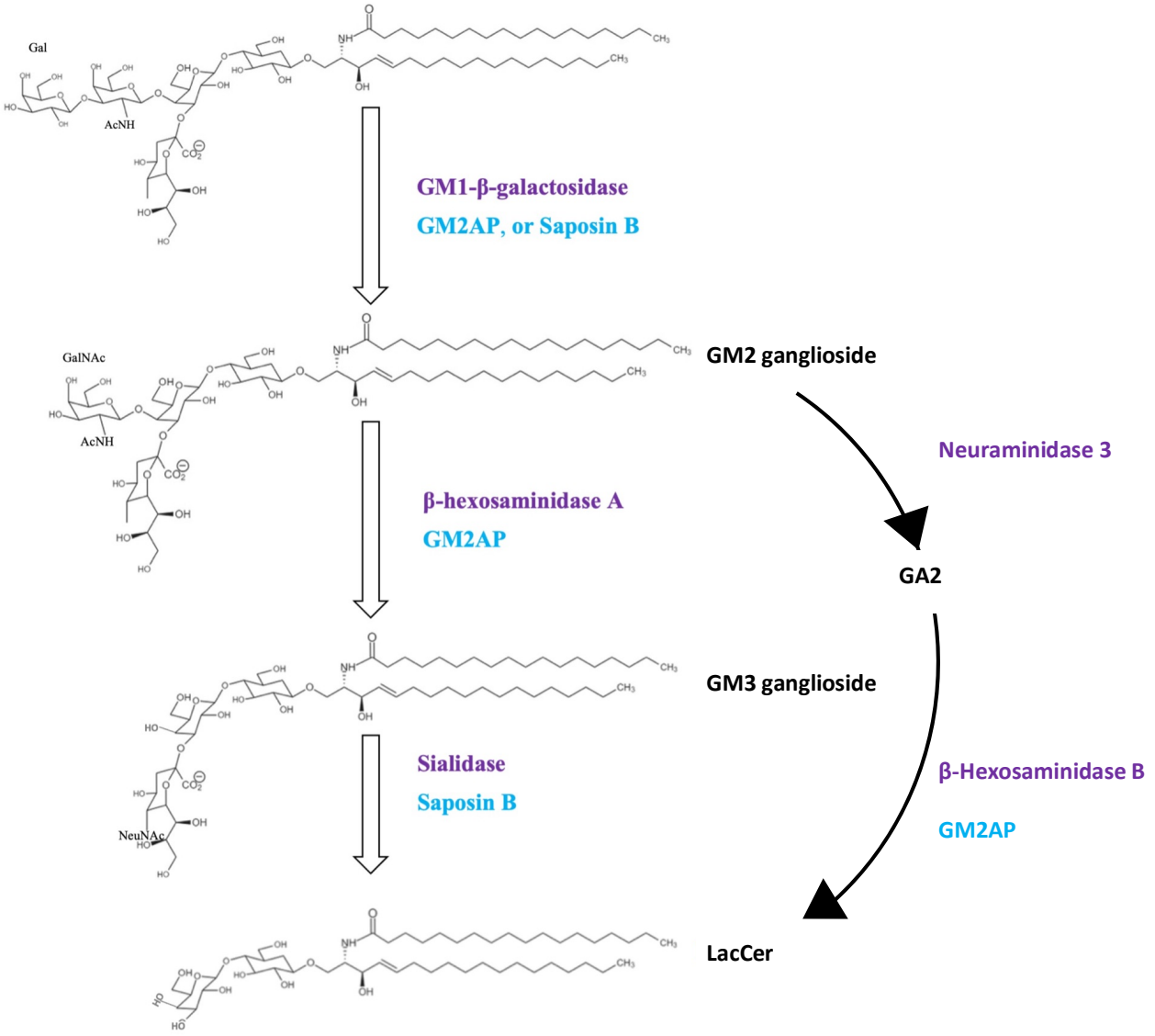

Figure 1-5. The murine-specific metabolic pathway in *Hexa*$^{-/-}$ knock out mouse.

The figure shows the metabolic pathway that degrades GM2 to GA2 ganglioside in *Hexa*$^{-/-}$knock out mouse and prevents severe GM2 ganglioside accumulation. Neuraminidase 3 is a murine specific sialidase which removes a terminal sialic acid from the glycosylated lipids and by doing so, converts the GM2 ganglioside to GA2 ganglioside which further can be degraded to lactosylceramide by the actions of HexB enzyme. Enzymes and coenzymes are indicated in purple and cyan respectively. Figure is recreated from Sandhoff et al. 2013 and Seyrantepe et al. 2018 (License Number: 5450990292971) [10,19,28].

Histological and behavioural characteristics of a mouse model with *Hexa*$^{-/-}$/*Neu3*$^{-/-}$ double-knock out were shown to be compatible with infantile form of TSD in humans with a progressive neuropathological accumulation of GM2 ganglioside [10]. Also, similarly our lab has recently recreated mouse models of the early and late-onset form of TSD using CRISPR/Cas9 methods to generate mice exhibiting the clinical phenotype of the disease (Emily Barker et al., unpublished). This model provides us with a reliable infantile TSD mouse model to further investigate the therapeutic potential of HexM or PhosHexM through ICV-ERT since previous research failed to assess the ERT approach in-vivo in a proper TSD animal model [65,99,101].

1.9 Thesis objectives

No approved treatment for TSD currently exists [118]. Distinctive characteristics of the HexM enzyme design such as stability, high expression, ease of purification in large quantities (in gram scale) using a mammalian cell expression system, and its ability to be hyperphosphated to improve cross-correction through M6PR-dependent manner in TSD fibroblasts potentially paves the way to develop an ERT-based approach for TSD [63,91]. However due to the lack of a proper TSD animal model to evaluate the ICV-ERT in previous research, in-vivo assessment of ICV-ERT impact was not possible for TSD [63,91]. Therefore, the intention of this study is to investigate the ICV-ERT of HexM and M6P-PhosHexM in a gene-edited mouse model of the infantile form of TSD. To accomplish this goal, three main objectives were established:

1- To produce and characterize HexM to be used for enzyme replacement therapy.
2- To examine M6P-HexM and M6P-PhosHexM's cellular uptake and evaluate the biodistribution of M6P-HexM and M6P-PhosHexM's in a TSD-like mouse model.

3- To determine if M6P-HexM or M6P-PhosHeXM has the capacity to degrade accumulating GM2 ganglioside in a TSD-like mouse model.

2 Materials and Methods

2.1 HexM enzyme production

To express and purify HexM, I used a cell line stably transfected with a HexM-expression construct (HEK293TABKO-HexM-His_6) which was previously generated by the laboratory of Dr. Don Mahuran [91]. HexM was secreted into the media under a doxycycline-induced promoter, in the absence of endogenous hexosaminidase α and β subunits from the original cell line, since both *HEXA* and *HEXB* genes were disrupted using the CRISPR-Cas9 genome editing system [91].

2.1.1 Cell culture

All cell culture manipulations were performed in a laminar flow hood under aseptic conditions and incubated in a humidified atmosphere containing 5% CO_2 at 37ºC following a previously described protocol [91]. A frozen cryovial of HEK293 expressing HexM was thawed quickly and transferred to pre-heated growth media (DMEM, 10% (v/v) FBS, 1 % (v/v) Penicillin-Streptomycin, 1 µg/ml doxycycline) followed by centrifugation, and the supernatant was discarded. The cell pellet was resuspended in the growth medium and transferred to a T75 flask.

2.1.2 HexM expression in the FiberCell system

Successful development of ERT for my study required the production of active and pure enzyme in high quantity. In the first aim of my project, this critical issue was addressed using a FiberCell system which was efficiently modified for large scale recombinant protein expression and used to generate sufficient pure enzyme for ERT (FiberCell Systems Inc. New Market, Md) [119].

Use of the FiberCell system addressed the challenges arising from traditional cell culture T-Flasks, specifically large-scale enzyme production, protein contamination in later purification steps due to the presence of FBS in the media, and the higher risk of contamination in long-term passages.

To produce the amount of HexM required for enzyme replacement therapy (ERT), I used a FiberCell system (catalogue number C2011, FiberCell Systems Inc. New Market, Md) according to a method established by Graeme Benzie et al. [63]. The FiberCell system allows high throughput recombinant protein production and the manufacturer's instructions were followed to inoculate the FiberCell cartridge (catalogue number C2011) with the HexM-expressing cell line. A serum-free growth media supplemented with 10% chemically defined medium (supplied from the FiberCell system manufacturer) for high density growth (CDM-HD) was used to grow cells. FiberCell maintenance, including exchanging to fresh media and harvesting the media containing the expressed protein was performed as described by the manufacturer (catalogue number C2011, FiberCell Systems Inc. New Market, Md). Media was collected, debris were removed by centrifugation and the supernatant was stored at -20 °C for further purification.

2.1.3 HexM purification

HexM purification from the collected media was performed following a previously described protocol [63,119,120]. Immobilized metal affinity chromatography (IMAC) (HisPurTM Ni-NTA resin, Qiagen) was used with Bis-Tris 10 mM, NaCl 100 mM pH 6 as wash buffer and wash buffer supplemented with 250 mM imidazole was used as elution buffer. Nickel columns used for IMAC contained nitrilotriacetic acid with a high affinity for His-tagged proteins (Bio-Rad Laboratories, Inc). Subsequently, HexM was purified from the eluate by size exclusion

chromatography (SEC) using HiLoad16/600 Superdex 200 (GE Life Sciences) and the wash buffer above. Collected HexM was stored at -20 °C until further use.

To examine the purified HexM after SEC, SDS-PAGE was conducted followed by Coomassie brilliant blue staining. A replica gel was transferred to a nitrocellulose membrane for western blot analysis using anti-HexA rabbit polyclonal antibody (Abcam, Cat #: ab91624, 1:1000 dilution) followed by incubation of the membrane in goat-anti-rabbit IgG (H+L)-HRP conjugated antibody (Bio-Rad, Cat #: 1706515, 1:3000 dilution) as a secondary antibody [119].

2.1.4 Assessment of HexM activity under different conditions

The stability of purified HexM was evaluated, with slight modifications from a previously described protocol [63,121,122].

Aliquots of the enzyme were prepared in artificial CSF (©2022 Durect Corporation, California [123]) or artificial CSF supplemented with 0.1% BSA and incubated at 37°C over seven days. Samples were collected daily and stored at -20°C for future enzyme assay. Once all the samples were collected, the MUGS assay was performed by preparing the reaction containing 100 pM HexM from the mentioned conditions followed by the addition of 1mM MUGS to start the reaction (final volume of 40 µl). After 30 minutes, the reaction was stopped by addition of Glycine-Carbonate (GC) buffer pH 10.2.

The fluorescence intensity was read with a SpectraMax iD5 plate reader (excitation:365 nm and emission:450 nm) and 4-MU levels were determined from a standard curve generated from known concentrations of 4-methylumbelliferone (4-MU). The results of enzyme activity in various conditions were plotted using GraphPad Prism 8 software.

We also used purified HexM to evaluate the impact of different conditions on the enzyme activity following a modified version of the previously described protocol [121,122].

Dilutions of HexM (100 nM) were made in citrate-phosphate buffer (CP buffer) (41.2 mM Na_2HPO_4, 29.4 mM citric acid; pH 4.2), CP buffer containing 0.5% BSA, or CP buffer containing 0.25 % (v/v) TritonX-100 in regular and low protein binding tubes.

For each buffer condition, a control reaction at t=0 was generated by adding Glycine-Carbonate (GC) buffer pH 10.2 to stop the reaction. The remaining aliquots were incubated for 60 minutes at 37 ℃ and then assayed with 1mM 4-MUGS. The reaction was stopped by addition of GC buffer. The fluorescence intensity was measured using known concentrations of 4-methylumbelliferone (4-MU) as a standard curve and plotted as mentioned above.

2.1.5 Cellular uptake with M6P-HexM and M6P-PhosHexM

To assess the cellular uptake of M6P-HexM and M6P-PhosHexM (Phosphorylated form of HexM) provided by our collaborators, M6P Therapeutics (M6PT), we used a previously described protocol with slight modifications [63].

A TSD fibroblast cell line known as TSD 1881, that was previously immortalized in our lab, was cultured in DMEM containing 10% (v/v) FBS and 1 % (v/v) each of Penicillin-Streptomycin, glutamax-100, and non-essential amino acids. Cells were seeded in 6 well plates (0.5×10^6 cells/well), and M6P-HexM (15 µg), M6P-PhosHexM (15 µg) or 10µl of 1x PBS was added to each well in duplicate and incubated for 24 hours. The media was removed, the wells were washed with 1x PBS, and the cells were harvested. After centrifugation, the cell pellet was lysed on ice for 15 minutes in PBS pH 6.6 containing 0.5% Triton-X 100 and 0.2% protease inhibitor [63]. The protein concentration in the supernatant was determined using a kit based on the

Bradford assay (BioRad, Protein Assay Dye Reagent Concentrate, #5000006)[63]. Known concentrations of gamma-globulin were assayed simultaneously to generate a standard curve. The Hex activity associated with the cell was determined using 30 µg of protein and MUGS as a substrate following the protocol above over 30 minutes. All samples were assayed in triplicate and the results were analyzed using Graphpad Prism 8 software.

2.2 Experimental Animals

A TSD-like model in mice was created by combining mutant alleles for the *Hexa* and *Neu3* genes to create *Hexa*$^{-/-}$*Neu3*$^{-/-}$ mice as described previously by Syrantepe team [10,110]. These mutant alleles were generated by the University of Manitoba Transgenic Service using CRISPR/Cas9 and have been characterized (Barker et al., manuscript in preparation). All studies were conducted under animal protocol 19-027 that was approved by the University of Manitoba Animal Care Committee. Animals were given free access to water and dried food with a light/dark cycle of 12 hours in a facility that is in full compliance with the Canadian Council on Animal Care.

2.3 Genotyping

DNA was isolated from ear punches as described previously [124–126].

Genotypes of animals were determined through standard PCR amplification of the DNA as previously described with slight optimizations (94°C for 3 min, followed by 35 cycles of 94°C, 55°C, and 72°C 30 s each) by using primers for both *Hexa* and *Neu3* genes followed by a previously described heteroduplexing method [126].

Briefly, the resulting PCR products were analyzed on an 8% polyacrylamide gel before and after annealing using PCR product from the same locus amplified from wild type mouse DNA. The presence of the mutant allele was indicated by the formation of heteroduplexes without mixing with wild type DNA when in the heterozygous state or after mixing with wild type DNA in the homozygous state. Oligonucleotide primer sequences are provided in Table 1.

Table 1-List of the oligonucleotides used for genotyping the experimental animals for *Hexa* and *Neu3* genes.

Primers	ID	Direction	Sequence
HexA	WPG1200	F	5 ’-CAACCCTGTCACTCACATCTAC-3’
	WPG1201	R	5 ’-CAAGAGCCAAGGCCAAGATA-3’
Neu3	WPG1251	F	5 ’-CTACTGATGGAGGCCACATTAC-3’
	WPG1252	R	5 ’-CTCCTCGGTCAAGTCTTTCAC-3’

2.4 M6P-HexM and M6P-PhosHexM biodistribution assessment[13]

2.4.1 Selection of animals

To assess the biodistribution of purified M6P-HexM and M6P-PhosHexM, animals that were deficient in β-hexosaminidase A activity (i.e., *Hexa*$^{-/-}$) were selected. These animals were healthy and between the ages of 10.2 and 47 weeks. For comparisons of M6P-HexM and M6P-PhosHexM, animal pairs were matched by age and sex.

[13] In all the animal interventions, both HexM and PhosHexM enzymes were provided by our collaborators; M6P therapeutics. They are referred to as M6P-HexM and M6P-PhosHexM.

2.4.2 Tail vein injection of M6P-HexM/M6P-PhosHexM in a mice model of TSD

A total number of 19 animals (7 M6P-HexM, 7 M6P-PhosHexM, and 5 saline) were used for tail vein injection.

Under surgical anesthesia, a catheter was placed in the lateral tail vein of the mice. Placement of the catheter was confirmed by the ease of saline injection and the presence of blood in the needle. Another syringe filled with 50 µl of saline or 0.5 mg/kg M6P-HexM/or M6P-PhosHexM was attached to the catheter and delivered. Once the injection was completed, blood samples were collected through the saphenous vein at 5, 20, and 60 minutes post-injection into capillary microtubes (Microvette). Serum was separated from the blood samples following the manufacturer's instructions.

120 minutes after the injection, the animal was euthanized by isoflurane overdose, and blood was collected by cardiac puncture. Serum was obtained by centrifugation of the blood sample at 1500 x g for 10 minutes.

Brain, liver, and other tissues were collected, and half of the brain and pieces of other tissues were instantly frozen on dry ice and stored at -80°C for further enzyme assay. The rest of the harvested tissues were fixed in 10% neutral-buffered formalin overnight, followed by tissue processing and embedding in paraffin wax.

2.4.3 Serum β-hexosaminidase activity assay

β-hexosaminidase A activity was determined following a previously established procedure [16,122]. Briefly, dilutions of serum in saline (1:50), were assayed in CP buffer (pH4.2) using 1mM 4-MUGS (4-Methylumbelliferyl-7-6-sulfo-2-acetamido-2-deoxy-β-D-

glucopyranoside) to start the reaction as described in the section 2.2.2 (in the serum enzyme activity assessment, BSA was excluded from the assay).

All assays were performed in triplicate and incubated at 37°C for 30 minutes. The reaction was stopped by the addition of 960 µl of Glycine-Carbonate Buffer pH 10.2. The samples were read with excitation of 365 nm and emission of 450 nm wavelength at room temperature and subsequently interpreted based on a standard curve consisting of known concentrations of 4-methylumbelliferone (4-MU).

2.4.4 Tissue β-hexosaminidase activity assay

Lysates from the collected brain and liver tissues were prepared following a modified version of the previously described protocol [127,128]. Half of the brain (~460 mg) or approximately 100 mg of liver was sonicated in 1000 µl of 1X PBS pH 6.6 supplemented with a protease inhibitor cocktail (2-3 times, 5 seconds each, with an interval of 30 seconds) in an ice bath. Cell debris were removed. Half of the collected supernatants were frozen instantly, and the other half was used to determine total protein concentrations by the Bradford method (described in section 2.1.5). The enzyme activity was determined using 20 µg protein from the brain or liver lysate following the endpoint assay described in section 2.2.2.

2.5 Short-term continuous ERT in an infantile TSD-like mouse model

Continuous enzyme delivery to the ventricular system of mice brains was conducted over seven days using intracerebroventricular (ICV) cannulation of Alzet osmotic pumps.

2.5.1 Selection of experimental animals

Animals were selected that were age (10-12 weeks) and sex-matched TSD mice (*Hexa*$^{-/-}$*/Neu3*$^{-/-}$ double knock-out). Additionally, age and sex-matched healthy mice (heterozygous for *Hexa* [*Hexa*$^{-/+}$] and knock-out for *Neu3* [*Neu3*$^{-/-}$]) were selected as controls.

2.5.2 Pump preparation

Alzet pumps (lot number 10395-18, ALZET Osmotic Pumps, Durect Corporation, California) were loaded with 50 µg with the total volume of 100 µl of M6P-HexM, M6P-PhosHexM or 100 µl of aCSF (artificial cerebrospinal fluid) in a laminar flow hood. Other parts of the pump, including the cannula and flow modulator, were assembled as described by the manufacturer's instructions (ALZET Osmotic Pumps, Durect Corporation, California).

The pumps were incubated in sterile saline at 37°C overnight to provide pumps with the initial osmotic pressure required for instant enzyme/or CSF delivery after implantation. The capacity of the pumps used for this study was 100 µl, with a predetermined flow rate of 0.48µl/min (ALZET Osmotic Pumps, Durect Corporation, California).

2.5.3 Intracerebroventricular cannulation and pump implantation

Stereotaxic surgery was performed for intracerebroventricular (ICV) cannulation and subcutaneous implantation of pumps following a previously described protocol [129].

Under aseptic conditions, animals were surgically anesthetized, and the head was properly positioned in the stereotaxic apparatus. Prior the operation, animals received 2mg/kg of meloxicam. After cleaning the skin with chlorhexidine and 70% alcohol, a blade was used to make a sagittal incision on the skin aligned with the interfrontal and sagittal suture on the skull to

make an opening between the eyes and base of the neck. The drill was used to prepare a hole for cannula insertion into the right lateral ventricle using coordinates with reference to bregma (AP -0.5, ML -1.1, DV -3).

While animals were anesthetized, the cannula was secured to the skull with cyanoacrylate glue **"**i.e., Crazy glue", and the pump was implanted in a subcutaneous pocket made under the skin on the back. The incision site was closed by suture, and after recovery, animals were housed separately.

Post-surgery, animals were provided wet food on the floor of the cage and a long sipper for water access. Animals received 2mg/kg of meloxicam a day after surgery. Mice were monitored daily for seven days after the surgery for signs of distress or illness, shaking, isolating behaviour, gait abnormalities, or 15% loss from initial weight were considered a humane endpoint resulting in euthanasia.

2.5.4 Tissue collection

Seven days after the surgery, animals were euthanized by isoflurane overdose and the brain, liver, spleen, lung, and heart were collected. The half of the brain containing the cannula insertion site, and pieces of other tissues were fixed, processed, and embedded in paraffin wax as described in section 2.4.2. The brain's left hemisphere and pieces of other organs were frozen on dry ice and stored at -80℃ for future assays.

2.5.5 Immunohistochemistry (IHC)

Immunohistochemical evaluation of GM2 ganglioside was performed with slight modifications of the previously described protocol [130]. All the procedures were performed at room temperature unless otherwise mentioned.

Half-brains embedded in paraffin were sectioned at 5 μm thickness in the sagittal plane. Sections were deparaffinized, rehydrated, and subjected to 95℃ citrate buffer for antigen retrieval. The internal peroxidase activity was blocked with hydrogen peroxide followed by incubation in the blocking solution to reduce non-specific staining. Endogenous biotin was blocked using the Avidin/Biotin Blocking Kit and following the manufacturer's instructions ([MJS]BioLynx Inc., VECTSP2001). Subsequently, sections were incubated with primary antibody (mouse monoclonal Anti-GM2 IgM, TCI, MK1-16, ,1/1000) overnight at 4 °C followed by biotinylated secondary antibody (goat anti-mouse IgM, Jackson ImmunoResearch Lab, 115-065-020) at 1/500. ABC Complex (Vector Labs, PK4000) was applied on sections as described by the manufacturer, followed by incubation with DAB substrate (ImmPACT® DAB EqV Substrate Kit, Peroxidase (HRP)). Sections were then submerged in Methyl Green as a counterstain before dehydration. Sections were covered with mounting medium and a coverslip was placed on the slide. The slides were viewed using a brightfield microscope.

2.6 Short-term bolus ERT in infantile TSD –like mouse model

2.6.1 Experimental animals

For short-term bolus ERT, animals were selected from 12-15 weeks old TSD mice (*Hexa*$^{-/-}$*/Neu3*$^{-/-}$ double knock-out). Age and sex-matched healthy animals (heterozygous for *Hexa* [*Hexa*$^{-/+}$] and knock-out for *Neu3* [*Neu3*$^{-/-}$]) were used as controls. Animal housing conditions were maintained as described in the section 2.2.

2.6.2 Making ICV cannulas and verification

Cannulas were made based on a modified version of a previously described method [131]. Guide cannulas were made with 26-gauge needles, and dummy cannulas and injectors were made with 33-gauge needles. Fast green and methylene blue were used to visualize the location of the cannula insertion. After the dye injection, animals were euthanized as previously described in section 2.5.4 (See supplementary **Fig. 7-3**).

2.6.3 Intracerebroventricular cannulation and injection

Stereotaxic surgery was performed to implant cannulas for short-term bolus ICV-ERT following a similar procedure as previously described in section 2.5.3.

Under aseptic conditions, animals were surgically anesthetized, and the head was properly positioned in the stereotaxic apparatus. After making the incision, bregma was identified and considered as an origin to obtain the coordination for the right lateral ventricle accordingly (AP -0.5, ML -1.1, DV -2.5).

To secure the cannula in place for multiple injections the cannula was attached to the skull with glue and fortified by implanting a metal screw and applying dental cement around it. When the cannulation was accomplished, TSD–like mice (*Hexa*$^{-/-}$*/Neu3*$^{-/-}$) received 5µl of M6P-HexM or M6P-PhosHexM (6.6 µg) or the same volume of saline as control (TSD control with *Hexa*$^{-/-}$*/Neu3*$^{-/-}$ genotype or healthy control with *Hexa*$^{-/+}$*/Neu3*$^{-/-}$ genotype). The delivery rate was adjusted to 1µl/min, and to prevent instant backflow the injector was kept in place for an extra minute after the injection was completed. The cannula was covered by gently placing a dummy in the cannula and the recovered animals were housed individually.

2.6.3.1 Post-operative procedure

Animals were provided with wet food on the floor, a long sipper, and diet gel after surgery. Animals were monitored for signs of illness or distress. A humane endpoint was used as described in section 2.5.3.

2.6.3.2 Weekly ICV injection

A week after the surgery, animals received a second dosage of M6P-HexM, M6P-PhosHexM, or saline as described earlier.

Animals were anesthetized to reduce their mobility. The dummy cannula was then removed and kept in the sterile area followed by gently placing the injector in the fixed cannula. Once the injection was completed, the dummy was gently re-inserted into the cannula. Animals were returned to their home cage after recovery.

2.6.3.3 Tissue collection

Ten to fourteen days after the surgery, animals were euthanized by isoflurane overdose, followed by intracardiac perfusion with 1 x PBS as previously described [127,130]. The brain was carefully removed and half of the brain containing the cannula was instantly frozen on crushed dry ice and stored at -80°C for further analysis.

Also, samples of other tissues including the liver, spleen, lung, and heart were immediately frozen on dry ice and stored at -80°C. The other half-brain and liver were fixed, processed, and embedded in paraffin wax as described in section 2.4.2.

2.6.4 Brain ganglioside mapping by MALDI-MSI mass spectrometry [14]

MALDI-MSI was performed following a modified version of a previously described method [132,133]. Sagittal 10 μm sections of fresh frozen half-brain containing the cannula insertion site were prepared on a cryostat, and thaw-mounted onto electrically conductive Indium-Tin-Oxide (ITO) slides. Slides were sublimated with a thin layer of 1,5-Diaminonapthalene (DAN) matrix and incubated in 5% methanol to rehydrate at −20 °C overnight. To calibrate the instrument, a 5-peptide standard was spotted off the matrix and MALDI images were acquired by a Sciex MALDI 5800 TOF/TOF instrument under negative ion reflectron mode. The section was scanned with a laser step size of 70 μm and 20 shots per spectrum in the range of 1100 -200 m/z. TissueView software was used to quantify the brain's ganglioside and generate the digital map of ganglioside. Ganglioside species including GM2 (d18:1 and d20:1 moieties), and GM3 d18:1 were detected and quantified for a total number of twenty-three anatomical regions of interest (ROIs) selected relative to the injection area. The extracted mass spectra for each ROI were filtered based on the defined peaks for each ganglioside (GM2 d18:1 in 1382.75-1385.62 m/z, GM2 d20:1; 1410.88-1413.67 m/z, GM3 d18:1; 1179.52-1182.37 m/z). To quantify MALDI-MSI results, area under the curves for each ganglioside species were measured for further analysis. $GM2_{total}$ obtained from d18:1 and d20:1 moieties was used to report changes in the ratio of GM3 to $GM2_{total}$ ganglioside. The results were graphed using the prism software.

[14] Matrix assisted laser desorption/ionization mass spectrometry imaging

3 Results

3.1 HexM production, and biochemical evaluation

3.1.1 HexM expression in FiberCell system

A cell line stably expressing HexM with a His-Tag on the C-terminus (HEK293TABKO-HexM-His_6) was used to inoculate a C2011 FiberCell system cartridge (**Fig. 3-1**). The endogenous *HEXA* and *HEXB* genes of the cell line were previously inactivated using the CRISPR-cas9 genome editing system to avoid formation of endogenous β-hexosaminidase isozymes [63,91]. The selected cartridge had a 4000 cm^2 surface area which enabled high density cell growth (2.5×10^5 cell/ cm^2) and maintained biologically homeostatic conditions in serum free media (FiberCell Systems Inc. New Market, Md). The extracapillary space retained the expressed HexM which allowed concentration of the protein for extraction.

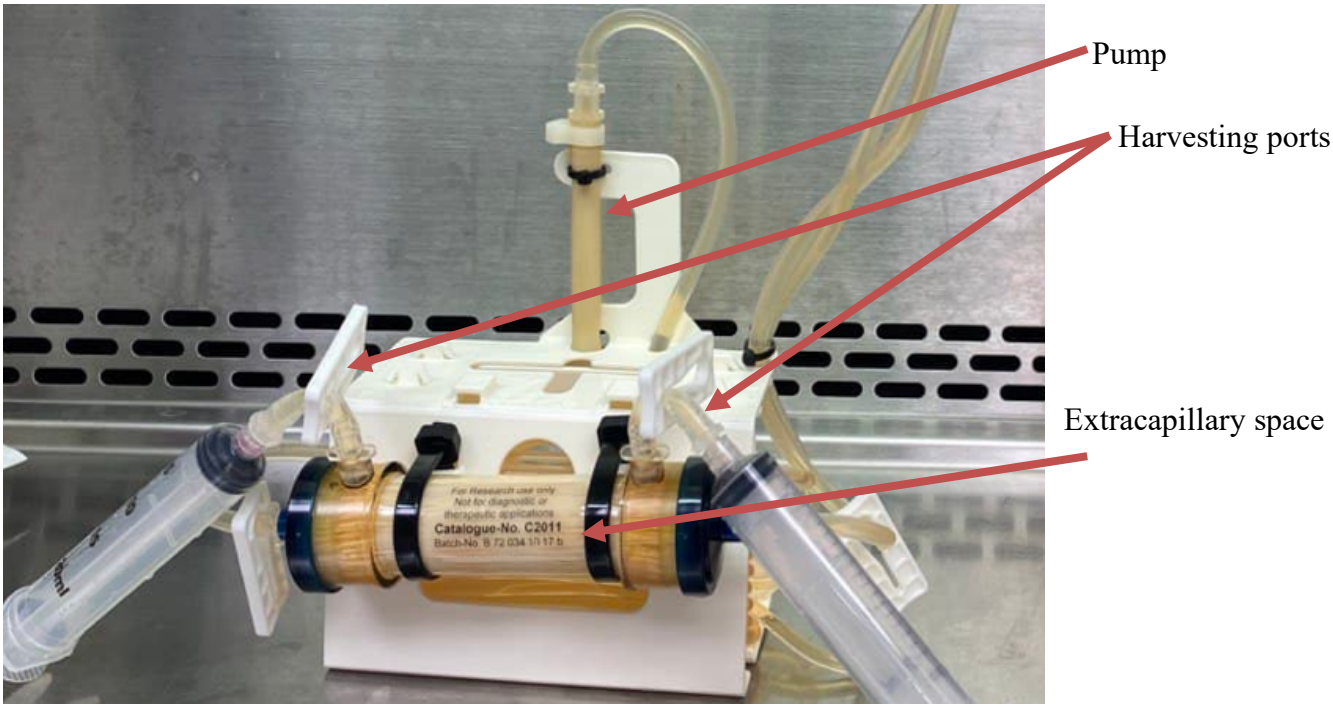

Figure 3-1. HexM production in FiberCell system.

The photograph shows the FiberCell system used to grow the HEK293TABKO-HexM-His6 cell line, with the endogenous *HEXA* and *HEXB* genes inactivated to avoid formation of endogenous

β-hexosaminidase isozymes. Cells are seeded on the hollow fiber membrane capillary surfaces which allow for the rapid exchange of nutrients and metabolites across 20 kDa cut-off pores within the fibers that traverse the cartridge. The pump enables controlled media flow through the cartridge and gas exchange via the fibers. The harvesting ports are used to remove the media containing the expressed HexM protein from the extra capillary space as well as dead cells. The collected media was centrifuged, and the supernatant was stored at -20 ℃ for further purification.

3.1.2 HexM purification

HexM purification was conducted in two steps. First, the media collected from the FiberCell were purified with IMAC to isolate the HexM from the media with Ni-NTA resin through its His-tag. In the second step, the obtained eluate was separated by SEC (size exclusion chromatography, HiLoad 16/600 Superdex 200, GE Life Sciences) to purify HexM. The chromatogram obtained from the SEC step showed only one peak with a high UV absorbance for the eluate, emphasizing the purity of the sample **(Fig. 3-2)**. Each 20 ml FiberCell harvest resulted in approximately 3.2 mg HexM yield.

The SDS-PAGE for the HexM samples derived from Nickel column and SEC purification showed that the eluted protein before (lane 4) and after (lane 5) size exclusion chromatography had no extra bands, verifying the purity of HexM **(Fig. 3-3A)**. Western blot analysis of the purified HexM using an anti-HexA antibody confirmed the presence of HexM (**Fig. 3-3B**). The detected band was in the same position as the Coomassie-staining band in Fig.3-3A. The activity of purified enzyme toward a negatively charged artificial substrate (MUGS), was assessed to confirm that it remained catalytically active after the purification (**Fig. 3-5**).

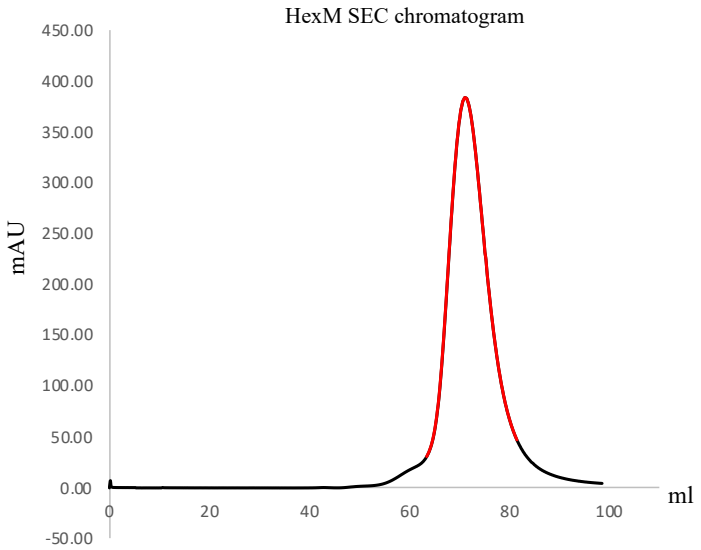

Figure 3-2. HexM chromatogram after running through SEC (S200).

The chromatogram shows the UV absorbance of the elution passing through the SEC. The red portion of the peak shows the fractions collected for HexM. Fractions were concentrated and stored in -20℃ for further analysis with SDS-PAGE, western blot, and enzyme assay.

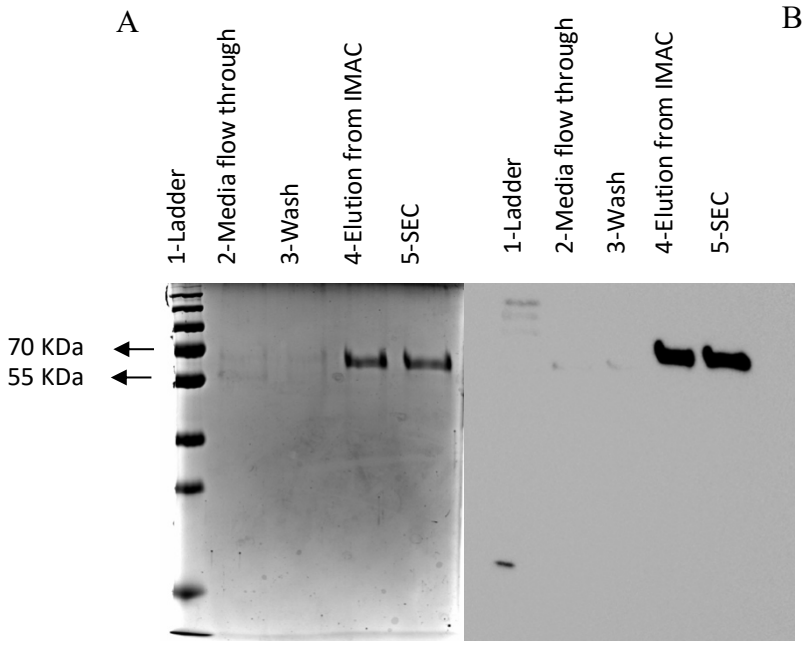

Figure 3-3. SDS-PAGE and western blot of the samples collected from HexM purification steps.

To confirm the efficacy of HexM isolation from the media, and its purity, samples were collected from both IMAC (the column flow through [lane 2], wash [lane 3], and elution [lane 4]

and the SEC [final step, lane 5]. A. Samples (1µg protein) were separated on an SDS-PAGE gel (12%), and reduced HexM (µ-subunits (MW ~62kDa) were visualized with Coomassie brilliant blue. B. An identical gel to that shown in the A panel, was used for western blot analysis with anti-HexA antibody (anti-HexA rabbit polyclonal antibody; Abcam, Cat #: ab91624, 1:1000 dilution) followed by secondary anti-rabbit IgG (H+L)-HRP conjugated antibody (Bio-Rad, Cat #: 1706515, 1:3000 dilution). After detection with HRP substrate, the membrane was imaged by a ChemiDoc Imaging System (Bio-Rad). Both IMAC and SEC isolation steps resulted in a single protein band, verified as HexM with the anti-HexA antibody (Lane 4 and 5 respectively).

3.1.3 Enzyme activity of HexM

In the enzyme assays, 4-methylumbelliferyl 6-sulfo-2-acetamido-2-deoxy-β-d-glucopyranoside potassium salt (MUGS) was used as a synthetic fluorogenic substrate that is negatively charged and binds specifically to the positively charged Arg residue within the active site the µ-subunit (which is identical to the alpha subunit of HexA) (**Fig. 3-4)** [91,134]. Cleavage of the MUGS substrate with HexM results in the formation of 4-MU, a fluorogenic product that can be readily detected at an excitation of 365 nm and emission of 450 nm.

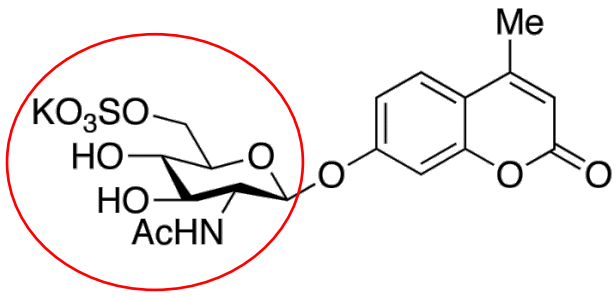

Figure 3-4. Molecular structure of MUGS molecule.

MUGS stands for 4-methylumbelliferyl 6-sulfo-2-acetamido-2-deoxy-β-d-glucopyranoside potassium salt (TRC, Canada). The negatively charged sulfate moiety present on the MUGS substrate interacts with the positively charged pocket of the active sites within the HexM enzyme

as they are derived from the α-subunit active site of HexA. This interaction then results in the cleavage of 4-MU from MUGS (indicated in red circle) and results in the formation of a detectable fluorogenic component [60,135].

3.1.4 Assessment of HexM activity in different conditions

In order to characterize some of the factors that might impact the use of purified HexM as an ERT, we determined the activity of HexM obtained from FiberCell under different conditions.

We chose the endpoint approach to measure the activity of HexM in different conditions. The same protocol was also followed for the post intervention studies using M6P-HexM and M6P-PhosHexM in different animal studies[122].

As shown in **Fig. 3-5**, the presence of BSA or TritonX-100 resulted in HexM activity being retained over the course of the experiment in both regular and low protein binding tubes. However, the enzyme activity in the absence of BSA in regular and low protein binding tubes dropped about 67% and 49% respectively. Similarly, in the absence of TritonX-100 the activity dropped about 68% and 49% in regular and low protein binding tubes respectively.

This results were consistent with the previously described methods to assess the activity of purified HexA and highlighted the necessity of adding a stabilizer molecule or anti-adhesive agent in the enzyme assay [122,136]. Also, the activity of the enzyme in CP buffer was identified to be higher in the low protein binding tubes compared to regular tubes indicating that there was adhesion of the enzyme in the regular tubes (**Fig. 3-5**).

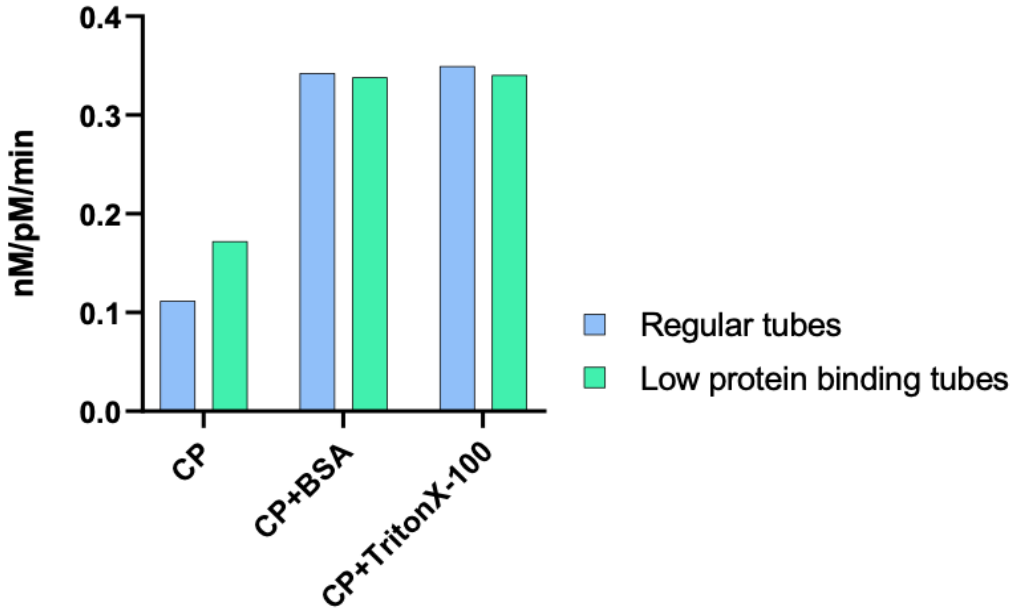

Figure 3-5. Assessment of HexM activity in different conditions.

Dilutions of purified HexM in CP buffer (100pM) was prepared in low protein binding and regular tubes in the presence of 0.5% BSA or 0.25 % (v/v) Triton X-100. The results showed that enzyme activity was remarkedly higher in the presence of 0.5% BSA or 0.25 % (v/v) Triton X-100. The HexM activity in the presence of BSA or Triton X-100 appeared similar when incubated in low protein binding tube and regular tubes. However, in the absence of 0.5% BSA or 0.25 % (v/v) Triton X-100, that activity appeared to be lower in regular tubes. The assay was performed in duplicate, and the average of the assay results was graphed. The activity is reported as nM 4-MU per pM of enzyme per minute.

3.1.5 HexM stability assay

Continuous ERT to treat an infantile mouse model of TSD over seven days requires infusion of pure and active HexM enzyme. To evaluate the activity of the enzyme over time in a solution that mimics the fluid into which the enzyme would be introduced, dilutions of purified HexM from the FiberCell were prepared in artificial cerebrospinal fluid (aCSF) or aCSF

supplemented with 0.1% BSA and kept at 37 °C. The results showed that the change in the enzyme activity over time in both conditions were minimal and the enzyme is relatively stable (**Fig. 3-6**). These results are consistent with the previous enzyme stability assay from our lab over 14 days [119], reinforcing the potential of using HexM as an ERT approach.

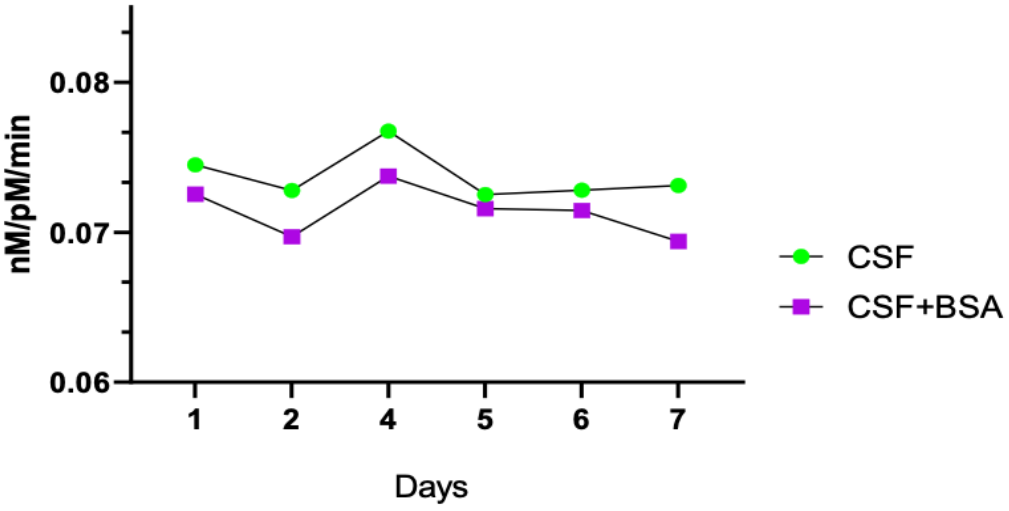

Figure 3-6. HexM stability assessment over 7 days.

The graph shows the results of an endpoint assay used to investigate HexM activity in aCSF over seven days in the presence or absence of 0.1% BSA. Assay was performed in the presence of 1mM MUGS as substrate using appropriate dilutions of enzyme collected over seven days. Each point represents the average for three technical replicates.

3.1.6 Cellular uptake of M6P-HexM and M6P-PhosHexM

Previously it was established that appropriate phosphorylation on the enzyme's oligosaccharides is critical for proper transport [137]. Also, according to previous studies regarding the impact of phosphorylation on the enzyme, it is now well established that the presence of

phosphate (M6P) tags on a higher proportion of high mannose chains improves the cross-correction mechanism through M6P receptors (CI- MPR[15] and CD-MPR[16] receptors) [63,138].

Previously, our lab in collaboration with M6P therapeutics (M6PT), generated a phosphorylated form of PhosHexM by co-expression of HexM with a catalytically active form of modified GlcNAc-1-phosphotransferase (S1S3 PTase)[63]. Further characterization of PhosHexM confirmed about 20% higher content of M6P tags on the enzyme at N157 glycosylation site, and about 3 times higher cellular uptake in the TSD fibroblast cells (1881) compared to HexM [63]. The PhosHexM previously was produced in T-Flasks through transfection of HexM expression cell line with GlcNAc-1-Phosphotransferase, however the low yields of phosphorylated enzyme purified from traditional T-Flasks and the risk of contamination introduced during the procedure highlighted the importance of a high throughput and real time system to scale up PhosHexM production for ERT assessment in preclinical study [63].

To facilitate efficient large-scale production of PhosHexM, M6P therapeutics (M6PT) developed a bicistronic vector for co-expression of M6P-HexM and a truncated active form of GlcNAc-1-Phosphotransferase (S1S3 PTase). The truncated form of the phosphotransferase facilitates higher phosphorylation levels of M6P-HexM on its N-linked high mannose glycan chains and forming a more highly phosphorylated form of M6P-HexM, M6P-PhosHexM (M6P Therapeutics, M6PT) [62,109].

[15]Cation-independent mannose-6-phosphate receptor

[16]Cation-dependent mannose-6-phosphate receptor

Here we were interested in assessing the mannose-6-phosphate mediated uptake of the provided M6P-HexM and M6P-PhosHexM enzymes to determine the benefit of generating large amounts of M6P-PhosHexM for pre-clinical experiments.

To assess the cellular uptake of M6P-HexM and the hyperphosphorylated form of M6P-HexM (M6P-PhosHexM) described above we used an immortalized version of the TSD fibroblast 1881 cell line. This cell line was derived from a patient with a complete deletion of the 5' end of *HEXA* and therefore no background alpha subunit or HexA activity was expected in this cell line.

Cells were grown in a 6 well plate and were provided with 15 µg of either M6P-HexM, M6P-PhosHexM or equivalent volumes of PBS as a control. After 24 hours, cells were collected, lysed and the total protein concentration of each sample was obtained through Bradford by using γ-protein to generate the standard curve. M6P-HexM / M6P-PhosHexM activity was assessed in triplicate. The intensity of fluorescence of each reaction was measured and the concentration of 4-MU was determined from a 4-methylumbelliferone (4-MU) standard curve. The graph shows that MUGS activity for M6P-PhosHexM treated cells was considerably higher than M6P-HexM treated cells (**Fig. 3-7**). MUGS activity for M6P-HexM treated cells was higher than PBS control (**Fig. 3-7**).

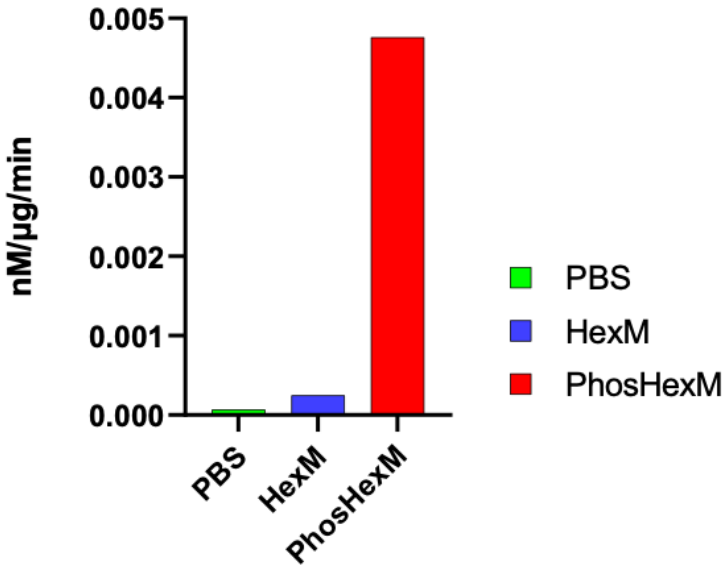

Figure 3-7. Cellular uptake with M6P-HexM and M6P-PhosHexM.

Sample lysates (30 ug protein) from fibroblasts incubated with PBS, M6P-HexM or M6P-PhosHexM were assayed with MUGS. The graph shows that M6P-PhosHexM treated cells has a considerably higher MUGS activity than M6P-HexM treated cells. However, M6P-HexM treated cells showed a slightly higher MUGS activity than PBS control. The graph shows the average of technical triplicates.

3.2 Biodistribution of intravenously injected M6P-HexM and M6P-PhosHexM

The biodistribution of M6P-HexM and M6P-PhosHexM provided by M6P in mice was assessed by injecting 0.5 mg/kg of enzyme into the tail vein of *Hexa*$^{-/-}$ (knock-out) mice. *Hexa*$^{-/-}$ mice were chosen because they do not have any alpha subunit protein and therefore should not have any forms of beta-hexosaminidase that hydrolyzes the synthetic substrate, MUGS. Saline was injected as a control. Once the needle-guided catheter was confirmed to be in the vein, 50 µl of either M6P-HexM, M6P-PhosHexM or saline was injected. Serums from the blood samples

collected through the saphenous vein at 5, 20, 60, and 120 minutes post injection were used for evaluation of enzyme activity toward MUGS. A series of tissues were also collected, and MUGS activity was measured in brain and liver lysates.

The measured serum activity toward 4-MUGS was analyzed with the One phase decay equation performed by Prism software. The One phase decay equation is used when a substance clearance rate is proportional to its remainder concentrations of the substrate at any given time within a defined timeframe (GraphPad Software). The results showed that half of the injected M6P-PhosHexM was cleared approximately in 8 mins, however this value for M6P-HexM was 17 minutes **(Fig. 3-8**). These results indicated the circulation of M6P-HexM in the blood was 2 times longer than M6P-PhosHexM (**Fig. 3-8**). As was expected, the levels of enzyme activity in the saline injected animals did not change from the baseline (**Fig. 3-8**).

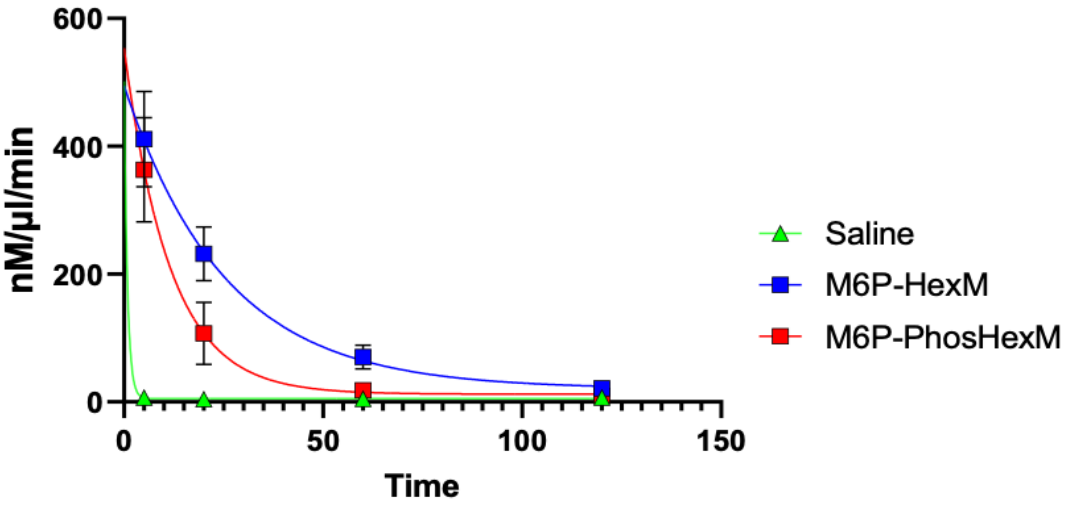

Figure 3-8. Blood clearance for M6P-HexM and M6P-PhosHexM.

The graph shows the blood clearance of M6P-HexM and M6P-PhosHexM and the best-fit line using a one-phase decay model. The calculated half-lives for M6P-HexM and M6P-PhosHexM was about 17 minutes and 8 minutes respectively (M6P-HexM R^2= 0.935, 95% confidence

intervals (CI) [12.29, 25.86] and M6P-PhosHexM R^2=0.915, 95% CI [5.195 to 11.69]). Each data point represents the mean, and the error bars are indicating standard deviation (Saline n=5, M6P-HexM n=6, M6P-PhosHexM n=6). The MUGS assay for the serum samples was performed in triplicate and 2 µl of the diluted serum sample was used for the experiment. The average fluorescence intensity by MUGS cleavage was measured using a plate reader and concentrations were derived from a standard curve generated with known concentrations of 4-MU (see methods). The results were analyzed through one-phase decay and a line of best fit was generated to connect the data points with Prism 8 software.

Biodistribution of M6P-HexM and M6P-PhosHexM in the collected brain and liver was assessed by evaluation of enzyme activity toward MUGS using 20 µg of brain or liver lysates. The results revealed that the enzyme activity of liver in *Hexa*$^{-/-}$ knock out animals which received M6P-HexM or M6P-PhosHexM was significantly higher than saline injected animals; approximately 54 and 62 times respectively (**Fig. 3-9**). There was no significant difference in the activity levels of M6P-PhosHexM and M6P-HexM injected mice (**Fig. 3-9**). The activity in the brains after IV injection of M6P-HexM, M6P-PhosHexM, or saline in *Hexa*$^{-/-}$ knock out animals showed a minimal increase in the M6P-PhosHexM injected animals, although the M6P-HexM injected animals showed a significant increase in the MUGS activity compared to saline injected animals (**Fig. 3-10**).

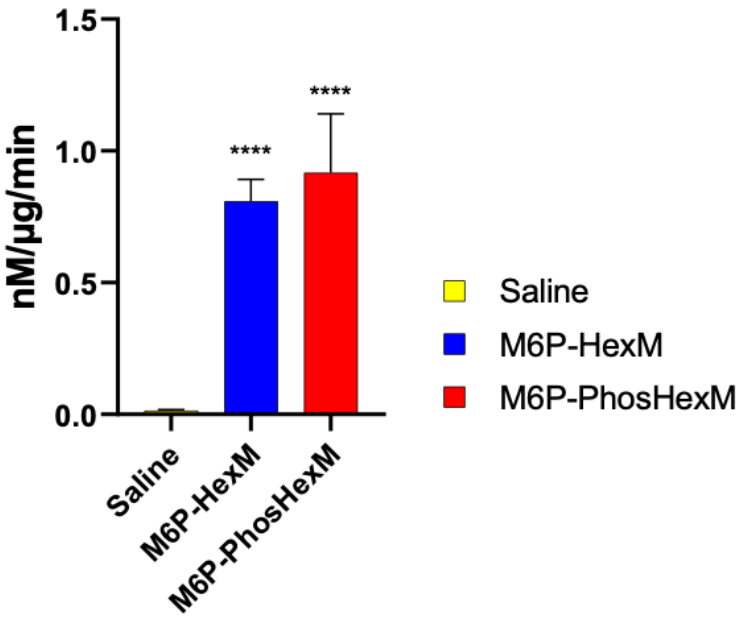

Figure 3-9. Uptake of M6P-HexM and M6P-PhosHexM in the liver post IV injection.

An activity assay toward MUGS was determined using 20 µg of protein lysate and it was performed in triplicate. The graph shows a statistically significant differences post injection for M6P-HexM ****$p<0.0001$; n=6, and M6P-PhosHexM ****$p<0.0001$; n=7 compared with saline injected animals (n=4) as a control. The columns are showing mean, and the bars are indicative of standard deviation. The results were analyzed by One-way ANOVA and graphed with prism.

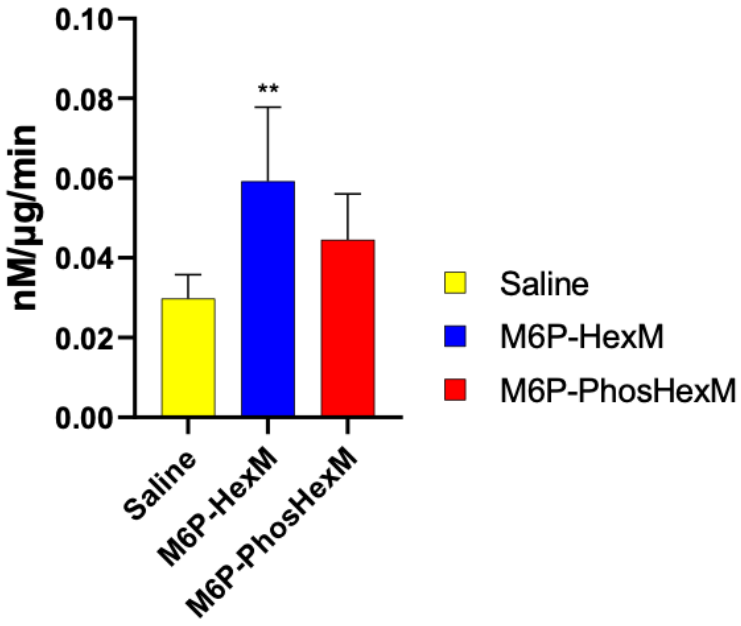

Figure 3-10. Tissue uptake of M6P-HexM and M6P-PhosHexM in the brain post IV injection.

The graph shows the enzyme activity assessment in the brain of *Hexa*$^{-/-}$ knock out animals after tail vein injection of M6P-HexM(n=6), M6P-PhosHexM(n=6) or saline(n=5). There was a trend toward increased activity in the enzyme injected animals, but the differences were only significant for the M6P-HexM mice (**$p<0.01$, n=6) compared to saline injected animals (n=5). The columns are showing mean, and the bars are indicative of standard deviation. The results were analyzed by One-way ANOVA and graphed with prism.

3.3 Short-term continuous ERT in infantile-like mouse model

Conzelmann and Sandhoff in 1992, demonstrated that residual enzyme activity above a certain threshold, which is defined as 10-15% of normal enzyme activity, can potentially rescue the normal turn over and prevent substrate storage [67].

Using an IV-ERT approach has been an effective treatment strategy in some of the LSDs including Gaucher, Fabry, and Pompe diseases to ameliorate visceral symptoms arising from

substrate accumulation [31,139,140]. IV-ERT has not been an efficient treatment to deliver enzyme to the CNS due to the presence of blood brain barrier [31,140]. To deliver enough enzyme to the brain and overcome the challenge posed by the BBB, an ICV-ERT approach that has been clinically approved for other lysosomal storage disorders was used [141].

To evaluate the impact of ICV-ERT of M6P-HexM or M6P-PhosHexM on GM2 ganglioside storage in the infantile Tay-Sachs disease-like mouse model, enzyme or aCSF was delivered to the lateral ventricle over seven days by using Alzet osmotic pumps. At 10-12 weeks of age, sex-matched animals with a *Hexa*$^{-/-}$/*Neu3*$^{-/-}$ double knock-out genotype were selected for M6P-HexM, M6P-PhosHexM or aCSF delivery. Age and sex-matched animals with *Hexa*$^{-/+}$/*Neu3*$^{-/-}$ genotype received aCSF as healthy controls. Pumps were filled with enzyme or aCSF and primed based on the manufacturer instructions. Stereotaxic surgery was performed on the animals under an aseptic condition to implant the cannula and pumps.

3.3.1 Immunohistochemistry (IHC)

It has been established that widespread GM2 ganglioside accumulation in the lysosomes results in cytoplasmic inclusions throughout the CNS in TSD patients [10]. These cytoplasmic inclusions in neurons are hallmarks of TSD [12]. In the infantile TSD-like mouse model used in this study, which are knockouts for both *Hexa* and *Neu3*, accumulation of GM2 ganglioside in the brain, especially in the hippocampus and cerebellum has been reported (Results from our lab are to be published) [10].

In this study to evaluate the efficacy of the ICV-ERT of M6P-HexM/or M6P-PhosHexM enzymes provided by M6P-Theraputics, mice were treated with enzyme for 7 days followed by

euthanasia. The GM2 ganglioside content and distribution was analyzed in the half-brains containing the cannula insertion site using immunohistochemistry with anti-GM2 antibody.

The results of ERT for after continuous injection of M6P-HexM/ or M6P-PhosHexM enzyme or saline for 7 days, indicated an overall reduction in the intensity of accumulated GM2 detected with anti-GM2 antibody in the hippocampus which is relatively close to the injection site (lateral ventricle) compared to *Hexa*$^{-/-}$ *Neu3*$^{-/-}$ double knockout mice as a control (**Fig. 3-11-A and Fig. 3-11-B**). This was observed in two experimental cohorts of treated mice compared to healthy and TDS controls (the other cohorts yet to be included). IHC results suggested that the ICV-ERT can effectively help to overcome the presence of the BBB and successively provide the catalytically active enzyme to the neurons where the neuropathological damage happens due to high amount of undegraded GM2 in the lysosomes. The promising results from IHC led us to further investigate the short-term bolus ICV-ERT approach for treating the TSD mouse model.

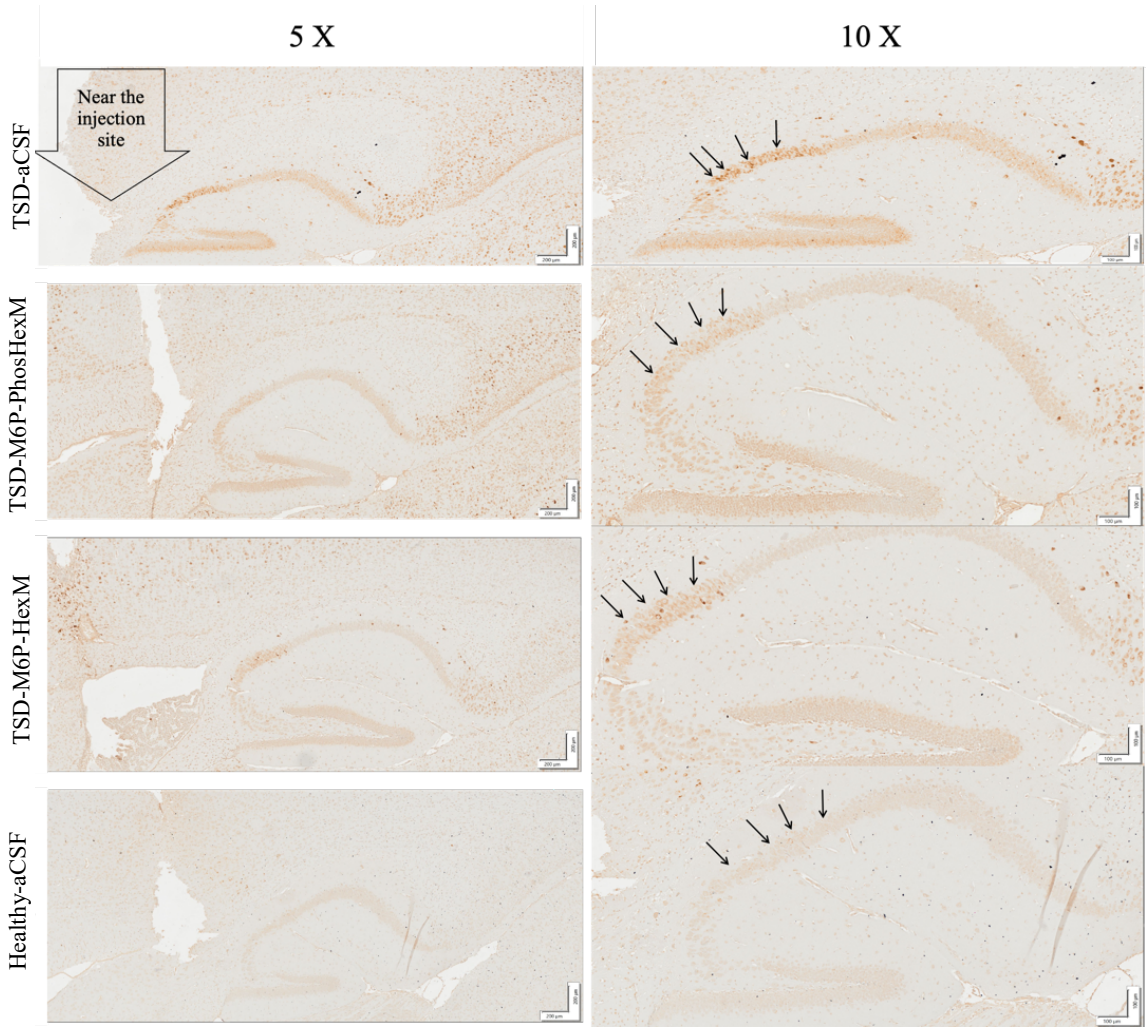

Figure 3-11-A. Immunodetection of GM2 ganglioside in TSD mouse model.

Anti-GM2 antibody was used to determine the impact of ICV-ERT on the neuronal storage of GM2 ganglioside in brain. Sagittal sections of 5µm were prepared from paraffin embedded brains collected after seven days of ICV-ERT. In the TSD mice (*Hexa*$^{-/-}$ *Neu3*$^{-/-}$double knockout) which received aCSF there is noticeable GM2 ganglioside visualized as dark brown spots in the hippocampus (black arrows). However, in the healthy age matched animals these accumulations are absent (black arrows in the healthy animals are pointing at the normal GM2 content in neurons). A reduction in the intensity of GM2 ganglioside was observed as is indicated with arrows in the hippocampi post ICV-ERT with M6P-HexM and M6P-PhosHexM in the TSD mice (*Hexa*$^{-/-}$ *Neu3*$^{-/-}$double knockout). Slides were scanned with an Olympus

VS200 microscope and images were extracted with OlyVia software. Scale bars in the 5X and 10X magnifications represent 200 µm and 100 µm respectively.

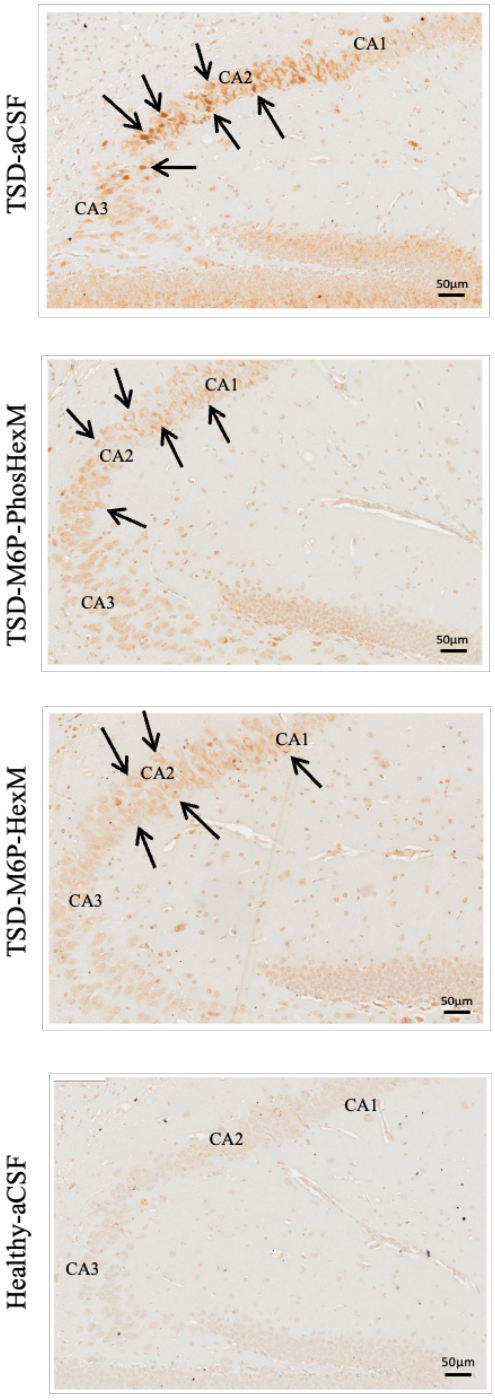

Figure 3-11-B. Immunodetection of GM2 ganglioside in TSD mouse model after continuous ICV-ERT.

Pictures in the panel represent TSD-aCSF, TSD-M6P-PhosHexM, TSD-M6P-HexM and Healthy-aCSF with 20X magnification after continuous ICV-ERT in the brains of TSD mouse model. Sagittal sections of the half-brains were subjected to anti-GM2 antibody. The sections were exposed to the biotinylated secondary antibody and were visualized by DAB substrate. Methyl Green was used as a counterstain and prepared slides were observed with a brightfield microscope. Black arrows indicate the swollen pyramidal cells due to the GM2 ganglioside accumulation which are detected by anti-GM2 antibody in the TSD-aCSF. In contrast this accumulation is absent in the healthy animal that received aCSF shown in the panel. Arrows in the panel TSD-M6P-PhosHexM and TSD-M6P-HexM show the lighter brown, showing a reduction in the GM2 content of pyramidal cells in CA2 and CA3 hippocampus regions post ERT. Animals used in this study were between 11-12 weeks old. Slides were scanned with an Olympus VS200 microscope and images were extracted with OlyVia software. Scale bars in the 20X magnification represent 50 µm.

3.4 Short-term bolus ERT in infantile TSD mouse model

To assess the impact of short-term bolus ICV-ERT, MALDI-MSI mass spectroscopy was employed. Cryosections of frozen half-brain containing the cannula insertion site were prepared following the described protocol (also see section 2.6.4.) [132,133]. Investigating the sections with MALDI allowed us to visualize the depth of enzyme infusion in the brain by assessing GM3 ganglioside levels and comparing the GM3/GM2 ganglioside ratio in different regions of brain.

The TSD mouse model used in this study was deficient in both *HexA* and *Neu3* genes (*Hexa*$^{-/-}$ and *Neu3*$^{-/-}$ double knock out), which leads to a broad accumulation of GM2 ganglioside throughout the body. In this aspect of study, the animals started the treatment between 12 to 16 weeks of age. The study was limited to only two bolus injections. This was due to the severity of symptoms in the model which in some cases led to sudden death (cardio-pulmonary related problems) during the surgical procedure or during the anesthesia required for bolus injections. This is in accordance with previously described TSD mouse model with the same genotype which was reported to have a high rate of sudden death [110].

Investigation of post ICV-ERT on the obtained brain sections with MALDI-MSI mass spectrometry allowed the semi-quantitative analysis of the specific ganglioside species (GM1, GM2, GM3) and their distribution within the tissue section.

In situ mapping of GM2 and GM3 ganglioside through MALDI-MSI allowed the spatial distribution of these gangliosides to be visualized in the brain sections (**Fig. 3-12**). As indicated in the figure, GM2 ganglioside has a wide distribution in the TSD-saline and TSD-enzyme injected animals. As expected, the GM2 ganglioside signal in the heterozygous animal (healthy control with *Hexa*$^{-/+}$/*Neu3*$^{-/-}$ genotype) brains is very low. To facilitate visualization, the GM2 and GM3 ganglioside signals were coloured with red and green respectively, and then overlaid.

In TSD mice treated with enzyme there is an increase in the intensity and extent of the green signal representing GM3 around the injection area (**Fig. 3-12**). The majority of the GM3 produced after treatment with the M6P-HexM enzyme is detected in the hippocampus. The distribution of GM3 is broader in the M6P-PhosHexM injected mice, and extends into the cerebral cortex, hippocampus, and in some areas in the cerebral nuclei. In contrast, the GM3 signal in the saline injected TSD animal is negligible (**Fig. 3-12**).

MALDI-MSI results for the other experimental animals used in this aspect of study (TSD model and healthy animals that received either of enzymes or saline as control) are presented below. Similar pattern for GM2 and GM3 ganglioside signal distribution for the animals that received treatment compared to healthy-saline and TSD-saline can be observed. In the overlaid coloured figures GM2 ganglioside and GM3 ganglioside signals are indicated with red and green respectively (**Fig. 3-13, 3-14, 3-15, 3-16**).

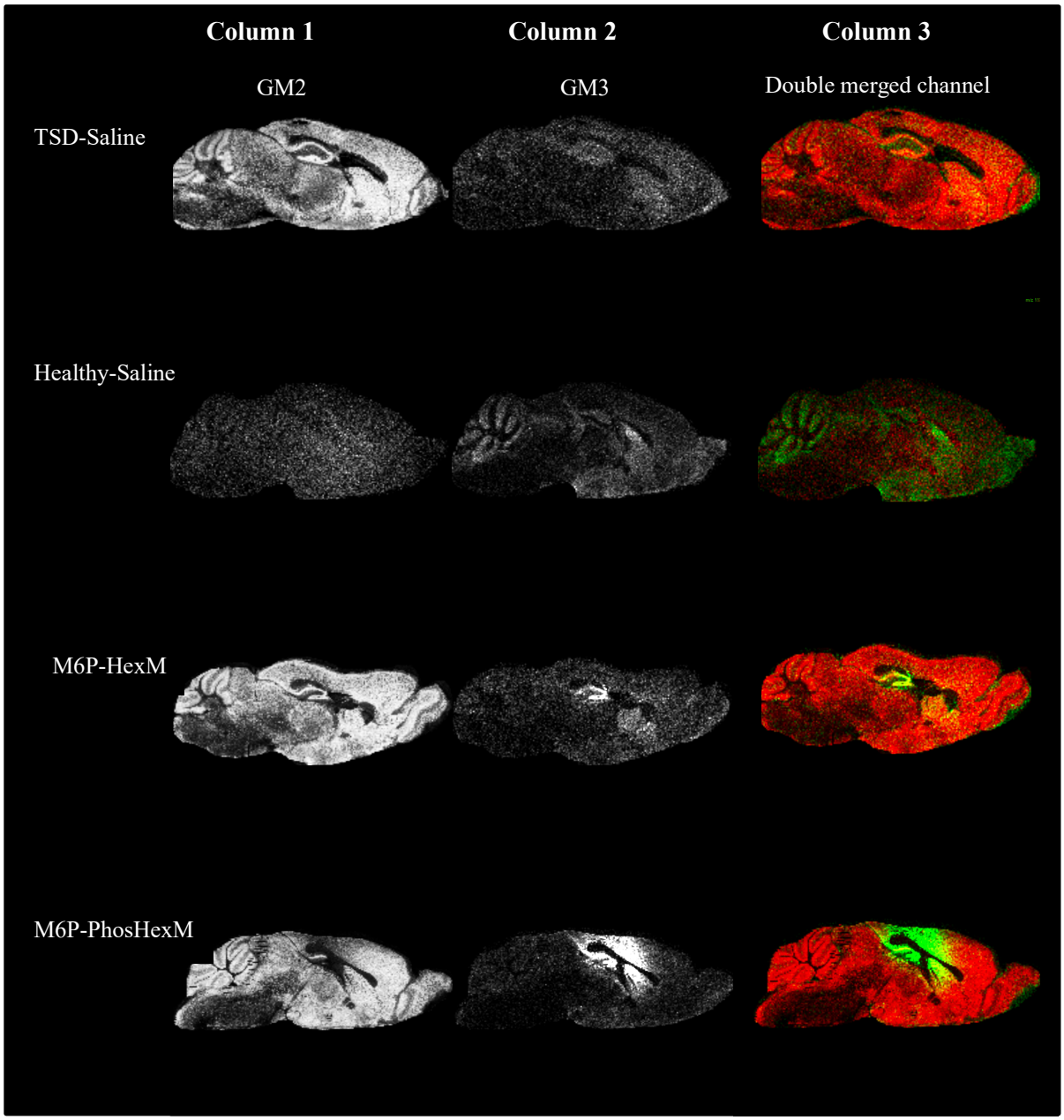

Figure 3-12. In situ mapping with MALDI-MSI mass spectrometry of GM2 and GM3 ganglioside in the brain section after short-term bolus ICV-ERT.

The MALDI-MSI images above in columns 1 and 2 show the presence of GM2 ganglioside and GM3 ganglioside with the intensity of the signal corresponding to the level of the molecules. The intensity of the GM3 signal is clearly elevated in the M6P-HexM and M6P-PhosHexM injected TSD mice compared to the saline injected TSD control. Ganglioside species were detected in the

defined range of laser intensities (GM2 d18:1; 1382.75-1385.62, GM2 d20:1; 1410.88-1413.67, GM3 d18:1; 1179.52-1182.37 m/z). In column 3 where the signals have been colourized and merged (GM2 with red and GM3 with green channels), GM3 is increased in M6P-HexM and M6P-PhosHexM injected mice, but there is a more intense and broader GM3 signal close to the lateral ventricle (cerebral cortex, hippocampus, and regions of cerebral nuclei). In the TSD animal that received saline the GM3 signal is not noticeable. These images represent one experimental cohort containing TSD-M6P-HexM, TSD-M6P-PhosHexM, TSD-saline (TSD with *Hexa*$^{-/-}$*/Neu3*$^{-/-}$ genotype) and heterozygous animals (healthy with *Hexa*$^{-/+}$*/Neu3*$^{-/-}$ genotype) used for short-term bolus ICV-ERT. Animals were sex/age matched and started their treatment at 12 weeks of age.

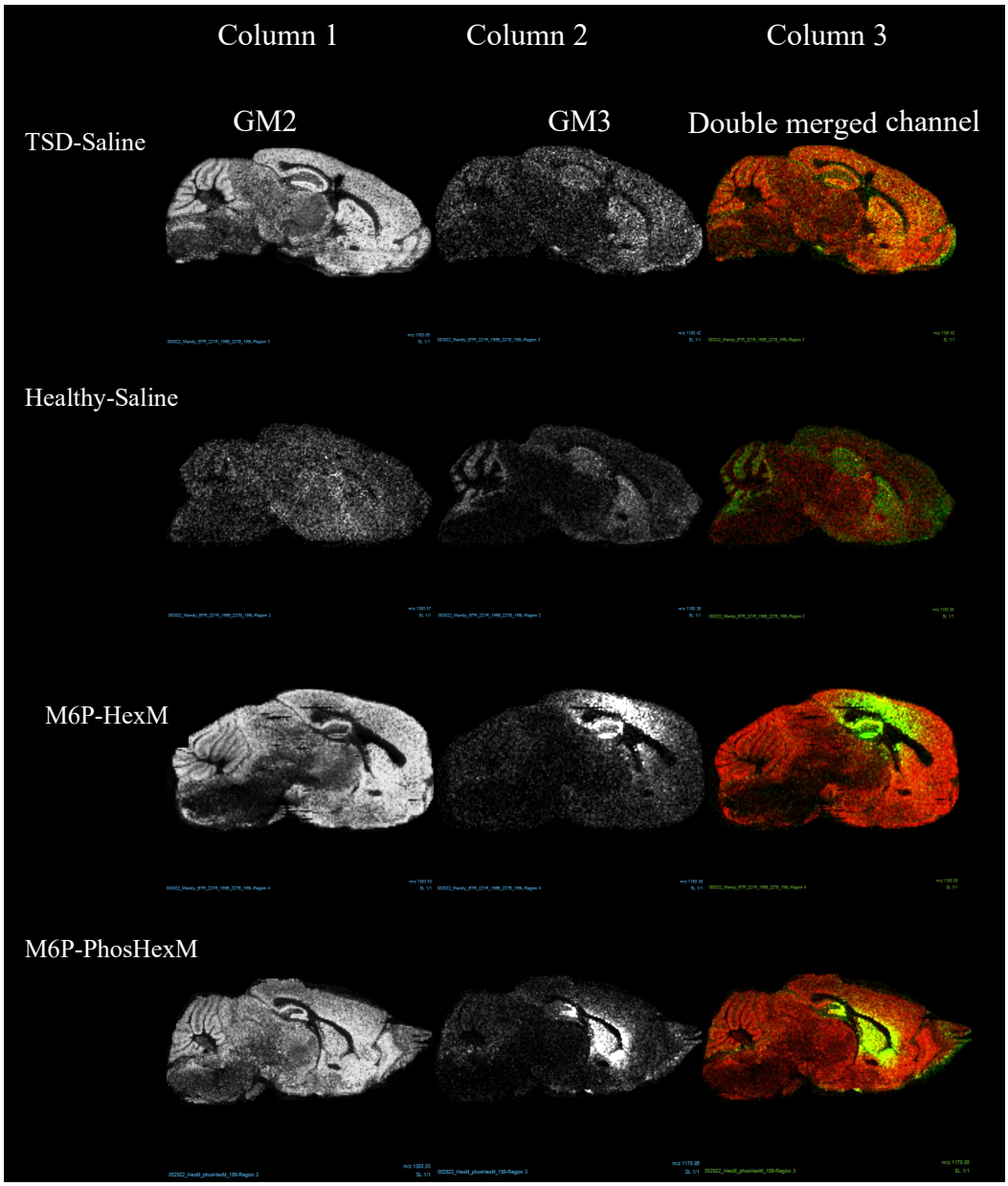

Figure 3-13. In situ mapping of GM2 and GM3 ganglioside in the brain section after short-term bolus ICV-ERT with MALDI-MSI mass spectrometry.

The MALDI-MSI images above in columns 1 and 2 show the presence of GM2 ganglioside and GM3 ganglioside with the intensity of the signal corresponding to the level of the molecules. The intensity of produced GM3 signal in the M6P-HexM and M6P-PhosHexM injected mice compared to saline injected TSD mouse is noticeable. Ganglioside species were detected in the

defined range of laser intensities (GM2 d18:1; 1382.75-1385.62, GM2 d20:1; 1410.88-1413.67, GM3 d18:1; 1179.52-1182.37 m/z). In column 3, where the signals have been colourized and merged (GM2 with red and GM3 with green channels), M6P-HexM injected animal shows an increase in the GM3 ganglioside signal which was detected to be higher compared to M6P-PhosHexM injected animal. The production of GM3 ganglioside in M6P-HexM mainly is concentrated around the hippocampal region and cerebral cortex. However, in M6P-PhosHexM injected animal, more prominent GM3 signal was observed in the hippocampal and in the septum (indicated as green channel). In the TSD animal which received saline this signal is not noticeable. The results represent a cohort of animals comprising of TSD-saline, heterozygous animal (healthy with *Hexa*$^{-/+}$*/Neu3*$^{-/-}$ genotype), TSD-M6P-HexM and TSD-M6P-PhosHexM used for short-term bolus ICV-ERT which received the treatment or saline in 15 weeks of age.

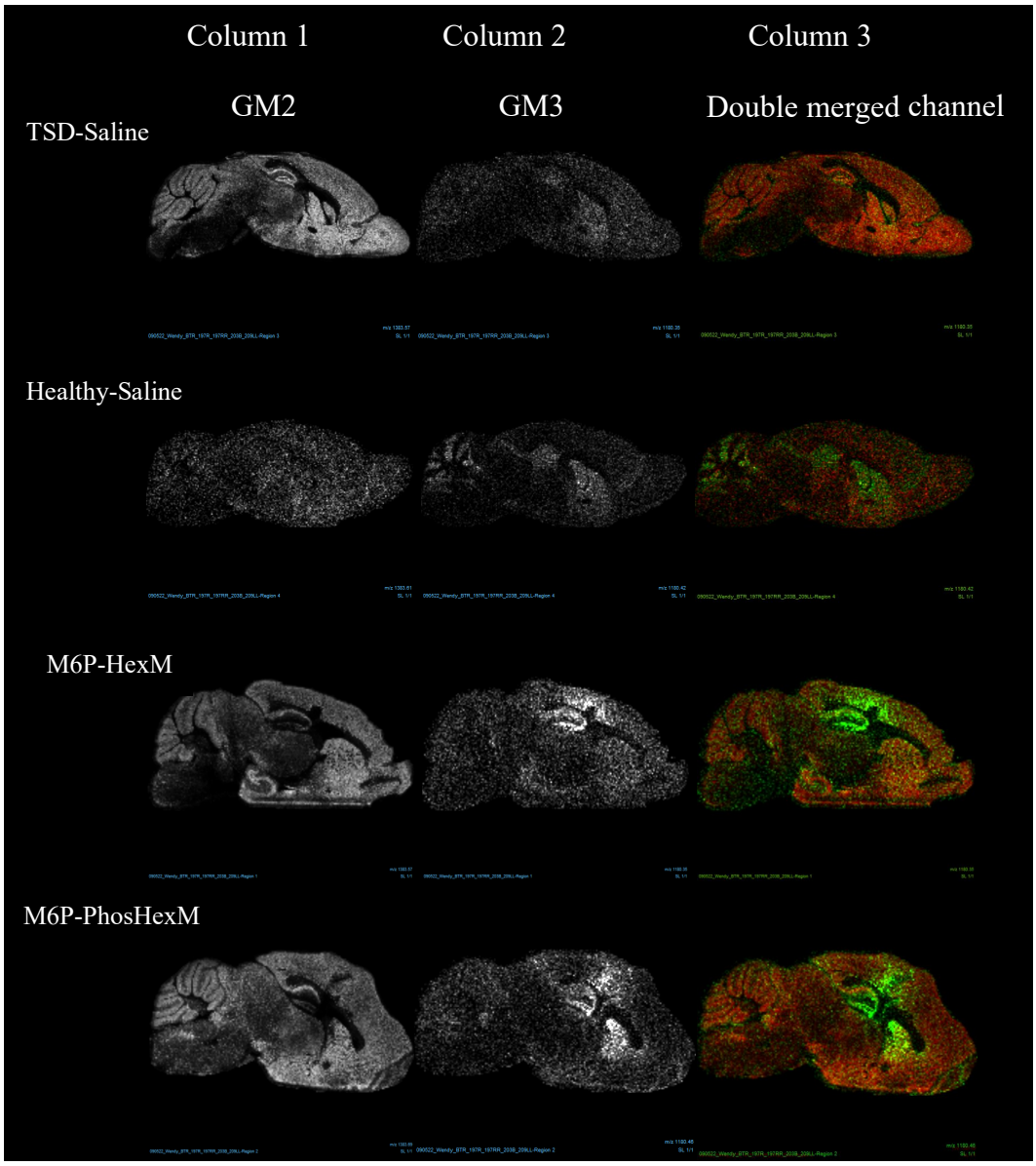

Figure 3-14. In situ mapping of GM2 and GM3 ganglioside in the brain section after short-term bolus ICV-ERT with MALDI-MSI mass spectrometry.

The MALDI-MSI images above in columns 1 and 2 show the presence of GM2 ganglioside and GM3 ganglioside with the intensity of the signal corresponding to the level of the molecules. The intensity of produced GM3 in the M6P-HexM and M6P-PhosHexM injected animal compared to TSD animal is evident. Ganglioside species were detected in the defined range of laser intensities (GM2 d18:1; 1382.75-1385.62, GM2 d20:1; 1410.88-1413.67, GM3 d18:1; 1179.52-1182.37 m/z). In column 3 where the signals have been colourized and merged (GM2 with red and GM3

with green channels), M6P-HexM injected animal shows an increase in the GM3 ganglioside signal in the cerebral cortex and hippocampal region. M6P-PhosHexM injected animal shows a higher and broader GM3 production (indicated as green channel) not only in the mentioned regions for M6P-HexM, but also in the septum is noticeable. In the TSD animal which received saline this signal is not noticeable. Presented results are indicative of one of the experimental cohorts containing TSD-M6P-HexM, TSD-M6P-PhosHexM, TSD-saline and Heterozygous animals (healthy with *Hexa*$^{-/+}$*/Neu3*$^{-/-}$ genotype) used for short-term bolus ICV-ERT which received the treatment or saline in 15 weeks of age.

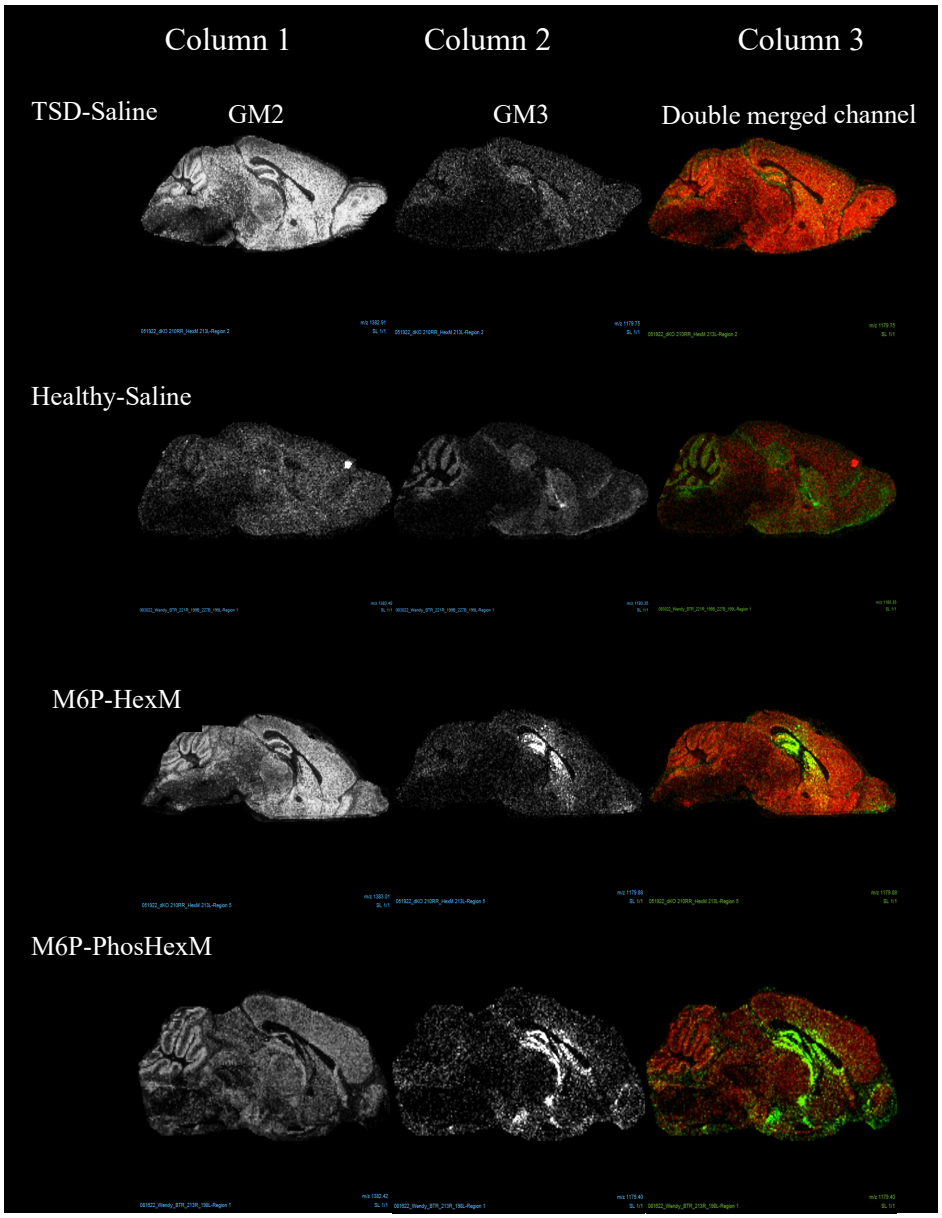

Figure 3-15. In situ mapping of GM2 and GM3 ganglioside in the brain section after short-term bolus ICV-ERT with MALDI-MSI mass spectroscopy.

The MALDI-MSI images above in columns 1 and 2 show the presence of GM2 ganglioside and GM3 ganglioside with the intensity of the signal corresponding to the level of the molecules. The intensity of produced GM3 in the M6P-HexM and M6P-PhosHexM injected animal compared to TSD animal is noticeable. Ganglioside species were detected in the defined range of laser intensities (GM2 d18:1; 1382.75-1385.62, GM2 d20:1; 1410.88-1413.67, GM3 d18:1;

1179.52-1182.37 m/z). In column 3 where the signals have been colourized and merged (GM2 with red and GM3 with green channels), M6P-HexM injected animal shows an increase in the GM3 ganglioside signal in the hippocampal region and in the caudate putamen. M6P-PhosHexM injected animal shows a higher and broader GM3 production not only in the hippocampal region but also in the areas away from injection area deeper in the brain like hypothalamus. In the TSD animal which received saline this signal is not noticeable. The results represent a cohort of animals comprising of TSD-saline, heterozygous animal (healthy with *Hexa*$^{-/+}$*/Neu3*$^{-/-}$ genotype), TSD-M6P-HexM and TSD-M6P-PhosHexM used for short-term bolus ICV-ERT which received the treatment or saline in 14-15 weeks of age.

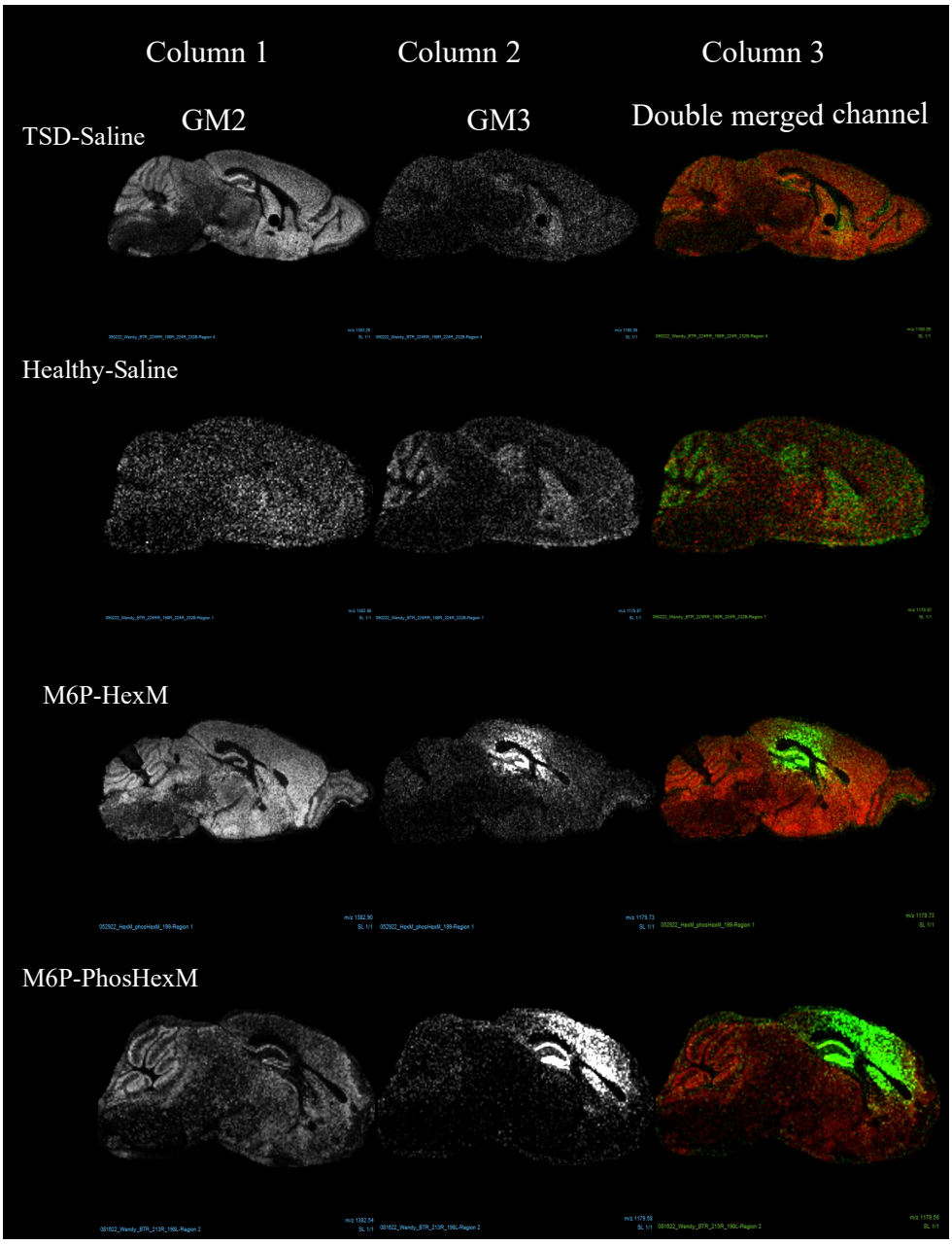

Figure 3-16. In situ mapping of GM2 and GM3 ganglioside in the brain section after short-term bolus ICV-ERT with MALDI-MSI mass spectrometry.

The MALDI-MSI images above in columns 1 and 2 show the presence of GM2 ganglioside and GM3 ganglioside with the intensity of the signal corresponding to the level of the molecules. The intensity of produced GM3 in the M6P-HexM and M6P-PhosHexM injected animal compared to TSD animal is noticeable. Ganglioside species were detected in the defined range of laser

intensities (GM2 d18:1; 1382.75-1385.62, GM2 d20:1; 1410.88-1413.67, GM3 d18:1; 1179.52-1182.37 m/z). In column 3 where the signals have been colourized and merged (GM2 with red and GM3 with green channels), M6P-HexM injected animal shows an increase in the GM3 ganglioside signal in the hippocampal region and in the cerebral cortex. M6P-PhosHexM injected animal shows GM3 signal not only in the observed areas for M6P-HexM with a greater signal but also its distribution around the lateral ventricle in the caudate putamen. In the TSD animal which received saline this signal is not noticeable. The results represent a cohort of animals comprising of TSD-saline, heterozygous (healthy with *Hexa*$^{-/+}$*/Neu3*$^{-/-}$ genotype) animal, TSD-M6P-HexM and TSD-M6P-PhosHexM used in their 15-16 weeks of age for short-term bolus ICV-ERT.

Analysis of twenty-three brain regions or ROIs indicated an increase in the GM3/GM2$_{total}$ ganglioside ratio mainly in the hippocampus area in the animals that received M6P-HexM enzyme (**Fig. 3-17** M6P-HexM).

What is striking about the ROI chart for the M6P-HexM injected animal compared to the TSD animal is that highest signals for the GM3/GM2$_{total}$ ganglioside ratio were observed in the areas anatomically closer to the injection area in the lateral ventricle (i.e., ROI-8) (**Fig. 3-17** HexM).

What is interesting about the chart for the M6P-PhosHexM injected animal is that a greater increase in the GM3/GM2$_{total}$ ganglioside ratio was observed (**Fig. 3-17** PhosHexM). Similarly, the highest increase in the GM3/GM2$_{total}$ ganglioside ratio for the M6P-PhosHexM injected animal was observed in the ROI number 8, as indicated in the **figure 3-17**. Moreover, a broader distribution of enzyme around the lateral ventricle specifically in the cerebral cortex, hippocampus, and in some areas in the cerebral nuclei were noticeable (**Fig. 3-17** M6P-PhosHexM).

Taken together, these results suggest that there is an overall higher $GM3/GM2_{total}$ ganglioside ratio in ICV-ERT for M6P-PhosHexM and M6P-HexM compared to TSD control animal, which only received saline (**Fig. 3-17**).

MALDI-MSI results for the other experimental animals used in this aspect of study are presented below. The changes in the GM3 and GM2 ganglioside signals are indicated as $GM3/GM2_{total}$ ganglioside ratio. The pattern of increase in the signal for the animals that received either of the enzymes are approximately similar, with the highest ratio observed closer to the canula injection site (**Fig. 3-18, 3-19, 3-20, 3-21**).

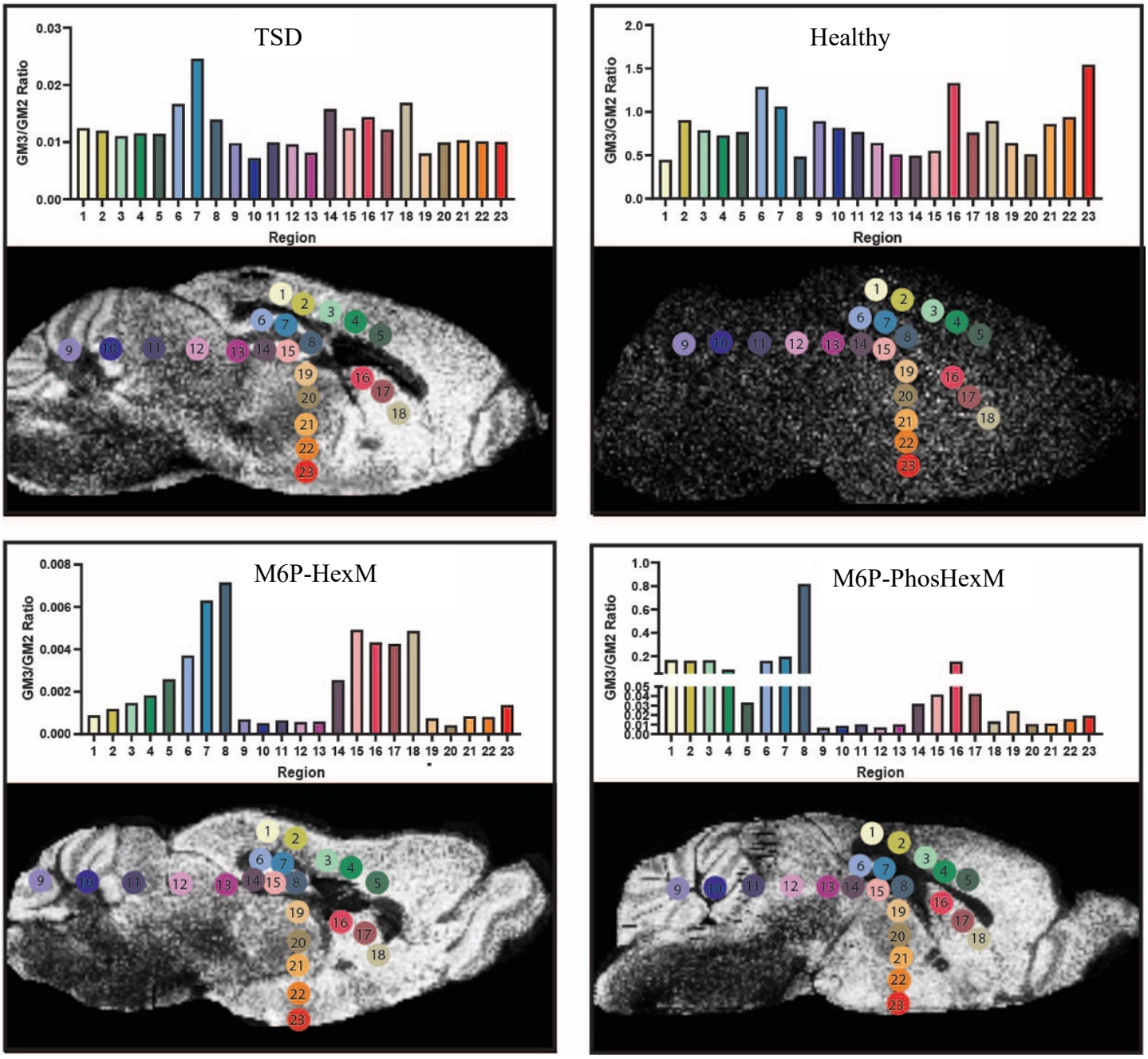

Figure 3-17. MALDI-MSI images following short-term bolus ICV-ERT.

Graphs show the GM3/$GM2_{total}$ ganglioside ratios for TSD, and heterozygous animals injected with saline, and TSD animals that received M6P-HexM and M6P-PhosHexM. Highest GM3/$GM2_{total}$ ratio was achieved in the ROI number 8 in both M6P-HexM and M6P-PhosHexM

enzymes compared to TSD animal. The obtained results after ICV- M6P-HexM injection revealed an increase in the GM3/$GM2_{total}$ ganglioside ratio resulted from GM2 ganglioside breakdown in the areas closer to the injection site. However, acquired results after ICV-M6P-PhosHexM injection showed an increase in the GM3/$GM2_{total}$ extended further from the injection site.

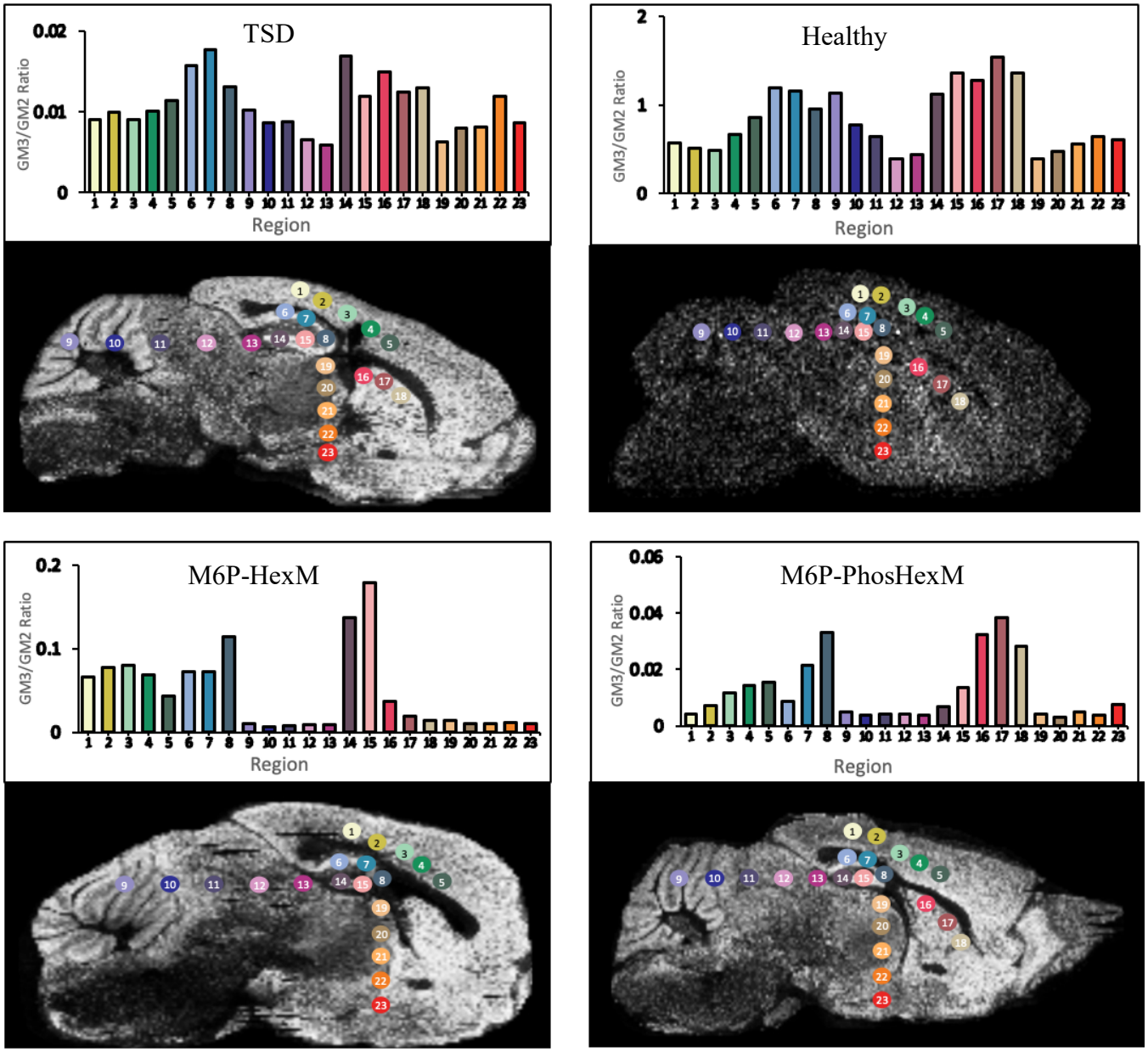

Figure 3-18. MALDI-MSI images following short-term bolus ICV-ERT.

Graphs show the quantification of GM3/$GM2_{total}$ ganglioside ratios for TSD, and heterozygous animals injected with saline, and TSD animals which received M6P-HexM and M6P-PhosHexM. Highest GM3/$GM2_{total}$ ratio was achieved in the ROIs closer to the injection site in the hippocampal area for the TSD-M6P-HexM compared to TSD-saline animal. This increase was greater and broader near the injection site and lateral ventricle for the TSD-M6P-PhosHexM

compared to TSD-saline animal. The animals in this cohort were sex-age matched. In 15 weeks of age, they received two doses of enzyme as treatment, or saline in control animals.

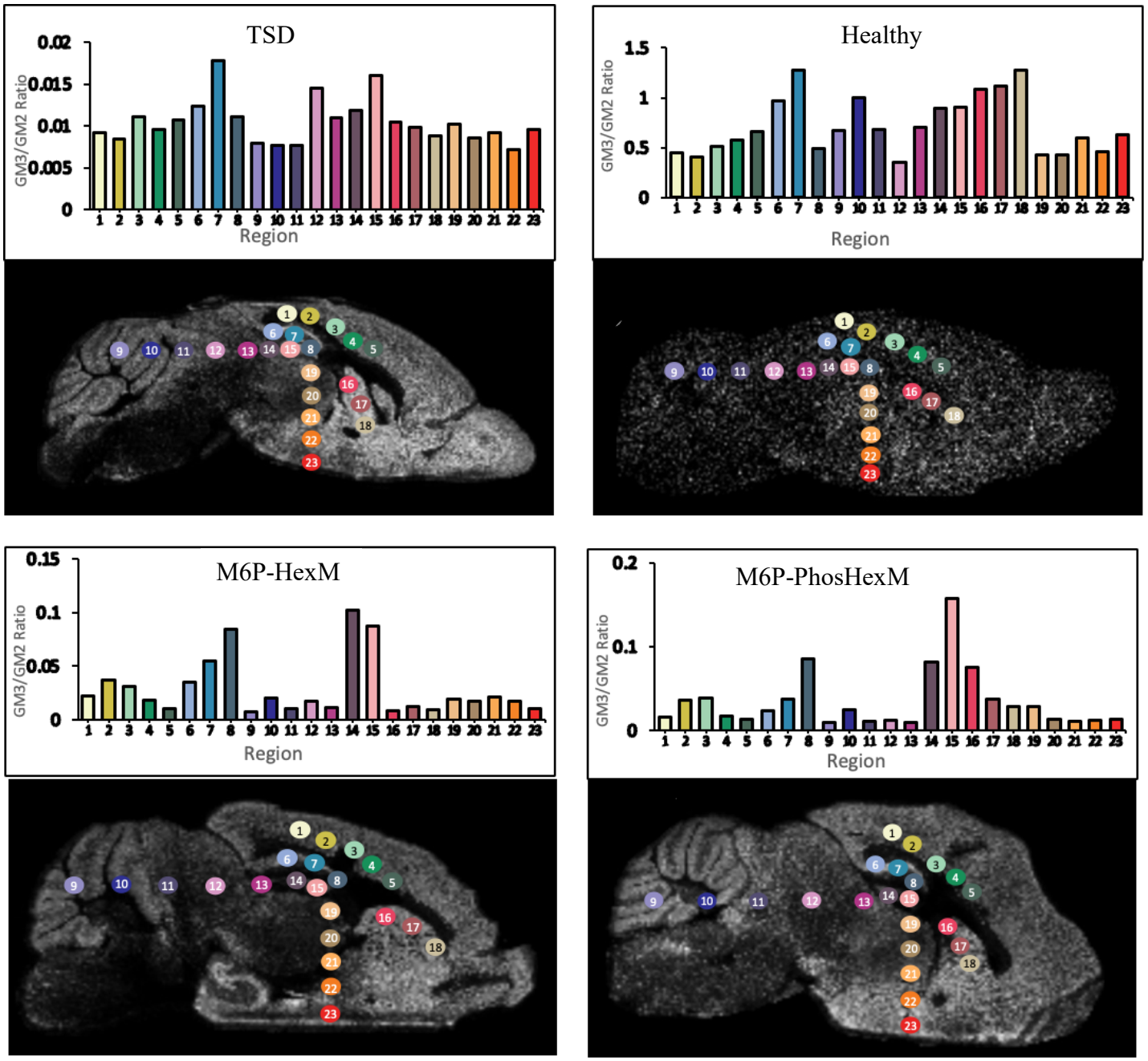

Figure 3-19. MALDI-MSI images following short-term bolus ICV-ERT.

Graphs show the quantification of GM3/$GM2_{total}$ ganglioside ratios for TSD, and heterozygous animals injected with saline, and TSD animals which received M6P-HexM and M6P-PhosHexM.

Highest GM3/$GM2_{total}$ ratio was achieved in the ROIs closer to the hippocampus for the TSD-M6P-HexM compared to TSD-saline. Acquired results for TSD-M6P-PhosHexM animal showed a greater increase in the GM3/$GM2_{total}$ ratio with an extended impact from the injection site. The animals in this cohort were sex/age matched. In 15 weeks of age, they received two doses of enzyme as treatment, or saline in control animals.

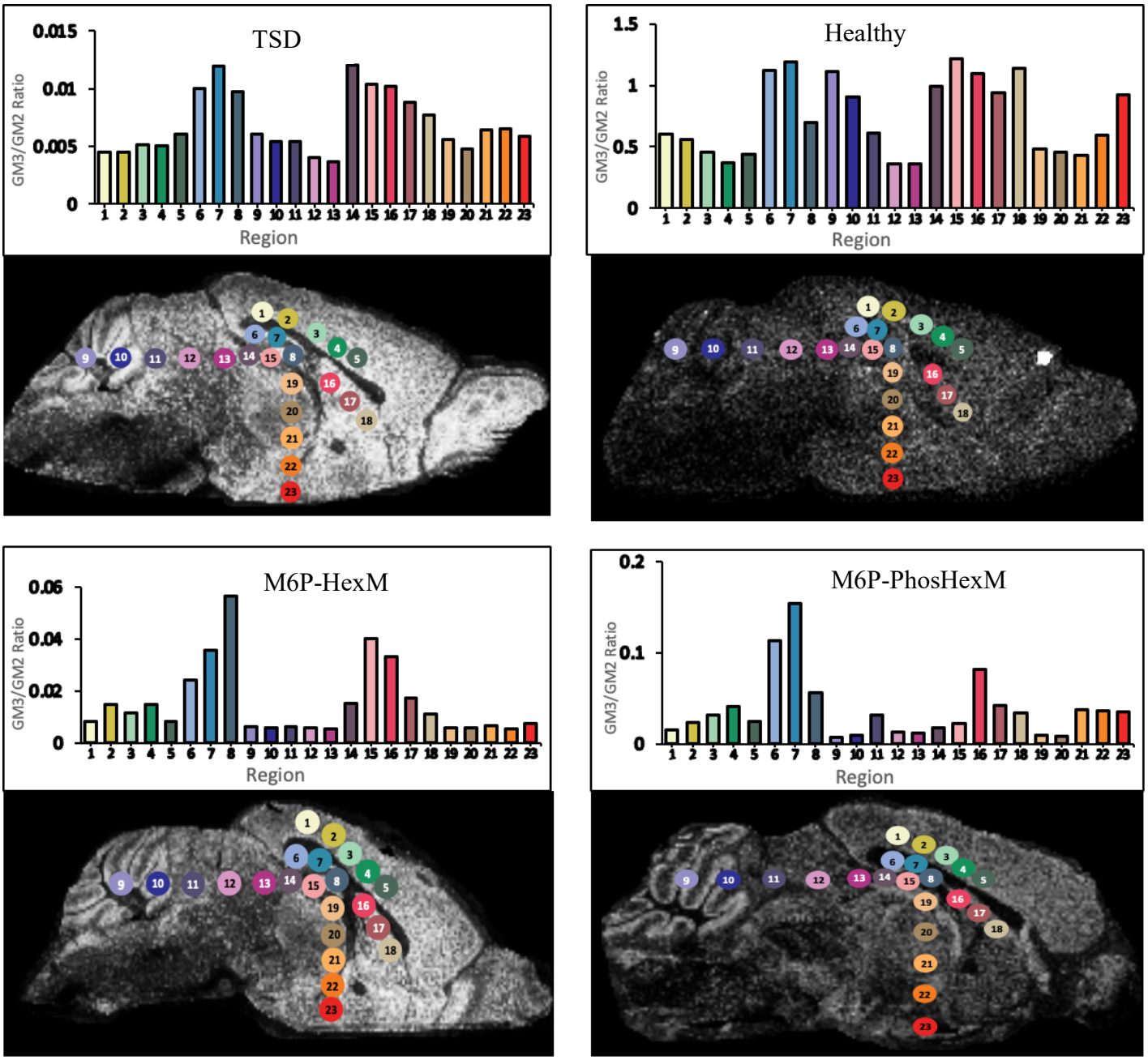

Figure 3-20. MALDI-MSI images following short-term bolus ICV-ERT. MALDI-MSI images following short-term bolus ICV-ERT.

Graphs show the quantification of GM3/GM2$_{total}$ ganglioside ratios for TSD, and heterozygous animals injected with saline, and TSD animals which received M6P-HexM and M6P-PhosHexM. Highest GM3/GM2$_{total}$ ratio for the TSD-M6P-HexM was achieved in the ROIs mainly near the

hippocampus which is located near the cannula injection site. However, obtained results for TSD-M6P-PhosHexM showed a higher GM3/$GM2_{total}$ ganglioside ratio and a broader effect away from the canulation site compared to TSD-saline animal. The animals in this cohort were sex/age matched. They received two doses of enzyme starting at 14-15 weeks of age, as treatment, or saline in control animals.

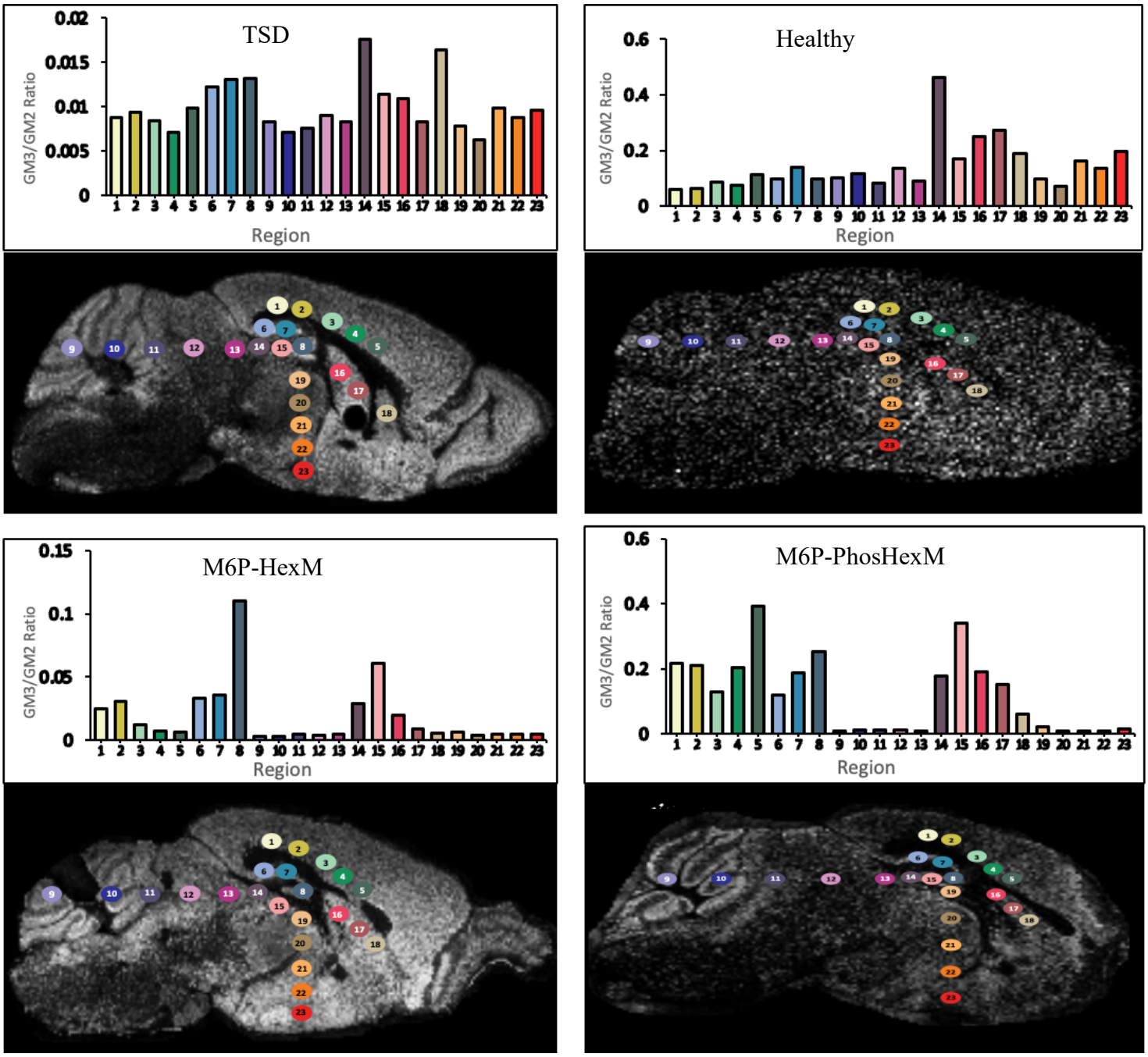

Figure 3-21. MALDI-MSI images following short-term bolus ICV-ERT. MALDI-MSI images following short-term bolus ICV-ERT.

Graphs show the quantification of GM3/$GM2_{total}$ ganglioside ratios for TSD, and heterozygous animals injected with saline, and TSD animals which received M6P-HexM and M6P-PhosHexM. Maximum GM3/$GM2_{total}$ ratio was achieved in the ROIs close to the injection site near the

hippocampus for TSD- M6P-HexM. However, acquired results for TSD-M6P-PhosHexM showed a greater increase in the ratio which was extended further away from the cannula injection site compared to TSD-saline animal. The animals in this cohort were sex/age matched. In 15-16 weeks of age, they received two doses of enzyme as treatment, or saline in control animals.

4 Discussion:

4.1 HexM production, and biochemical evaluation

4.1.1 HexM expression in FiberCell system

One of the main aims of the current study was to produce high quality and active HexM enzyme in large scale for downstream ERT. To produce HexM, a modified mammalian cell line known as HEK293TABKO-HexM-His6 was used. HEK-293 cell line was genetically modified to secrete HexM in the media [91].

The importance of proper glycosylation has been detailed in previous studies [61,104,142]. In contrast with yeast and bacteria based production systems, the mammalian cell line has the required glycosylation enzymes essential for optimal folding and trafficking of HexA to the lysosomes [99].

Another advantage of using the mammalian expression system to produce the enzyme is that it provides the enzyme with the glycan structures present in mammals and thus reduces the potential antigenicity in ERT [99]. Moreover, because the endogenous *HEXA* and *HEXB* genes are inactivated in this cell line, there are no wild type alpha or beta subunits creating homo or heterodimers that could be secreted into the media and included in the subsequent purification steps [91]. To scale up the production of HexM in this study a FiberCell system was used, which resulted in high yields of purified HexM (~ 0.16 mg/mL of harvested media) **(Fig. 1-1).**
For the *in vivo* ERT trials performed in this thesis, HexM and PhosHexM enzyme were provided for ERT by M6P-Theraputics. ERT in humans requires a large amount of enzyme, with treatments such as Fabrazyme® for Fabry's disease and Myozyme® for Pompe disease using dosages of 1mg/kg and 20 mg/kg, respectively [94].

4.1.2 HexM purification from the FiberCell system

The purity of HexM was an important factor for ERT. Harvested media was purified through Nickel-NTA resin via a C-terminus His-tag, and subsequently through size exclusion chromatography (SEC). The presence of one major peak in the SEC chromatogram eluted from the column indicated the production of a high purity protein product (**Fig. 3-2**). The results from SDS-PAGE and western blot analysis verified that the protein product was highly pure and identified it as HexM (**Fig. 3-3-A** and **Fig. 3-3-B**).

4.1.3 Assessment of HexM activity in different conditions

With respect to the first research aim, purified HexM was used for biochemical characterizations. This step was important to guide us in selecting appropriate buffer conditions for further enzyme activity evaluation after ERT.

The results showed that the presence of 0.5% BSA or 0.25 % (v/v) TritonX-100 in CP buffer was crucial to assess purified HexM activity as otherwise the activity would drop drastically. This result was consistent with other studies which demonstrated the importance of a stabilizer molecule or anti-adhesive agent during the β-hexosaminidase activity assays (**Fig. 3-5**) [122,136].

In the next step, the enzyme stability of HexM was assessed in the aCSF with or without BSA. This was important since short-term continuous ICV-ERT with pumps over seven days required the aCSF preparation of enzymes (Alzet Osmotic Pumps, ©2023 DURECT Corporation). aCSF has relatively similar electrolyte properties to the previously described CSF in different species [143,144].

The results revealed that the enzyme was relatively stable over seven days in both artificial CSF/or artificial CSF supplemented with 0.1% BSA (**Fig. 3-6**). This result was consistent with the results of prior experiments on the stability of HexM over 14 days by our lab [119].

4.2 M6P-HexM and M6P-PhosHexM's cellular uptake and biodistribution after intravenous injection

4.2.1 Cellular uptake of M6P-HexM and M6P-PhosHexM

It has been established that exogenous lysosomal enzymes can be captured and internalized to lysosomes through the MPR receptors on the cell surface [63,82,91]. Also, the presence of M6P-tags on the enzyme facilitates the enzyme's endocytosis to cells and therefore improves cross-correction [109].

To ensure consistency with studies between our laboratories and those occurring at M6P therapeutics (M6PT), it was decided that animal trials for the ERT studies of HexM and PhosHexM would be carried out using enzyme produced by M6P therapeutics (M6P-HexM and M6P-PhosHexM) as opposed to using the enzyme produced at the University of Manitoba. Further, M6P therapeutics has optimized their co-expression system with S1S3 GlcNAc-1-phosphotransferase to maximize M6P-PhosHexM production, thereby producing higher yields than is possible in our laboratory [63,119].

Therefore, prior to *in-vivo* ICV-ERT, the M6P-HexM and M6P-PhosHexM's cellular uptake was assessed. When M6P-HexM enzymes were administered to a TSD cell line, a higher cellular uptake for M6P-PhosHexM compared to M6P-HexM was clearly observed (**Fig. 3-7**).

The observed increase in the cellular uptake is attributed to the higher levels of M6P-tags present on the M6P-PhosHexM. This confirms that the engineered bicistronic construct containing both M6P-HexM and S1S3 cDNA hyper-phosphorylates M6P-HexM enzyme effectively which subsequently facilitated the enzyme's endocytosis to cells.

4.2.2 Biodistribution of intravenously injected M6P-HexM and M6P-PhosHexM

Optimization of glycosylation levels and glycan structure can affect the pharmacokinetic characteristics of lysosomal enzymes [59,61,104,105].

Previous studies have demonstrated that exogenous lysosomal enzymes can be captured and internalized to the lysosomes through N-glycan recognizing receptors on the cell surface, including mannose 6-phosphate (M6P) receptors, CI-MPR [17], Ashwell–Morell receptor (AMR), and mannose receptor (MR) [59,145]. It has been proven that the cellular uptake levels are determined by the availability and frequency of M6PR receptors on the cell surface [108] and that the biodistribution, cellular uptake and clearance time of injected enzymes are reliant on the mentioned receptors [59].

Previous studies using MALDI-MS to analyze HexM and PhosHexM confirmed the presence of terminal mannose on both enzymes which subsequently can facilitate their uptake through the mannose receptor (MR) [59,63,119]. The increased presence of mannose 6-phosphate tags on M6P-PhosHexM compared to M6P-HexM was implicated by the cellular uptake assay (**Fig. 3-7**).

[17] Cation-independent mannose-6-phosphate receptor

Studies of injected enzymes indicated that the M6P-PhosHexM gets taken up from the blood circulation two times faster than M6P-HexM when administered to *Hexa*$^{-/-}$ mice (**Fig. 3-8**). These results suggest that phosphorylation in M6P-PhosHexM improved the cellular uptake of enzyme through MPRs.

Assessment of liver enzyme activity post IV-injection with M6P-HexM or M6P-PhosHexM in *Hexa*$^{-/-}$ knock out animals revealed 49 and 52 times increase in the enzyme activity levels, respectively, compared to saline injected animals (**Fig. 3-9**).

Intravenous injection of enzymes led to rapid hepatic uptake of M6P-PhosHexM versus M6P-HexM from blood circulation as it was previously reported about hepatic uptake of IV injected enzymes [21]. This indicates that intravenous delivery may be an ineffective route for ERT, as it leaves only a small amount of active enzyme available for targeting other affected tissues [59].

Comparison of the brains' enzyme activity after IV injection with M6P-HexM and M6P-PhosHexM in *Hexa*$^{-/-}$ knock out animals showed a minimal increase in the M6P-PhosHexM injected animals. However, the M6P-HexM injected animals showed a statistically significant increase in the MUGS activity compared to saline injected animals (**Fig. 3-10**). Although there was a statistically significant increase, the overall increase is less than 2-fold compared to the 54-fold increase the liver, indicating that the BBB was not overcome by the increased M6P present on the glycan chains.

Urayama and his colleagues showed that sulfamidase can effectively pass through the brain's parenchyma in a M6P receptor mediated manner when it was delivered to newborn mice or in early postnatal stages. However, the enzyme transport after 8 weeks of age was reported as

negligeable, demonstrating a developmentally related reduction in the BBB's ability to allow passage of the enzyme due to downregulation of M6P receptors [146].

A solution to increasing the ability for M6P-HexM to pass through the BBB may involve reducing the presence of its terminal mannose. A previous study found that chemically cleaving the terminal sugars on β-glucuronidase, another lysosomal enzyme used for ERT, increased its plasma half-life by 100-fold, allowed for a greater amount of transcytosis in a non-M6P dependent manner across the BBB [147].

The animals used in this aspect of my study varied between 10-48 weeks of age, which indicated that the BBB was not more permeable to the M6P-PhosHexM with increased M6P tags than the M6P-HexM. However, the availability of PhosHexM to enter through the BBB was reduced because it was more quickly removed from the blood circulation. This could explain the increased uptake of M6P-HexM into the brain compared to M6P-PhosHexM.

One possible method to increase the efficacy of the IV-ERT approach in mouse model, is to start the treatment in the early stages of life (early after birth) [146,147]. In this stage of life, the phosphorylated enzyme can more readily pass through the BBB by means of M6P/IGF2R. This permissibility of the BBB is downregulated in mice older than 2 weeks, highlighting the absence of enzyme delivery to the brain in adult mice [148]. Furthermore, the enzyme uptake in the ERT approach relies on receptors that can be saturated [108]. Providing the enzyme in a higher dose over a prolonged period of time would maintain a high concentration of circulating enzyme. It has been suggested that the excess of circulating enzyme could promote passage through BBB by uncharacterized pathways which permits the movement of large molecules [147,148]. The requirement to start early after birth is also dictated by the disease itself as GM2 ganglioside begins to accumulate even before birth in the infantile forms of the disease.

4.3 Short-term continuous ICV-ERT in infantile TSD mouse model

The present study was designed to determine the effect of M6P-HexM and M6P-PhosHexM in the infantile TSD-like mouse model. Previous studies on a similar *Hexa*$^{-/-}$*/Neu3*$^{-/-}$ double knock-out mouse model revealed an great increase in stored GM2 ganglioside in the CNS making this animal model compatible to assess ERT efficacy [10].

BBB restricts the efficacy of IV-ERT [20,96,97], therefore ICV-ERT was employed as a clinically approved method to overcome BBB impermeability for M6P-HexM and M6P-PhosHexM infusion [141].

The results of continuous enzyme delivery to double knockout mice demonstrated that there is a reduction in the intensity of stored GM2 ganglioside in the areas relatively close to the injection site compared to saline injected. One of the areas demonstrating the most noticeable decrease in GM2 ganglioside was the hippocampus (**Fig. 3-11-A and Fig. 3-11-B**). These results provide further support for the previously established results regarding HexM's potential to degrade GM2 ganglioside [91].

4.4 Short-term bolus ERT in infantile TSD-like mouse model

It has been established that introducing exogenous lysosomal enzymes can decrease storage of their corresponding substrate through cellular uptake [82–84]. Improving the residual enzyme activity to nearly 10% of normal enzyme activity is considered to be effective in counteracting the pathological accumulation of GM2 ganglioside to treat TSD with ERT [33].

The results of ICV-ERT with M6P-HexM and M6P-PhosHexM after two bolus injections in the infantile TSD-like mouse model indicated that the enzyme infusion caused an increase in

GM2 ganglioside degradation in the areas closer to the cannula (**Fig. 3-12**). This was most evident in the double merged channel images showing GM3 ganglioside detected by MALDI-MSI in the brains of the treated and untreated *Hexa*$^{-/-}$*/Neu3*$^{-/-}$ mice. These studies also consistently showed an increased and more broadly distributed GM3 signal in the M6P-PhosHexM-treated mice compared to the M6P-HexM treated mice.

The applied double merged channel with green and red colour for GM3 and GM2 ganglioside respectively indicated an in-situ distribution map of these gangliosides in the brain section (**Fig. 3-12)**. The green colour representing the produced GM3 signal is distinguished in the hippocampus area and close to the injection site for M6P-HexM. However, for M6P-PhosHexM injected animal the produced GM3 signal showing in green is noticeable in cerebral cortex (in somatosensory and somatomotor areas), hippocampal region and in regions close to the lateral ventricle such as cerebral nuclei (caudoputamen region) (**Fig. 3-12)**.

Also, we attempted to compare the ratios of GM3/$GM2_{total}$ levels in these mice in the regions of interest at varying distances from the cannula entrance. Overall, the GM3/$GM2_{total}$ ganglioside ratio exhibited was higher in a larger region surrounding the cannula insertion site for M6P-PhosHexM than forM6P-HexM (**Fig. 3-17**). However, isolating the precise section containing the cannula insertion site was challenging and complicates the comparison of the M6P-PhosHexM and M6P-HexM enzymes.

These results are in accordance with recent studies indicating that human based recombinant hexosaminidase enzymes are capable of restoring the residual enzyme activity and degrading GM2 ganglioside [97,101]. Furthermore, the obtained results are in agreement with previous studies regarding the impact of phosphorylation level on improving the enzyme's ability to reduce GM2 ganglioside in the *Hexb*$^{-/-}$ SD mouse model [97].

5 Conclusion:

The present study was designed, for the first time, to assess the M6P-HexM and M6P-PhosHexM's potential to be used as ICV-ERT in the infantile TSD-like mouse model.

HexM is an enzyme that was designed to be more efficiently delivered through ERT (**Fig. 1-4**) [91]. The unique design of the μ-subunit incorporates the essential areas from both α and β subunits of HexA to form a functional homodimer [91].

HexM's unique features include the presence of two catalytic sites, specific function towards negatively charged substrate, interaction with GM2A protein, enhanced heat stability (T_m), high stability over time and scalable production. These features make it an ideal candidate for ERT [63,91,119].

The biochemical assessment of HexM shows that the enzyme is relatively stable over a week, which is critical for the enzyme to be used in pumps in the short-term continuous ICV-ERT (**Fig. 3-5,6)**.

Moreover, hyperphosphorylation of HexM or M6P-PhosHexM was made possible through a S1S3 co-expression platform technology developed by M6P Therapeutics (M6PT, M6P THERAPEUTICS). S1S3 is a truncated GlcNac1-PT enzyme which actively enhances the M6P content of co-expressed enzyme (M6PT, M6P THERAPEUTICS). This boosts the cross-correction mechanism of M6P-PhosHexM which was observed after providing the enzymes to a TSD cell line in comparison to M6P-HexM (**Fig. 3-7**) [109].

In this investigation, for the first time, the capabilities of M6P-HexM/ M6P-PhosHexM for ERT was assessed in an infantile TSD-like mouse model developed and characterized by our lab (Emily Barker et al., unpublished). Similar to the previously described model by Seyrantepe et al., the mice were deficient in both *Hexa*$^{-/-}$ and *Neu3*$^{-/-}$ genes which manifests a widespread and excessive GM2 ganglioside accumulation mainly in CNS [10] (Emily Barker et al.,

unpublished).

The model is described with the pathological onset starting at 12-13 weeks of age and an approximate humane endpoint of 22 weeks (Emily Barker et al., unpublished).

The biodistribution study of M6P-PhosHexM showed a quicker clearance from the blood circulation than M6P-HexM compared to *Hexa*$^{-/-}$ control animals (**Fig. 3-8)**. This could be due to the presence of higher M6P-tags on the M6P-PhosHexM enzyme which consequently facilities the enzyme uptake through MPRs in the visceral organs such as liver and spleen after intravenous injection [147].

The liver enzyme activity revealed a significant increase for both enzymes compared to *Hexa*$^{-/-}$ control animals, with the higher amount being M6P-PhosHexM (**Fig. 3-9**).

The brains enzyme activity post IV-injection showed a higher increase in the M6P-HexM injected animals than M6P-PhosHexM compared to saline injected *Hexa*$^{-/-}$ control animals. The observed results support the idea that the prolonged circulation time for M6P-HexM enhances its ability to increase the brain's enzyme activity post-IV injection in adult mice (**Fig. 3-10**).

With the exception of neonates, mice older than two weeks undergo a downregulation in the BBB's M6P receptor which adversely affects the efficiency of IV-ERT in the adults' CNS [149–151]. Therefore, the observed increase in the brain's activity did not reach the defined critical threshold (10% of normal enzyme activity in healthy animals) (data not shown) [67]. There are possibly several other mechanisms involved in the detected increase in brain's activity; including dosage-dependent pinocytosis [152], transcytosis by other glycoprotein receptors, or extracellular routes of entry influenced by the higher circulation time [147].

Further study could investigate the prolonged IV-infusion's impact as an adjuvant treatment on visceral and CNS GM2 ganglioside reduction.

The IHC data from continuous enzyme infusion in the infantile TSD mouse model indicated a reduction in the intensity of detected GM2 ganglioside in the affected brain's pyramidal cell layer (**Fig. 3-11**). This result suggests that the short-term continuous ICV-ERT with M6P-HexM and M6P-PhosHexM was an effective approach to surmount BBB and delivering the active enzyme to the lysosomes beyond the injection site.

MALDI-MSI results after short-term bolus ICV-ERT with M6P-HexM and M6P-PhosHexM indicated a maximum increase in the ratio of GM3/GM2 ganglioside compared to TSD-saline control near the implanted cannula (**Fig. 3-12 and Fig. 3-17**). Based on the obtained MALDI-MSI digital distribution map for GM2 and GM3 ganglioside after two bolus injections, both M6P-HexM and M6P-PhosHexM exhibited a diffusion pattern of produced GM3 near the cannula, mainly in the hippocampal region. A reduction in the GM3/GM2 ganglioside ratio was observed by increasing the distance from the cannula towards the posterior region of the brain.

The present study makes several noteworthy contributions to developing an enzyme replacement therapy by using an engineered human based HexA enzyme to provide an effective strategy to treat fatal infantile TSD. These promising results can further be translated into using M6P-HexM and M6P-PhosHexM in clinical applications.

6 Limitations and future directions

This study was limited by the presence of several factors that need to be addressed in future investigations.

The short-term continuous ICV-ERT on TSD animals was started in 10-12 weeks of age, in which animals have already started to manifest progressive neuropathological symptoms. Thus, the study was limited due to the severity of phenotype in the TSD mouse model included but not limited to cardio-pulmonary related problems, locomotor dysfunction, tremor, and excessive weight loss.

To use the osmotic pump for the short-term continuous enzyme infusion, the implanted pumps in the experiment would require a replacement or usage of a bigger reservoir. However, one of the downsides was that pump replacement would require performing another surgery. This would increase the chance of inflammation in the incision area. Furthermore, it could interrupt the predetermined rate of diffusion and fluctuate the amount of treatment received by each animal as a result of developing fibrous pockets/adhesions surrounding the implanted pump [153]. Additionally, after pump implantation, some animals exhibited self-harming behaviors by scratching and making scars in the pump area. Using a bigger reservoir is not ideal either as it would encourage the self-harming behavior and hinder locomotion due to its increased weight. Finally, the amount and the activity of the enzyme's remnant in the pumps had variations, which could alter the amount of enzyme delivered to the animals. Considering the posed issues in using the osmotic pumps, an alternative method of infusion using the implanted cannula and weekly injection was employed for short-term bolus ICV-ERT.

Using this method was an improvement to deliver active enzyme directly into the lateral ventricle though an implanted cannula. The animals used in this aspect of the study were between 12-15 weeks of age. We noticed that using isoflurane in the defined amount to restrain

the animals for surgery or weekly injections had a negative impact on the animals through increasing the risk of cardiac arrest and unexpected death. Therefore, unfortunately we could not exceed the short-term bolus ICV-ERT more than two injections for each animal, and thus it became a short-term discontinuous study.

Further research is required to determine short-term bolus ICV-ERT's impact on the neurobehavioral restoration and alteration in the locomotion functions in the TSD mouse model.

In the future, experiments should be carried out to establish the degree of immune reaction after enzyme infusion as antibodies can be developed due to the introduction of new epitopes (human-based enzyme in mouse and novel sequence) [154].

An issue that can be addressed in the future is whether the enzyme can diffuse through the septum pellucidum to reach the other ventricle through MALDI-MSI analysis.

It has been established that diffusion of water-soluble small molecules after ICV infusion has a logarithmic reduction in the concentration per millimeter away from the injection site [155]. To address this issue, a bilateral ICV-ERT with higher dosage of enzymes can alternatively be used to improve the effectiveness of treatment, starting in an earlier age.

More broadly, research is also needed to determine the glycosylation status and phosphorylation levels on the M6P-HexM and M6P-PhosHexM and possibly to optimize the glycosylation levels to promote the cross-correction mechanism.

Agents like epinephrine, insulin, and retinoic acid has been recognized to improve the brain's uptake of other lysosomal enzymes post IV-injection [156]. Thus, a future study could assess the short-term bolus effects of intravenous enzyme infusion accompanied by BBB manipulation.

Generating engineered enzymes tagged with a peptide sequence recognized by the BBB receptors known as trojan horses is another approach which can result in improving the transcytosis of lysosomal enzymes. This method has shown promising results in other studies using LSD mouse models [157].

Ultimately, further experimental investigations are needed to evaluate gene therapy not only to overcome the BBB, but also to alleviate the visceral symptoms in a less invasive way. Currently, AAV viruses have shown a great capability in delivering the target genes to neurons throughout the CNS after intravenous injection with the least off target impact on the liver. Taken together, the findings of this study demonstrate the potential of HexM as a treatment for the individuals who are affected by TSD.

7 Appendix:

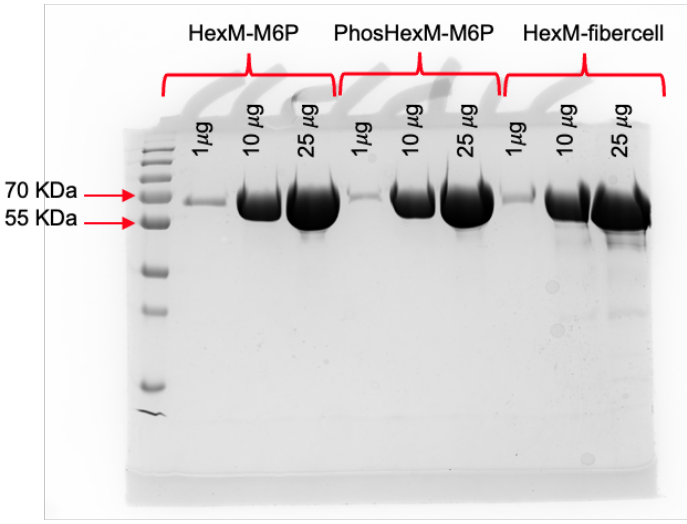

Figure 7-1. SDS-PAGE gel of HexM (purified from FiberCell), M6P-HexM and M6P-PhosHexM.

Different concentrations of FiberCell HexM, M6P-HexM, and M6P-PhosHexM (1, 10 and 25 µg protein) were reduced and separated on an SDS-PAGE gel (12%). Enzyme monomers are visualized with Coomassie brilliant blue at an apparent molecular weight of ~62kDa. The provided enzyme by M6P-Theraputics with the HPC4 tag don't show any extra bands in the higher concentrations (10, and 25 µg protein) on the gel. 10, and 25 µg protein loaded from HexM FiberCell shows a few faint smear bands on the SDS-PAGE.

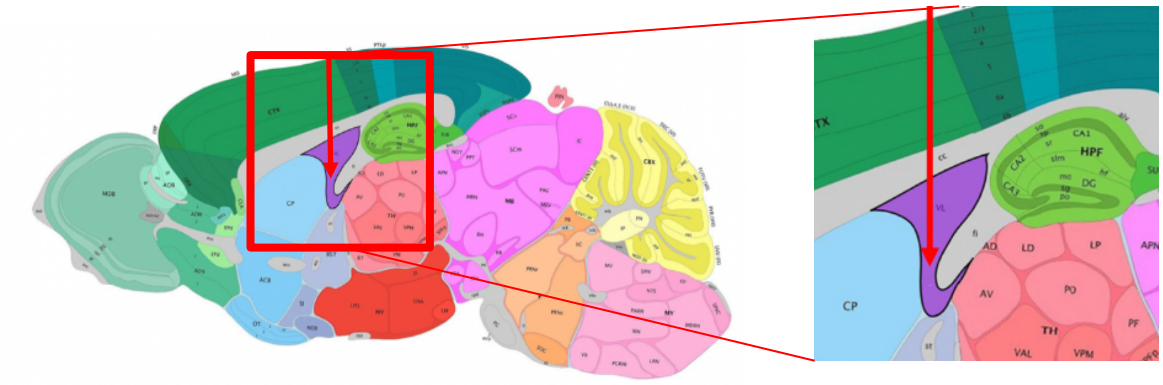

Figure 7-2. Cannula location in the lateral ventricle.

The area shown in magenta is the lateral ventricle and the red arrow shows the injection site. The coordination was obtained in accordance with bregma for the right lateral ventricle to implant the cannula (AP -0.5, ML -1.1, DV -2.5). Figure is adapted from Mouse Brain, Allen Mouse Brain

Atlas, available from atlas.brain-map.org [158]. (AP; Anterior-Posterior, ML; Medial-Lateral, and DV; Dorsal-Ventral)[159–164].

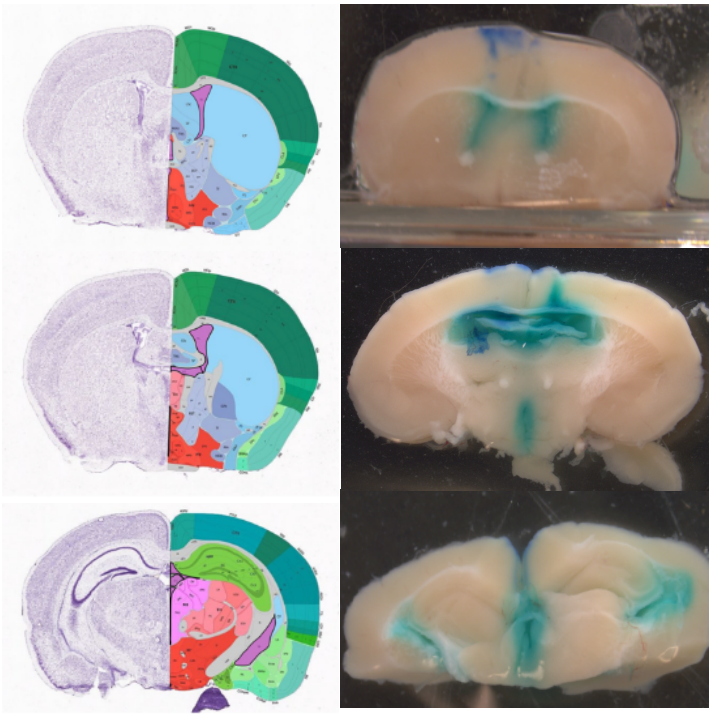

Figure 7-3. Verifying the cannula placement.

To confirm the correct placement of cannula for the mentioned coordination for the lateral ventricle (AP -0.5, ML -1.1, DV -2.5), methyl green dye was used. The figures on the right show the coronal brain sections after dye injection. Sections from different coronal plane show the dye dispersion thorough the ventricular system. The cartoons on the left are anatomically similar brain sections from Allen mouse brain atlas in which the lateral ventricle is indicated with magenta. Images are obtained from Mouse Brain, Allen Mouse Brain Atlas, available from atlas.brain-map.org [158–164]

8 References:

1. Sabatini, D. D. & Adesnik, M. Christian de Duve: Explorer of the cell who discovered new organelles by using a centrifuge. doi:10.1073/pnas.1312084110.
2. Bonam, S. R., Wang, F. & Muller, S. Lysosomes as a therapeutic target. *Nat. Rev. Drug Discov. 2019 1812* **18**, 923–948 (2019).
3. Settembre, C., Fraldi, A., Medina, D. L. & Ballabio, A. Signals from the lysosome: a control centre for cellular clearance and energy metabolism. *Nat. Rev. Mol. Cell Biol. 2013 145* **14**, 283–296 (2013).
4. Appelqvist, H., Wäster, P., Kågedal, K. & Öllinger, K. The lysosome: from waste bag to potential therapeutic target. *J. Mol. Cell Biol.* **5**, 214–226 (2013).
5. Colsch, B., Jackson, S. N., Dutta, S. & Woods, A. S. Molecular Microscopy of Brain Gangliosides: Illustrating their Distribution in Hippocampal Cell Layers. *ACS Chem. Neurosci.* **2**, 213 (2011).
6. Sands, M. S. & Davidson, B. L. Gene therapy for lysosomal storage diseases. *Mol. Ther.* **13**, 839–849 (2006).
7. Rastall, D. P. W. & Amalfitano, A. Recent advances in gene therapy for lysosomal storage disorders. *Appl. Clin. Genet.* **8**, 157–169 (2015).
8. Li, M. Enzyme replacement therapy: A review and its role in treating lysosomal storage diseases. *Pediatr. Ann.* **47**, e191–e197 (2018).
9. Uyama, E. *et al.* Hydrocephalus, corneal opacities, deafness, valvular heart disease, deformed toes and leptomeningeal fibrous thickening in adult siblings: a new syndrome associated with beta-glucocerebrosidase deficiency and a mosaic population of storage

cells. *Acta Neurol. Scand.* **86**, 407–420 (1992).

10. Seyrantepe, V. *et al.* Murine Sialidase Neu3 facilitates GM2 degradation and bypass in mouse model of Tay-Sachs disease. *Exp. Neurol.* **299**, 26–41 (2018).
11. Charria-Ortiz, G. A. The GM2 gangliosidoses. in *Lysosomal Storage Disorders* 229–256 (McGraw-Hill, 2007). doi:10.1007/978-0-387-70909-3_16.
12. Solovyeva, V. V. *et al.* New approaches to Tay-Sachs disease therapy. *Front. Physiol.* **9**, 1–11 (2018).
13. Carlos R. Ferreiraa, b, c, and W. A. G. Lysosomal storage disease. **53**, 2911–2914 (2017).
14. Tandon, A. Therapeutic Options for Tay-Sachs Disease. *Einstein Quart. J. Biol. Med.* **40**, 2002 (2002).
15. Robinson, D. & Stirling, J. L. N-Acetyl-beta-glucosaminidases in human spleen. *Biochem. J.* **107**, 321–327 (1968).
16. Maegawa, G. H. B. *et al.* Pyrimethamine as a potential pharmacological chaperone for late-onset forms of GM2 gangliosidosis. *J. Biol. Chem.* **282**, 9150–9161 (2007).
17. Klenk, E. Beiträge zur Chemie der Lipoidosen [3. Mitteilung]. Niemann-Picksche Krankheit und amaurotische Idiotie. **262**, 128–143 (1939).
18. Klenk, E. Die Fettstoffe des Gehirns bei Amaurotischer Idiotie und Niemann-Pick'scher Krankheit. *Ber Ges Physiol* **96**, 659–660 (1937).
19. Sandhoff, K. & Harzer, K. Gangliosides and gangliosidoses: Principles of molecular and metabolic pathogenesis. *J. Neurosci.* **33**, 10195–10208 (2013).
20. Leal, A. F. *et al.* Gm2 gangliosidoses: Clinical features, pathophysiological aspects, and current therapies. *International Journal of Molecular Sciences* vol. 21 1–27 at https://doi.org/10.3390/ijms21176213 (2020).

21. Lawson, C. A. & Martin, D. R. Animal models of GM2 gangliosidosis: Utility and limitations. *Appl. Clin. Genet.* **9**, 111–120 (2016).

22. Schnaar, R. L. Brain gangliosides in axon-myelin stability and axon regeneration. *FEBS Lett.* **584**, 1741–1747 (2010).

23. Svennerholm, L. CHROMATOGRAPHIC SEPARATION OF HUMAN BRAIN GANGLIOSIDES. *J. Neurochem.* **10**, 613–623 (1963).

24. Svennerholm, L. The gangliosides. *J. Lipid Res.* **5**, 145–155 (1964).

25. Walkley, S. U., Siegel, D. A. & Dobrenis, K. GM2 ganglioside and pyramidal neuron dendritogenesis. *Neurochem. Res. 1995 2011* **20**, 1287–1299 (1995).

26. Svennerholm, L. The chemical structure of normal human brain and Tay-Sachs gangliosides. *Biochem. Biophys. Res. Commun.* **9**, 436–441 (1962).

27. Sandhoff, R. & Sandhoff, K. Emerging concepts of ganglioside metabolism. *FEBS Lett.* **592**, 3835–3864 (2018).

28. Sandhoff, K. & Kolter, T. Glykolipide der Zelloberfläche -Biochemie ihres Abbaus. *Naturwissenschaften* **82**, 403–413 (1995).

29. W., T. Symmetrical changes in the region of the yellow spot in each eye of an infant. *Trans Opthalmol Soc* **1**, 55–57 (1881).

30. Sachs, B. AMAUROTIC FAMILY IDIOCY AND GENERAL LIPOID DEGENERATION. *Arch. Neurol. Psychiatry* **21**, 247–253 (1929).

31. Toro, C., Zainab, M. & Tifft, C. J. The GM2 gangliosidoses: Unlocking the mysteries of pathogenesis and treatment. *Neurosci. Lett.* **764**, (2021).

32. Flotte, T. R. *et al.* AAV gene therapy for Tay-Sachs disease. *Nat. Med.* **28**, 251–259 (2022).

33. Conzelmann, E. & Sandhoff, K. Partial enzyme deficiencies: residual activities and the development of neurological disorders. *Dev. Neurosci.* **6**, 58–71 (1983).

34. Regier, D. S., Proia, R. L., D'Azzo, A. & Tifft, C. J. The GM1 and GM2 Gangliosidoses: Natural History and Progress toward Therapy. *Pediatric endocrinology reviews : PER* vol. 13 663–673 at (2016).

35. Toro, C., Zainab, M. & Tifft, C. J. The GM2 gangliosidoses: Unlocking the mysteries of pathogenesis and treatment. *Neurosci. Lett.* **764**, 136195 (2021).

36. Lopez Vasquez, K. Tay-Sachs disease. *J. Neonatal Nurs.* **26**, 316–318 (2020).

37. Terry, R. D. & Korey, S. R. Membranous Cytoplasmic Granules in Infantile Amaurotic Idiocy. *Nat. 1960 1884755* **188**, 1000–1002 (1960).

38. McColl, B. & Vadolas, J. Animal models of β-hemoglobinopathies: Utility and limitations. *J. Blood Med.* **7**, 263–274 (2016).

39. Kaback, M. M. Tay–Sachs Disease. in (eds. Brenner, S. & Miller, J. H. B. T.-E. of G.) 1941–1943 (Academic Press, 2001). doi:https://doi.org/10.1006/rwgn.2001.1273.

40. Kaback, M. *et al.* Tay-Sachs Disease— Carrier Screening, Prenatal Diagnosis, and the Molecular Era: An International Perspective, 1970 to 1993. *JAMA* **270**, 2307–2315 (1993).

41. Maegawa, G. H. B., Stockley, T. & Tropak, M. Erratum: The natural history of juvenile or subacute GM2 gangliosidosis: 21 New cases and literature review of 134 previously reported (Pediatrics (November 2006) 118, (e1550-e1562) DOI: 10.1542/peds.2006-0588). *Pediatrics* **120**, 936 (2007).

42. Triggs-Raine, B. L. *et al.* Screening for carriers of Tay-Sachs disease among Ashkenazi Jews. A comparison of DNA-based and enzyme-based tests. *N. Engl. J. Med.* **323**, 6–12

(1990).

43. Resnik, R. *et al.* Creasy and Resnik's Maternal-Fetal Medicine: Principles and Practice 8th Edition. 1408 (2018).

44. Martin, D. C., Mark, B. L., Triggs-Raine, B. L. & Natowicz, M. R. Evaluation of the risk for Tay-Sachs disease in individuals of French Canadian ancestry living in New England. *Clin. Chem.* **53**, 392–398 (2007).

45. Mahuran, D. J., Triggs-Raine, B. L., Feigenbaum, A. J. & Gravel, R. A. The molecular basis of Tay-Sachs disease: Mutation identification and diagnosis. *Clin. Biochem.* **23**, 409–415 (1990).

46. Cao, Z. *et al.* A second mutation associated with apparent beta-hexosaminidase A pseudodeficiency: identification and frequency estimation. *Am. J. Hum. Genet.* **53**, 1198 (1993).

47. Triggs-Raine, B. L. *et al.* A pseudodeficiency allele common in non-Jewish Tay-Sachs carriers: Implications for carrier screening. *Am. J. Hum. Genet.* **51**, 793 (1992).

48. Kaback, M. M., Nathan, T. J. & Greenwald, S. Tay-Sachs disease: heterozygote screening and prenatal diagnosis--U.S. experience and world perspective. *Prog. Clin. Biol. Res.* **18**, 13–36 (1977).

49. Myerowitz, R. & Hogikyan, N. D. Different mutations in Ashkenazi Jewish and non-Jewish French Canadians with Tay-Sachs disease. *Science* **232**, 1646–1648 (1986).

50. Sheth, J. *et al.* Identification of deletion-duplication in HEXA gene in five children with Tay-Sachs disease from India. *BMC Med. Genet.* **19**, 1–5 (2018).

51. Triggs-Raine, B., Richard, M., Wasel, N., Prence, E. M. & Natowicz, M. R. Mutational analyses of Tay-Sachs disease: Studies on Tay-Sachs carriers of French Canadian

background living in New England. *Am. J. Hum. Genet.* **56**, 870–879 (1995).

52. Navon, R. & Proia, R. L. The mutations in Ashkenazi Jews with adult GM2 gangliosidosis, the adult form of Tay-Sachs disease. *Sci. (American Assoc. Adv. Sci.* **243**, 1471–1474 (1989).

53. Myerowitz, R. Splice junction mutation in some Ashkenazi Jews with Tay-Sachs disease: Evidence against a single defect within this ethnic group. *Proc. Natl. Acad. Sci. U. S. A.* **85**, 3955–3959 (1988).

54. Myerowitz, R. & Costigan, F. C. The major defect in Ashkenazi Jews with Tay-Sachs disease is an insertion in the gene for the α-chain of β-hexosaminidase. *J. Biol. Chem.* **263**, 18587–18589 (1988).

55. Dersh, D., Iwamoto, Y. & Argon, Y. Tay-Sachs disease mutations in HEXA target the ? chain of hexosaminidase A to endoplasmic reticulum-associated degradation. *Mol. Biol. Cell* **27**, 3813–3827 (2016).

56. Frisch, A. *et al.* Origin and spread of the 1278insTATC mutation causing Tay-Sachs disease in Ashkenazi Jews: genetic drift as a robust and parsimonious hypothesis. *Hum. Genet.* **114**, 366–376 (2004).

57. Lew, R. M., Burnett, L., Proos, A. L. & Delatycki, M. B. Tay-Sachs disease: current perspectives from Australia. *Appl. Clin. Genet.* **8**, 19–25 (2015).

58. Maier, T. *et al.* The X-ray crystal structure of human β-hexosaminidase B provides new insights into Sandhoff disease. *J. Mol. Biol.* **328**, 669–681 (2003).

59. Tian, W. *et al.* The glycosylation design space for recombinant lysosomal replacement enzymes produced in CHO cells. *Nat. Commun.* **10**, 1–13 (2019).

60. Mark, B. L. *et al.* Crystal Structure of Human β-Hexosaminidase B: Understanding the

Molecular Basis of Sandhoff and Tay–Sachs Disease. *J. Mol. Biol.* **327**, 1093 (2003).

61. Weitzs, G. & Proiaq, R. L. Analysis of the glycosylation and phosphorylation of the alpha-subunit of the lysosomal enzyme, beta-hexosaminidase A, by site-directed mutagenesis. *J. Biol. Chem.* **267**, 10039–10044 (1992).

62. Braulke, T. & Bonifacino, J. S. Sorting of lysosomal proteins. *Biochim. Biophys. Acta - Mol. Cell Res.* **1793**, 605–614 (2009).

63. Benzie, G. *et al.* Increased phosphorylation of HexM improves lysosomal uptake and potential for managing GM2 gangliosidoses. *BBA Adv.* **2**, (2022).

64. Wendeler, M. *et al.* The enzyme-binding region of human GM2-activator protein. *FEBS J.* **273**, 982–991 (2006).

65. Akeboshi, H. *et al.* Production of human beta-hexosaminidase A with highly phosphorylated N-glycans by the overexpression of the Ogataea minuta MNN4 gene. *Glycobiology* **19**, 1002–1009 (2009).

66. Demir, S. A., Timur, Z. K., Ateş, N., Martínez, L. A. & Seyrantepe, V. GM2 ganglioside accumulation causes neuroinflammation and behavioral alterations in a mouse model of early onset Tay-Sachs disease. *J. Neuroinflammation* **17**, 1–18 (2020).

67. Leinekugel, P., Michel, S., Conzelmann, E. & Sandhoff, K. Quantitative correlation between the residual activity of β-hexosaminidase A and arylsulfatase A and the severity of the resulting lysosomal storage disease. *Hum. Genet.* **88**, 513–523 (1992).

68. Favret, J. M., Weinstock, N. I., Feltri, M. L. & Shin, D. Pre-clinical Mouse Models of Neurodegenerative Lysosomal Storage Diseases. *Front. Mol. Biosci.* **7**, 1–27 (2020).

69. Ries, M. Enzyme replacement therapy and beyond—in memoriam Roscoe O. Brady, M.D. (1923–2016). *J. Inherit. Metab. Dis. 2017 403* **40**, 343–356 (2017).

70. Liguori, L. *et al.* Pharmacological Chaperones: A Therapeutic Approach for Diseases Caused by Destabilizing Missense Mutations. *Int. J. Mol. Sci.* **21**, (2020).

71. Germain, D. P. *et al.* Treatment of Fabry's Disease with the Pharmacologic Chaperone Migalastat. *N. Engl. J. Med.* **375**, 545–555 (2016).

72. Shapiro, B. E., Pastores, G. M., Gianutsos, J., Luzy, C. & Kolodny, E. H. Miglustat in late-onset Tay-Sachs disease: A 12-month, randomized, controlled clinical study with 24 months of extended treatment. *Genet. Med.* **11**, 425–433 (2009).

73. Treiber, A., Morand, O. & Clozel, M. The pharmacokinetics and tissue distribution of the glucosylceramide synthase inhibitor miglustat in the rat. *Xenobiotica.* **37**, 298–314 (2007).

74. Ficicioglu, C. Review of miglustat for clinical management in Gaucher disease type 1. *Ther. Clin. Risk Manag.* **4**, 425 (2008).

75. Bembi, B. *et al.* Substrate reduction therapy in the infantile form of Tay-Sachs disease. *Neurology* **66**, 278–280 (2006).

76. Chen, Y. *et al.* Progranulin associates with hexosaminidase A and ameliorates GM2 ganglioside accumulation and lysosomal storage in Tay-Sachs disease. *J. Mol. Med.* **96**, 1359–1373 (2018).

77. Bley, A. E. *et al.* Natural History of Infantile GM2 Gangliosidosis. *Pediatrics* **128**, e1233 (2011).

78. Prasad, V. K. *et al.* Unrelated donor umbilical cord blood transplantation for inherited metabolic disorders in 159 pediatric patients from a single center: influence of cellular composition of the graft on transplantation outcomes. *Blood* **112**, 2979 (2008).

79. Jacobs, J. F. M., Willemsen, M. A. A. P., Groot-Loonen, J. J., Wevers, R. A. & Hoogerbrugge, P. M. Allogeneic BMT followed by substrate reduction therapy in a child

with subacute Tay-Sachs disease. *Bone Marrow Transplant.* **36**, 925–926 (2005).

80. Stepien, K. M. *et al.* Haematopoietic stem cell transplantation arrests the progression of neurodegenerative disease in late-onset tay-sachs disease. in *JIMD Reports* vol. 41 17–23 (Wiley-Blackwell, 2018).

81. Sala, D. *et al.* Therapeutic advantages of combined gene/cell therapy strategies in a murine model of GM2 gangliosidosis. (2022) doi:10.1016/j.omtm.2022.03.011.

82. Guidotti, J.-E., Akli, S., Castelnau-Ptakhine, L., Kahn, A. & Poenaru, L. *Retrovirus-mediated enzymatic correction of Tay-Sachs defect in transduced and non-transduced cells*. *Human Molecular Genetics* vol. 7 (1998).

83. Neufeld, E. F. Mucopolysaccharidoses: The Biochemical Approach. *Hosp. Pract.* **7**, 107–113 (1972).

84. Neufeld, E. F., Lim, T. W. & Shapiro, L. J. Inherited disorders of lysosomal metabolism. *Annual review of biochemistry* vol. 44 357–376 at https://doi.org/10.1146/annurev.bi.44.070175.002041 (1975).

85. Martino, S. *et al.* A direct gene transfer strategy via brain internal capsule reverses the biochemical defect in Tay–Sachs disease. *Hum. Mol. Genet.* **14**, 2113–2123 (2005).

86. Akli, S. *et al.* Restoration of hexosaminidase A activity in human Tay-Sachs fibroblasts via adenoviral vector-mediated gene transfer. *Gene Ther.* **3**, 769–774 (1996).

87. Guidotti, J. E. *et al.* Adenoviral Gene Therapy of the Tay-Sachs Disease in Hexosaminidase A-Deficient Knock-Out Mice. *Hum. Mol. Genet.* **8**, 831–838 (1999).

88. Begoacachon-González, M. *et al.* Gene transfer corrects acute GM2 gangliosidosispotential therapeutic contribution of perivascular enzyme flow. *Mol. Ther.* **20**, 1489–1500 (2012).

89. Cachón-González, M. B. *et al.* Effective gene therapy in an authentic model of Tay-Sachs-related diseases. *Proc. Natl. Acad. Sci. U. S. A.* **103**, 10373–10378 (2006).

90. Walia, J. S. *et al.* Long-Term Correction of Sandhoff Disease Following Intravenous Delivery of rAAV9 to Mouse Neonates. *Mol. Ther.* **23**, 414 (2015).

91. Tropak, M. B. *et al.* Construction of a hybrid β-hexosaminidase subunit capable of forming stable homodimers that hydrolyze GM2 ganglioside in vivo. *Mol. Ther. - Methods Clin. Dev.* **3**, 15057 (2016).

92. Karumuthil-Melethil, S. *et al.* Novel Vector Design and Hexosaminidase Variant Enabling Self-Complementary Adeno-Associated Virus for the Treatment of Tay-Sachs Disease. *Hum. Gene Ther.* **27**, 509–521 (2016).

93. Gray-Edwards, H. L. *et al.* Adeno-Associated Virus Gene Therapy in a Sheep Model of Tay-Sachs Disease. *Hum. Gene Ther.* **29**, 312–326 (2018).

94. Table 5, FDA-approved label dose regimens for ERT products. (2013).

95. Picache, J. A., Zheng, W. & Chen, C. Z. Therapeutic Strategies For Tay-Sachs Disease. *Front. Pharmacol.* **13**, (2022).

96. Johnson, W. G. *et al.* Intravenous injection of purified hexosaminidase A into a patient with Tay-Sachs disease. *Birth Defects Orig. Artic. Ser.* **9**, 120–124 (1973).

97. Tsuji, D. *et al.* Highly phosphomannosylated enzyme replacement therapy for GM2 gangliosidosis. *Ann. Neurol.* **69**, 691–701 (2011).

98. Jakóbkiewicz-Banecka, J., Węgrzyn, A. & Węgrzyn, G. Substrate deprivation therapy: a new hope for patients suffering from neuronopathic forms of inherited lysosomal storage diseases. *J. Appl. Genet. 2007 484* **48**, 383–388 (2007).

99. Akeboshi, H. *et al.* Production of recombinant β-hexosaminidase A, a potential enzyme

for replacement therapy for Tay-Sachs and Sandhoff diseases, in the methylotrophic yeast Ogataea minuta. *Appl. Environ. Microbiol.* **73**, 4805–4812 (2007).

100. Sun, A. Lysosomal storage disease overview. *Ann. Transl. Med.* **6**, 476.-476. (2018).

101. Matsuoka, K. *et al.* Therapeutic potential of intracerebroventricular replacement of modified human B-hexosaminidase B for GM2 gangliosidosis. *Mol. Ther.* **19**, 1017–1024 (2011).

102. Vu, M. *et al.* Neural stem cells for disease modeling and evaluation of therapeutics for Tay-Sachs disease. *Orphanet J. Rare Dis.* **13**, 1–15 (2018).

103. Lemieux, M. J. *et al.* Crystallographic Structure of Human β-Hexosaminidase A: Interpretation of Tay-Sachs Mutations and Loss of GM2 Ganglioside Hydrolysis. *J. Mol. Biol.* **359**, 913–929 (2006).

104. Mark, B. L. *et al.* Crystal Structure of Human β-Hexosaminidase B: Understanding the Molecular Basis of Sandhoff and Tay-Sachs Disease. *J. Mol. Biol.* **327**, 1093–1109 (2003).

105. Sonderfeld-Fresko, S. & Proia, R. L. Analysis of the glycosylation and phosphorylation of the lysosomal enzyme, β-hexosaminidase B, by site-directed mutagenesis. *J. Biol. Chem.* **264**, 7692–7697 (1989).

106. Lemieux, M. J. *et al.* Crystallographic Structure of Human β-Hexosaminidase A: Interpretation of Tay-Sachs Mutations and Loss of GM2 Ganglioside Hydrolysis. *J. Mol. Biol.* **359**, 913 (2006).

107. Mahuran, D. J. Biochemical consequences of mutations causing the GM2 gangliosidoses. *Biochim. Biophys. Acta - Mol. Basis Dis.* **1455**, 105–138 (1999).

108. Condori, J. *et al.* Enzyme replacement for GM1-gangliosidosis: Uptake, lysosomal

activation, and cellular disease correction using a novel β-galactosidase: RTB lectin fusion. *Mol. Genet. Metab.* **117**, 199–209 (2016).

109. Liu, L., Lee, W. S., Doray, B. & Kornfeld, S. Engineering of GlcNAc-1-Phosphotransferase for Production of Highly Phosphorylated Lysosomal Enzymes for Enzyme Replacement Therapy. *Mol. Ther. - Methods Clin. Dev.* **5**, 59–65 (2017).

110. Demir, S. A., Timur, Z. K., Ateş, N., Martínez, L. A. & Seyrantepe, V. GM2 ganglioside accumulation causes neuroinflammation and behavioral alterations in a mouse model of early onset Tay-Sachs disease. *J. Neuroinflammation* **17**, 1–18 (2020).

111. Moro, C. A. & Hanna-Rose, W. Animal Model Contributions to Congenital Metabolic Disease. in *Advances in Experimental Medicine and Biology* vol. 1236 225–244 (2020).

112. Bertani, V. *et al.* A pathogenic HEXA missense variant in wild boars with Tay-Sachs disease. *Mol. Genet. Metab.* **133**, 297–306 (2021).

113. Story, B. *et al.* Natural history of Tay-Sachs disease in sheep. *Mol. Genet. Metab.* **134**, 164–174 (2021).

114. Phaneuf, D. *et al.* Dramatically different phenotypes in mouse models of human Tay-Sachs and Sandhoff diseases. *Hum. Mol. Genet.* **5**, 1–14 (1996).

115. Taniike, M. *et al.* Neuropathology of mice with targeted disruption of Hexa gene, a model of Tay-Sachs disease. *Acta Neuropathol.* **89**, 296–304 (1995).

116. Bertoni, C., Li, Y. T. & Li, S. C. Catabolism of Asialo-GM2 in Man and Mouse: SPECIFICITY OF HUMAN/MOUSE CHIMERIC GM2 ACTIVATOR PROTEINS *. *J. Biol. Chem.* **274**, 28612–28618 (1999).

117. Yuziuk, J. A. *et al.* Specificity of Mouse GM2 Activator Protein and β-N-Acetylhexosaminidases A and B: SIMILARITIES AND DIFFERENCES WITH THEIR

HUMAN COUNTERPARTS IN THE CATABOLISM OF GM2. *J. Biol. Chem.* **273**, 66–72 (1998).

118. Okpala, P. & Okpala, S. Citation: Peterchris Okpala, Sandra Okpala. Effectiveness of Enzyme Replacement and Enhancement Therapies on the Management of Tay-Sachs. *Genet Mol Med* **3**, 1–4 (2021).

119. Benzie, G. Elucidating the structure and improving the cellular uptake of HexM, a candidate for enzyme replacement therapy of GM2 gangliosidosis. (2020).

120. Benzie, G., Grisel, B. & Abidali, M. 111A Dogwood Street Neither 111A Dogwood Street.

121. Dong, D. L. Y. & Hart, G. W. Purification and characterization of an O-GlcNAc selective N-acetyl-β-D- glucosaminidase from rat spleen cytosol. *J. Biol. Chem.* **269**, 19321–19330 (1994).

122. Wendeler, M. & Sandhoff, K. Hexosaminidase assays. *Glycoconj. J.* **26**, 945–952 (2009).

123. Preparation of Artificial CSF - ALZET® Osmotic Pumps. https://www.alzet.com/guide-to-use/preparation-of-artificial-csf/.

124. Zhu, X. *et al.* An efficient genotyping method for genome-modified animals and human cells generated with CRISPR/Cas9 system. *Sci. Rep.* **4**, (2014).

125. Foster, S. D., Glover, S. R., Turner, A. N., Chatti, K. & Challa, A. K. A mixing heteroduplex mobility assay (mHMA) to genotype homozygous mutants with small indels generated by CRISPR-Cas9 nucleases. *MethodsX* **6**, 1–5 (2019).

126. Ota, S. *et al.* Efficient identification of TALEN-mediated genome modifications using heteroduplex mobility assays. (2013) doi:10.1111/gtc.12050.

127. Kitakaze, K. *et al.* Protease-resistant modified human β-hexosaminidase B ameliorates

symptoms in GM2 gangliosidosis model. *J. Clin. Invest.* **126**, 1691–1703 (2016).

128. Osmon, K. J. L. *et al.* Systemic Gene Transfer of a Hexosaminidase Variant Using an scAAV9.47 Vector Corrects G M2 Gangliosidosis in Sandhoff Mice. doi:10.1089/hum.2016.015.

129. DeVos, S. L. & Miller, T. M. Direct intraventricular delivery of drugs to the rodent central nervous system. *J. Vis. Exp.* 1–10 (2013) doi:10.3791/50326.

130. Osmon, K. J. L. *et al.* Systemic Gene Transfer of a Hexosaminidase Variant Using an scAAV9.47 Vector Corrects GM2 Gangliosidosis in Sandhoff Mice. *Hum. Gene Ther.* **27**, 497–508 (2016).

131. Kazanskaya, R. B., Lopachev, A. V., Fedorova, T. N., Gainetdinov, R. R. & Volnova, A. B. A low-cost and customizable alternative for commercial implantable cannula for intracerebral administration in mice. *HardwareX* **8**, e00120 (2020).

132. Park, D. H., Wang, L., Pittock, P., Lajoie, G. & Whitehead, S. N. Increased Expression of GM1 Detected by Electrospray Mass Spectrometry in Rat Primary Embryonic Cortical Neurons Exposed to Glutamate Toxicity. *Anal. Chem.* **88**, 7844–7852 (2016).

133. Whitehead, S. N. *et al.* Imaging Mass Spectrometry Detection of Gangliosides Species in the Mouse Brain following Transient Focal Cerebral Ischemia and Long-Term Recovery. *PLoS One* **6**, e20808 (2011).

134. Tropak, M. B. *et al.* A sensitive fluorescence-based assay for monitoring GM2 ganglioside hydrolysis in live patient cells and their lysates. *Glycobiology* **20**, 356–365 (2009).

135. Sharma, R., Deng, H., Leung, A. & Mahuran, D. *Identification of the 6-Sulfate Binding Site Unique to α-Subunit-Containing Isozymes of Human β-Hexosaminidase †. Biochemistry* vol. 40 (2001).

136. Tomoyasu, T., Tabata, A., Ishikawa, Y., Whiley, R. A. & Nagamune, H. Small heat shock protein AgsA: An effective stabilizer of enzyme activities. *J. Biosci. Bioeng.* **115**, 15–19 (2013).

137. Weitz, G. & Proia, R. L. Analysis of the glycosylation and phosphorylation of the alpha-subunit of the lysosomal enzyme, beta-hexosaminidase A, by site-directed mutagenesis. *J. Biol. Chem.* **267**, 10039–10044 (1992).

138. Cachon-Gonzalez, M. B., Zaccariotto, E. & Cox, T. M. Genetics and Therapies for GM2 Gangliosidosis. *Curr. Gene Ther.* **18**, 68–89 (2018).

139. Haslett, L. Lysosomal storage disorders and neurodegenerative disease: related mechanisms of pathogenesis and identification of novel therapeutic targets. *PQDT - UK Irel.* (2015).

140. Dickson, P. *et al.* Intrathecal enzyme replacement therapy: Successful treatment of brain disease via the cerebrospinal fluid. *Molecular Genetics and Metabolism* vol. 91 61–68 at https://doi.org/10.1016/j.ymgme.2006.12.012 (2007).

141. Schwering, C. *et al.* Development of the "Hamburg Best Practice Guidelines for ICV−Enzyme Replacement therapy (ERT) in CLN2 Disease" Based on 6 Years Treatment Experience in 48 Patients. *J. Child Neurol.* **36**, 635–641 (2021).

142. Sonderfeld-Freskos, S. & Proiae, R. L. THE JOURNAL OF BIOLOGICAL CH'YISTRY Analysis of the Glycosylation and Phosphorylation of the Lysosomal Enzyme, @-Hexosaminidase B, by Site-directed Mutagenesis*. *J. Biol. Chem.* **264**, 7692–7697 (1989).

143. *Handbook of Neurochemistry*. *Handbook of Neurochemistry* vol. 2 (Springer Science+ Business Media New York Originally, 1969).

144. Preparation of Artificial CSF - ALZET® Osmotic Pumps. https://www.alzet.com/guide-

to-use/preparation-of-artificial-csf/.

145. Ashwell, G. & Harford, J. Carbohydrate-specific receptors of the liver. *Annu. Rev. Biochem.* **51**, 531–554 (1982).

146. Urayama, A., Grubb, J. H., Sly, W. S. & Banks, W. A. Mannose 6-Phosphate Receptor–mediated Transport of Sulfamidase Across the Blood–brain Barrier in the Newborn Mouse. *Mol. Ther.* **16**, 1261 (2008).

147. Grubb, J. H. *et al.* Chemically modified β-glucuronidase crosses blood-brain barrier and clears neuronal storage in murine mucopolysaccharidosis VII. *Proc. Natl. Acad. Sci. U. S. A.* **105**, 2616–2621 (2008).

148. Vogler, C. *et al.* Overcoming the blood-brain barrier with high-dose enzyme replacement therapy in murine mucopolysaccharidosis VII. *Proc. Natl. Acad. Sci. U. S. A.* **102**, 14777–14782 (2005).

149. Urayama, A., Grubb, J. H., Sly, W. S. & Banks, W. A. Developmentally regulated mannose 6-phosphate receptor-mediated transport of a lysosomal enzyme across the blood-brain barrier. *Proc. Natl. Acad. Sci. U. S. A.* **101**, 12658 (2004).

150. Ballesteros, M., Scott, C. D. & Baxter, R. C. Developmental regulation of insulin-like growth factor-II/mannose 6-phosphate receptor mRNA in the rat. *Biochem. Biophys. Res. Commun.* **172**, 775–779 (1990).

151. Sklar, M. M., Kiess, W., Thomas, C. L. & Nissley, S. P. Developmental Expression of the Tissue Insulin-like Growth Factor II/Mannose 6-Phosphate Receptor in the Rat: Measurement by Quantitative Immunoblotting. *J. Biol. Chem.* **264**, 16733–16738 (1989).

152. Baldo, G., Giugliani, R. & Matte, U. Lysosomal enzymes may cross the blood–brain-barrier by pinocytosis: Implications for Enzyme Replacement Therapy. *Med. Hypotheses*

82, 478–480 (2014).

153. Devos, S. L. & Miller, T. M. Direct Intraventricular Delivery of Drugs to the Rodent Central Nervous System. *J. Vis. Exp* 50326 (2013) doi:10.3791/50326.

154. Kishnani, A., Dickson, P. S. & Muldowney, P. I. Immune response to enzyme replacement therapies in lysosomal storage diseases and the role of immune tolerance induction. (2015) doi:10.1016/j.ymgme.2015.11.001.

155. Pardridge, W. M. Blood-brain barrier delivery for lysosomal storage disorders with IgG-lysosomal enzyme fusion proteins. *Adv. Drug Deliv. Rev.* **184**, 114234 (2022).

156. Urayama, A., Grubb, J. H., Sly, W. S. & Banks, W. A. Pharmacologic manipulation of lysosomal enzyme transport across the blood-brain barrier. *J. Cereb. Blood Flow Metab.* **36**, 476–486 (2016).

157. Boado, R. J., Hui, E. K. W., Lu, J. Z., Zhou, Q. H. & Pardridge, W. M. Reversal of lysosomal storage in brain of adult MPS-I mice with intravenous Trojan horse-iduronidase fusion protein. *Mol. Pharm.* **8**, 1342–1350 (2011).

158. Allen Institute for Brain Science. Interactive Atlas Viewer: Atlas Viewer. *Allen Mouse Brain Atlas* http://atlas.brain-map.org/atlas?atlas=2&plate=100883888#atlas=2&plate=100883888&resolution=20.94&x=7720&y=4576.000061035156&zoom=-4&structure=73 (2004).

159. Allen Institute for Brain Science (2004). Allen Mouse Brain Atlas [dataset]. Available from mouse.brain-map.org.Allen Institute for Brain Science (2011). doi:mouse.brain-map.org.

160. Oh, S. W. *et al.* A mesoscale connectome of the mouse brain. *Nature* **508**, 207–214 (2014).

161. Harris, J. A. *et al.* Hierarchical organization of cortical and thalamic connectivity. *Nature* **575**, 195–202 (2019).

162. Lein, E. S. *et al.* Genome-wide atlas of gene expression in the adult mouse brain. *Nature* **445**, 168–176 (2007).

163. Allen Reference Atlas-Mouse Brain. atlas.brain-map.org. doi:atlas.brain-map.org.

164. Daigle, T. L. *et al.* A Suite of Transgenic Driver and Reporter Mouse Lines with Enhanced Brain-Cell-Type Targeting and Functionality. *Cell* **174**, 465-480.e22 (2018).